INFORMATION TO USERS

The most advanced technology has been used to photograph and reproduce this manuscript from the microfilm master. UMI films the original text directly from the copy submitted. Thus, some dissertation copies are in typewriter face, while others may be from a computer printer.

In the unlikely event that the author did not send UMI a complete manuscript and there are missing pages, these will be noted. Also, if unauthorized copyrighted material had to be removed, a note will indicate the deletion.

Oversize materials (e.g., maps, drawings, charts) are reproduced by sectioning the original, beginning at the upper left-hand corner and continuing from left to right in equal sections with small overlaps. Each oversize page is available as one exposure on a standard 35 mm slide or as a 17″ × 23″ black and white photographic print for an additional charge.

Photographs included in the original manuscript have been reproduced xerographically in this copy. 35 mm slides or 6″ × 9″ black and white photographic prints are available for any photographs or illustrations appearing in this copy for an additional charge. Contact UMI directly to order.

Accessing the World's Information since 1938

300 North Zeeb Road, Ann Arbor, MI 48106-1346 USA

Order Number 8820854

Interaction of electromagnetic waves and electrons with solid surfaces and small particles

Das, Sanjukta, Ph.D.

City University of New York, 1988

U·M·I
300 N. Zeeb Rd.
Ann Arbor, MI 48106

PLEASE NOTE:

In all cases this material has been filmed in the best possible way from the available copy. Problems encountered with this document have been identified here with a check mark __✓__.

1. Glossy photographs or pages _____
2. Colored illustrations, paper or print _____
3. Photographs with dark background _____
4. Illustrations are poor copy _____
5. Pages with black marks, not original copy __✓__
6. Print shows through as there is text on both sides of page _____
7. Indistinct, broken or small print on several pages __✓__
8. Print exceeds margin requirements _____
9. Tightly bound copy with print lost in spine _____
10. Computer printout pages with indistinct print _____
11. Page(s) _____ lacking when material received, and not available from school or author.
12. Page(s) _____ seem to be missing in numbering only as text follows.
13. Two pages numbered _____. Text follows.
14. Curling and wrinkled pages __✓__
15. Dissertation contains pages with print at a slant, filmed as received _____
16. Other _____

_____

_____

INTERACTION OF ELECTROMAGNETIC WAVES AND ELECTRONS WITH SOLID SURFACES AND SMALL PARTICLES

by

Sanjukta Das

A dissertation submitted to the Graduate Faculty in Physics in partial fulfilment of the requirements for the degree of Doctor of Philosophy, The City University of New York.

1988

This manuscript has been read and accepted for the Graduate Faculty in Physics in satisfaction of the dissertation requirement for the degree of Doctor of Philosophy.

Dec. 7, 1987
Date

Chairman of Examining Committee

Dec. 7, 1987
Date

Executive Officer

V. Sahni

M. Lax

T. Boyer

F. Smith

Supervisory Committee

The City University of New York

Abstract

INTERACTION OF ELECTROMAGNETIC WAVES AND ELECTRONS WITH SOLID SURFACES AND SMALL PARTICLES

by

Sanjukta Das

Advisor: Professor Joel. I. Gersten

In this dissertation I study both the interaction of electromagnetic waves and the interaction of electrons with solid state surfaces and small particles. In the electromagnetic problem I construct a theory to explain the continuum Raman scattering from the surface of a solid. This theory is then generalized to the case of a spherical particle. I find that the surface and particle problems have somewhat different features due to quantum size effects. Resonance Raman scattering appears to play an important role in the case of the spherical particles. In the study of the interaction of electrons with solid state surfaces, I examine the role played by interference effects in electron energy loss spectroscopy. As in the case of low energy electron diffraction, scattering from the ionic lattice leads to an interference effect. This causes additional features to appear in the excitation spectrum for plasmon emission. In addition the effects of electron-hole pairs are considered. I have also studied the interaction of an electron with a solid state particle and derived expressions for the various excitation cross sections. The nonlocal nature of the dielectric constant is included.

Acknowledgement

I am acknowledging my gratitude to my thesis advisor Prof. J. I. Gersten for his constant guidance and help without which this piece of work could not be done.

I wish to acknowledge the advice and help of various professors in the Physics department of City College. I also wish to acknowledge Prof. V. Sahni for many useful discussions during the work.

I also wish to thank Dr. C. L. Wang for helping alot in computation. I wish to thank specially Dr. K. Arya and Dr. S. Gayen for many helpful discussions. Lastly I wish to thank all my friends for many helpful discussions.

To my mother

CONTENTS

Part II. Electron scattering from solid surfaces and small particles.

PART I.

INTERACTION OF LIGHT WITH SURFACES AND SMALL PARTICLES

INTRODUCTION

The field of surface physics has experienced considerable development in recent years. This follows a fairly exhaustive study of the bulk properties of solids in the last half century. The analysis of bulk properties is simplified by the fact that one may regard it as having infinite extent in all directions. The surface properties play a secondary role since the ratio of the number of surface atoms to the number of bulk atoms is small. However, certain experimental probes are sensitive only to the surface properties and in analyzing these experiments one must obviously understand the surface physics. In addition, thin films and small particles are dominated by surface effects. Some processes such as crystal growth, catalysis, corrosion, adhesion, etc. can only really be understood as surface processes. The topic of this thesis relates to two tools that have proven to be very fruitful in studying surfaces: light scattering and electron scattering. My goal here is to gain a greater insight into how these tools operate and to exploit their potential by proposing some new experiments.

Let me briefly review some salient features of surface physics. In the case of bulk solids one has two major categories: crystalline and non-crystalline. In the former case the problem is simplified by the presence of translational periodicity. This leads to a well developed theory of electronic band structure and a fine description of the lattice structure and excitations. In the latter case the theory is less well developed but some of the concepts such as bands and phonons do carry over. When a surface is

introduced both the excitations and the structure get modified. Surface electronic states and their associated bands appear in the band gaps and surface phonons appear. These come about because of the breaking of the translational symmetry in the direction normal to the surface. The surface layers may also relax or undergo a restructuring due to an asymmetry of the forces acting on them. Surface dipole layers may be built up. In addition, the possible presence of adsorbates complicates the situation. Finally, the surface is likely to possess new sets of collective excitations, such as surface plasmons and surface phonons etc.

The problems of surface physics are further complexified by morphological effects. Surfaces are not always smooth and roughness can modify the surface properties considerably. As the scale of surface roughness gets to be smaller and smaller the roughness features begin to take on properties related to those of small solid state particles. To a first approximation one may regard a rough surface as a hybrid between a smooth surface and a collection of particles. Aside from their intrinsic interest in their own right, the study of small particles is seen to be of interest as it can serve as a model for surface roughness.

In recent years some strange anomalies have been reported for systems containing rough surfaces or small particles. Included in these effects are various enhanced electromagnetic processes such as surface-enhanced Raman scattering[1], enhanced infrared absorption and second harmonic generation. In addition some optical processes such as enhanced photoemission[2] have been observed. More recently anamolies relating to the sticking coefficient[3] and interparticle forces have been reported. Our understanding of these effects, at present, is incomplete. One of the goals of this work is to develop tools by which one may study such systems.

Small particle's properties are quite different from those of bulk solids since the electronic energy levels are discrete. The various phenomena due to this are loosely called 'quantum size effects'. The spacing between the levels, on the average is inversely propertional to the volume of the particles. At low temperatures, when the thermal energy is small compared to the level spacing, this discreteness should be exhibited in the physical properties. Kubo[4] first pointed out that due to the atomic roughness on the surface the levels should have a statistical distribution and the physical properties which depend on the transition between two levels, should depend on a two level correlation function. Gorkov and Eliasberg[5] had calculated the two level correlation function corresponding to four different types of statistical distributions. They are the Poisson distribution, orthogonal distribution, unitary distribution and symplectic distribution[6]. Another important property is that due to discreteness of the levels the Knight shift has a different temperature dependence for the case of even and odd electrons per particles. Due to the discreteness of the energy levels, theoretically one should expect to observe oscillations in the infrared absorption, but this oscillation is very difficult to see experimentally due to the polydisperse nature of the size distribution.

The rate of progress in surface science is slowed both due to difficulties in carrying out experiments as well as difficulties in performing realistic calculations. Surface studies entail the need for the precise characterization of the morphology, chemical composition, geometrical arrangement and electronic density distribution. Nevertheless, a substantial amount of progress has been made.

Real interest in the study of surfaces began, after ultrahigh vacuum techniques had been developed, by which well-defined surfaces could be

produced. To date the most widely used UHV spectroscopies include Electron Loss Spectroscopy (ELS), Auger Electron Spectroscopy (AES), Ultraviolet and X-ray photoelectron spectroscopy (UPS and XPS) and Secondary Ion Mass Spectroscopy (SIMS). However, UHV techniques are also not universal in the sense that they can not be applied to the solid-liquid interfaces. Surface electronic X-ray absorption spectroscopy (SEXAFS)[7] and surface infrared vibrational spectroscopy remedied these limitations encountered in UHV techniques. The former is less surface sensitive due to large penetration depths of optical photons. On the other hand surface vibrational spectroscopy is used for characterizing molecules adsorbed on surfaces. Among these techniques Surface Raman Spectroscopy is applicable to most surface environments, though the normal Raman intensity is very small. However after the discovery of Surface Enhanced Raman Scatterings (SERS), it has been widely used to study the surface. Recently there is growing interest in the study of surfaces and small solid state particles due to the advent of a new generation of high resolution experimental apparati, like scanning tunneling microscopes, by which one can precisely probe the structure of the surface.

One of the most extensively studied surface spectroscopy is the surface enhanced Raman scattering, so let me briefly review this topic.

Surface Enhanced Raman Scattering.

In the phenomenon of Surface Enhanced Raman Scattering (SERS) the intensity of Raman-scattered light from an adsorbed molecule is found to be up to six orders of magnitude greater than from an isolated molecule. SERS was originally observed for pyridine molecules adsorbed on a silver surface in an electrochemical cell. In recent years the experimental works has been extended to include a wide variety of adsorbates for both

the solid/vacuum interface as well as the solid/liquid interface. The field has been adequately reviewed[8].

In the experimental observations it was determined that surface roughness played an important role in governing the degree of enhancement that was observed. The rougher the surface was, the stronger the Raman scattering was. The present day understanding of this phenomenon is that there are two mechanisms operating - one an electrodynamic mechanism and the other a chemical mechanism. In the electrodynamic mechanism the local field in the vicinity of the molecule is enhanced both due to a 'lightning rod' effect as well as due to the excitation of localized excitations (such as plasmons) on the surface roughness features. The chemical mechanism for the enhancement is due to charge transfer excitations between the molecule and the substrate. Both of these effects contribute substantial factors to the scattered signal and hence account for the observed enhancement effects.

One puzzling feature observed in the SERS experiments is the observation of a continuum background[9] upon which the Raman scattered lines are superimposed. This continuum radiation extends on the Stokes side out to 4000cm^{-1}. Recently it has been found that even without the presence of surface roughness the continuum background is present. This would indicate that the electrodynamic mechanism is not responsible for this effect. This feature has never been adequately explained although some attempts have been made. It had been conjectured, for example, that in a charge transfer mechanism electrons can tunnel back to the molecular ion from anywhere below the Fermi surface. One could therefore envision a process in which simultaneous tunneling and emission of photons was occuring and this could give rise to the continuum. However, it is difficult to obtain

quantitative, estimates for this effect and the low tunneling rates might act to supress this mechanism. Additional mechanisms include electron-hole excitations, surface plasmon polaritons, superimposed weak Raman lines, unspecified fluorescence mechanisms and various luminescence mechanisms. There is some evidence that an adsorbate is not needed to see the continuum. This therefore seems to say that the chemical effect acting in SERS is also not of any relevance to the phenomenon. It appears that the continuum radiation is an intrinsic property of the substrate itself.

In the first chapter of the first part of this thesis we have done the explicit calculation for the continuum background spectrum, taking electronic Raman scattering as the mechanism. In the second chapter we have extended the above formalism to a spherical geometry. In the second part of the thesis we study electron energy loss spectroscopy. In the first chapter of the second part we consider the interference effect in EELS due to ionic planes. There we also consider the contribution of electron-hole pair and bulk plasmon contributions to the inelasic background. In the second chapter we consider energy loss of a charged particle scattered from a sphere. There we consider the excitation of higher order multipoles and also include the non-local dielectric function.

A major distinction between part one and two of the thesis concerns the single-particle versus the collective excitations. In our Raman studies we focus our attention on processes in which a single electron is excited. This process is sensitive to the finite size of the system because the energy levels are well separated from each other. In the second part of the thesis, however we focus primarily on collective excitations. Since such an excitation represents a many-body effect, the role of quantized energy levels is not that important and the more traditional quantum models are

applicable. In the second part we have described the excitation spectrum of the solid and small particles in terms of the dielectric function.

References

1. R. P. VanDuyne, J. Phys. (Paris) 38, c5-239 (1977)

2. A. Schmidt-Ott, P. Schurtenberger, and H. C. Seigmann. Phys. Rev. Lett. 45, 1284 (1980)

3. U. Muller, A. Schmidt-Ott, and H. Burtscher. Phys. Rev. Lett. 58, 1684, (1987)

4. R. Kubo, J. Phys. Soc. Japan. 17, 975 (1962)

5. L. P. Gorkov and G. M. Elliashberg. Sov. Phys. JETP. 21, 5, 940, (1965)

6. W. P. Halperin, Rev. Mod. Phys. 58, 3, 533, (1986)

7. R. H. Muller, in "Advances in Electrochemistry and Electrochemical Engineering", (R. H. Muller, ed), Vol. 9, p-1, Wiley-Interscience, New-York, 1973.

8. "Surface Enhanced Raman Scattering", ed. by R. K. Chang and T. E. Furtak (Plenum, New York, 1981)

9. J. I. Gersten, R. L. Birke, and J. R. Lombardi, Phys. Rev. Lett. 43, 71, (1979)

1. Theory of continuum surface Raman scattering from electrons in metals.

1. Introduction.

An interesting phenomenon associated with the observation of surface enhanced Raman scattering (SERS)[1] from molecules adsorbed on metal surfaces has been the observation of a continuum background[2-5] on the Stokes side of the incident laser field. It appears that adsorbed molecules are not needed to observe this background[6-9] indicating that the continuum is a property of the metal substrate. A number of mechanisms have been proposed to account for the origin of this radiation. These include luminescence associated with charge transfer,[10] electron-hole excitations,[11] surface plasmon polaritons,[12] superimposed weak Raman lines,[13] unspecified fluorescence mechanisms,[14] and various luminescence mechanisms.[5,15,16] While all these mechanisms are plausible the relative contribution of the various mechanisms has not been determined due to a lack of detailed calculations. This provides the motivation for the present study.

We start with a very simple process - Raman scattering from a gas of electrons bounded by a surface potential but otherwise free and try to calculate from first principles what the yield for secondary radiation is. Rather than attempt to study the case of complicated surface morphology we consider the plane surface. The process consists of a photon promoting an electron from an occupied state within the Fermi sea, followed by the coherent radiation of a scattered photon along with a lowering of the electron energy to another vacant state.

In Sec. 2 we develop the basic theory for the Raman scattering process. First the theory is applied to the case of a step potential. Then the theory is generalized to the case of a more realistic potential. Finally the

results of the calculations are discussed and their significance is analyzed. It will be concluded that Raman scattering may be used as a valuable tool to probe the density of states of metals near the Fermi energy.

2. Theory

The physical process we are considering is one in which an incident photon characterized by a frequency w_1 and polarization ϵ_1 virtually excites an electron from an occupied state below the Fermi level to a state above the Fermi level . The excited electron then relaxes to some empty state above the Fermi level emitting a secondary photon characterized by frequency w_2 and polarization ϵ_2. Our goal is to calculate the yield for this Raman process. The electrons in the solid are described by the Sommerfeld model in which they are bounded by a translationally symmetric surface potential. The electromagnetic field corresponding to the photons at frequencies w_1 and w_2 are described by the vector potentials $\vec{A}_1$ and $\vec{A}_2$. We are working in the long wave length limit, so that retardation effects are neglected and $\vec{A}_1$ and $\vec{A}_2$ can be taken as spatially homogeneous. We also neglect the 'eletron-electron' interaction. Atomic units are used, so that m=e= $\hbar$=1. The one electron Schrodinger equation is given by

$$\left\{ \tfrac{1}{2}[\vec{P} + \frac{1}{c}(\vec{A}_1 + \vec{A}_2)]^2 + V(\vec{r}) - i\frac{\partial}{\partial t} \right\} \psi(\vec{r},t) = 0 \qquad (2.1)$$

Making a gauge transformation of the type

$$\psi(\vec{r},t) = e^{i[(\alpha_1+\alpha_2)\cdot\vec{p}+\beta]}\chi(\vec{r},t) \qquad (2.2)$$

where

$$\alpha_j = -\frac{1}{c}\int_0^t A_j(t')dt' \qquad (2.3)$$

$$\beta = -\frac{1}{2c^2}\int_0^t [A_1(t')+A_2(t')]^2 dt' \tag{2.4}$$

and making use of the commutation relation $[\vec{p}_k, \vec{r}_l] = -i\,\delta_{kl}$, Eq. (2.1) can be rewritten as

$$\left[\frac{\vec{p}^2}{2}+V(\vec{r}-\alpha_1-\alpha_2) - i\frac{\partial}{\partial t}\right]\chi(\vec{r},t) = 0 \tag{2.5}$$

Thus in this gauge the electrons respond to a time-dependent potential which oscillates at the frequency of both the incident and the out-going photons.

In discussing Raman scattering we are only interested in terms bilinear in $\vec{A}_1$ and $\vec{A}_2$, so we will make a perturbation expansion of V. Thus

$$V(\vec{r}-\alpha_1-\alpha_2) \approx V(r) - (\alpha_1+\alpha_2).\nabla V + \tfrac{1}{2}(\alpha_1\alpha_2+\alpha_2\alpha_1):\nabla\nabla V \tag{2.6}$$

The Hamiltonian may be written as the sum of three terms

$$H = H_0 + H_1 + H_2 \tag{2.7}$$

where H_0 is the unperturbed Hamiltonian describing the quiescent solid

$$H_0 = \frac{\vec{p}^2}{2} + V(\vec{r}) \tag{2.8}$$

H_1 is the part of the Hamiltonian linear in the electromagnetic field

$$H_1 = -(\alpha_1+\alpha_2).\nabla V \tag{2.9}$$

and H_2 is bilinear in the fields.

$$H_2 = \tfrac{1}{2}(\alpha_1\alpha_2+\alpha_2\alpha_1):\nabla\nabla V = \alpha_1\alpha_2:\nabla\nabla V \tag{2.10}$$

In our calculation to lowest order in perturbation theory we consider the second order perturbation produced by H_1 and the first order perturbation by H_2. If we quantize the electromagnetic field we may write α_1 and α_2 in terms of the creation and annihilation operators for the photons. Since we are only interested in the process in which photon w_1 is absorbed and photon w_2 is emitted we have

$$\alpha_1 = -\hat{\epsilon}^1 a_1 (2\frac{\pi}{\Omega w_1^3})^{1/2} \tag{2.12}$$

$$\alpha_2 = -\hat{\epsilon}^2 a_2^+ (2\frac{\pi}{\Omega w_2^3})^{1/2} \tag{2.13}$$

where Ω is the quantization volume of all space. The second quantized Hamiltonian for the system may now be written in terms of the matrix elements involving the eigenstates of the unperturbed Hamiltonian

$$(\epsilon_\lambda - H_0)\,|\lambda> = 0 \tag{2.13}$$

Thus

$$H = w_1(a_1^+ a_1 + 1/2) + w_2(a_2^+ a_2 + 1/2) - (\frac{2\pi}{\Omega w_1^3})^{1/2} \sum_{\lambda\lambda',\sigma} <\lambda'|\hat{\epsilon}^1.\nabla V\,|\lambda> \times$$

$$a_1 b_{\lambda'\sigma}^+ b_{\lambda\sigma} - (\frac{2\pi}{\Omega w_2^3})^{1/2} \sum_{\lambda\lambda'\sigma} <\lambda'|\hat{\epsilon}^2.\nabla V\,|\lambda> a_2^+ b_{\lambda'\sigma}^+ b_{\lambda\sigma} -$$

$$\frac{2\pi}{\Omega}(w_1 w_2)^{-\frac{3}{2}} \sum_{\lambda\lambda'\sigma} <\lambda'|\hat{\epsilon}^1.\nabla\hat{\epsilon}^2.\nabla V\,|\lambda> a_2^+ a_1 b_{\lambda'\sigma}^+ b_{\lambda\sigma} \tag{2.14}$$

where σ is the spin index, a_μ and $b_{\lambda\sigma}$ are the destruction operators for photons and electrons, a_μ^+ and $b_{\lambda\sigma}^+$ are the corresponding creation operators.

The physical processes corresponding to Raman Scattering are shown in Fig. (1) by the 5 diagrams. In each process a photon of frequency w_1 is

absorbed and a photon of frequency w_2 is emitted. A hole is produced in state $|\lambda>$ and an electron is excited to state $|\lambda'>$. In diagrams (a) and (c) the intermediate state involves a hole whereas in diagram (b) and (d) it involves an electron. In (b) and (c) the absorption occurs prior to emission whereas the reverse is true for diagrams (a) and (d). Diagram (e) is a process in which absorption and emission occurs simultaneously. The explicit expression for the matrix element corresponding to these five diagrams are

$$M_a = -\frac{2\pi}{(w_1 w_2)^{3/2}} \sum_{\lambda''} f^{-}_{\lambda''} \frac{<\lambda'|\hat{\epsilon}_2.\nabla V|\lambda''><\lambda''|\hat{\epsilon}_1.\nabla V|\lambda>}{\epsilon_{\lambda''}-\epsilon_{\lambda'}-w_2} \qquad (2.15a)$$

$$M_b = +\frac{2\pi}{(w_1 w_2)^{3/2}} \sum_{\lambda''} f^{+}_{\lambda''} \frac{<\lambda'|\hat{\epsilon}_2.\nabla V|\lambda''><\lambda''|\hat{\epsilon}_1.\nabla V|\lambda>}{\epsilon_{\lambda}-\epsilon_{\lambda''}-w_1} \qquad (2.15b)$$

$$M_c = -\frac{2\pi}{(w_2 w_1)^{3/2}} \sum_{\lambda''} f^{-}_{\lambda''} \frac{<\lambda'|\hat{\epsilon}_1.\nabla V|\lambda''><\lambda''|\hat{\epsilon}_2.\nabla V|\lambda>}{\epsilon_{\lambda''}-\epsilon_{\lambda'}+w_1} \qquad (2.15c)$$

$$M_d = +\frac{2\pi}{(w_1 w_2)^{3/2}} \sum_{\lambda''} f^{+}_{\lambda''} \frac{<\lambda'|\hat{\epsilon}_1.\nabla V|\lambda''><\lambda''|\hat{\epsilon}_2.\nabla V|\lambda>}{\epsilon_{\lambda}-\epsilon_{\lambda''}-w_2} \qquad (2.15d)$$

$$M_e = \frac{2\pi}{(w_1 w_2)^{3/2}} <\lambda'|\hat{\epsilon}_1.\nabla\hat{\epsilon}_2.\nabla V|\lambda> \qquad (2.15e)$$

For convenience the vacuum level is taken at ϵ=0. Conservation of energy for the overall process demands that $w_1+\epsilon_\lambda = w_2+\epsilon_{\lambda'}$. Matrix elements M_a and M_b can be added togather, even at finite temperature, to give an expressions no longer involving the Fermi factor of intermediate state. Similarly M_c and M_d can be added togather. Thus the total matrix element will be the sum of three terms and is given by

$$M = 2\frac{\pi}{(w_1 w_2)^{3/2}} <\lambda'|[\hat{\epsilon}^2.\nabla V G(w_1+\epsilon_\lambda)\hat{\epsilon}^1.\nabla V +$$

$$\hat{\epsilon}^1.\nabla V G(\epsilon_\lambda - w_2)\hat{\epsilon}^2.\nabla V + \hat{\epsilon}^1.\nabla\hat{\epsilon}^2.\nabla V]|\lambda> \qquad (2.16)$$

where we have introduced the Greens function $G(\epsilon)$ defined by

$$G(\epsilon) = \sum_{\lambda'} |\lambda'><\lambda'| \frac{1}{\epsilon - H_0} \tag{2.17}$$

The boundary condition corresponding to this function is chosen to result in outgoing states.

Evaluation of Eq.(2.16) is further simplified by introducing states $|u>$ and $|v>$ defined by

$$|u> = G(w_1+\epsilon_\lambda)\hat{\epsilon}_1.\nabla V |\lambda> \tag{2.18a}$$

and

$$|v> = G(\epsilon_\lambda - w_2)\hat{\epsilon}_2.\nabla V |\lambda> \tag{2.18b}$$

so that the total matrix element becomes

$$M = \frac{2\pi}{(w_1 w_2)^{3/2}}[<\lambda'|\hat{\epsilon}_2.\nabla V |u> + <\lambda'|\hat{\epsilon}_1.\nabla V |v> + <\lambda'|\hat{\epsilon}_1.\nabla\hat{\epsilon}_2.\nabla V |\lambda>] \tag{2.19}$$

The advantage of introducing $|u>$ and $|v>$ is that they may be found by simply solving the inhomogeneous equations

$$(\epsilon_\lambda + w_1 - H_o)|u> = \hat{\epsilon}_1.\nabla V |\lambda> \tag{2.20}$$

and

$$(\epsilon_\lambda - w_2 - H_o)|v> = \hat{\epsilon}_2.\nabla V |\lambda> \tag{2.21}$$

Then the matrix elements in Eq.(2.19) may be obtained by direct integration.

We are interested in obtaining the yield for producing outgoing photons that reach the detector per incident photon. We calculate the scattering rate by using Fermi's Golden Rule and dividing by the incident flux of photons. Thus summing over the initial and the final states of the electron and final states of the photon , the yield is given by

$$Y = \frac{2\pi}{c} \sum_{k_2,\lambda,\lambda',\sigma} f_{\lambda}^{-} f_{\lambda'}^{+} |M|^2 \delta(w_1 - w_2 + \epsilon_{nl} - \epsilon_{n'l'}) \qquad (2.22)$$

Here ϵ_{nl} and $\epsilon_{n'l'}$ are the initial and final state energy of the electron and $\vec{k}_2$ is the direction of final photon wave vector. The summation over final states is given by the integral

$$\sum_{k_2} = \int w_2^2 dw_2 \frac{d\Omega_2}{(2\pi c)^2} \qquad (2.23)$$

The differential yield for producing a photon in a frequency range dw_2 around w_2 and a solid angle range $d\Omega_2$ is given by

$$\frac{dY}{dw_2 d\Omega_2} = \frac{w_2^2}{4\pi^2 c^4} \sum_{\lambda,\lambda',\sigma} f_{\lambda}^{-} f_{\lambda'}^{+} |M|^2 \delta(w_1 - w_2 + \epsilon_{nl} - \epsilon_{n'l'}) \qquad (2.24)$$

where σ is the spin index. f_{λ}^{-} is the Fermi factor for an occupied electron state $|\lambda>$ while f_{λ}^{+} is the Fermi factor for the unoccupied state $|\lambda>$. Note that $f_{\lambda}^{-} + f_{\lambda}^{+} = 1$. In our work we are primarily concerned with situations in which thermal effects are not important, so we have used the relation

$$f_{\lambda}^{-} = \Theta(\epsilon_f - \epsilon_{\lambda}) \qquad (2.25)$$

Θ being the unit step function, and $-\epsilon_f$ is the work function. For convenience the vacuum level is taken at $\epsilon = 0$. Conservation of energy for the overall process demands $w_1 + \epsilon_{\lambda} = w_2 + \epsilon_{\lambda'}$.

So far the form of $V'(\vec{r})$ has been left general. Let us now restrict our attention to the case of a simple metal, which we will model as a set of free electrons in a potential well. The surface of the solid is taken to lie in the x-y plane with a characteristic surface reference point at z=0. The potential will be assumed to be of the form V(z) so that as far as the x or y motion is concerned the electrons are free particles. Let

$$<r \mid \lambda> = \phi_\mu(z)\exp(iK_p . r) \tag{2.26}$$

where we have expanded the notation so that the index λ now denotes (K_p, μ), where K_p is the wave vector parallel to the surface. The function $\phi_\mu(z)$ now satisfies the Schrodinger equation

$$\left[E_\mu + \frac{1}{2}\frac{d^2}{dz^2} - V(z)\right]\phi_\mu(z) = 0 \tag{2.27}$$

where

$$\epsilon_\lambda = E_\mu + \frac{K_p^2}{2}$$

Similarly we may factor $<r \mid u>$ and $<r \mid v>$ as

$$<r \mid u> = U(z)\hat{\epsilon}_1.\hat{K}\exp(iK_p . r) \tag{2.28}$$

$$<r \mid v> = W(z)\hat{\epsilon}_2.\hat{K}\exp(iK_p . r) \tag{2.29}$$

So that $U(z)$ and $W(z)$ satisfy the inhomogeneous equations

$$\left[E_\mu + w_1 + \frac{1}{2}\frac{d^2}{dz^2} - V(z)\right]U(z) = V'(z)\phi_\mu(z) \tag{2.30}$$

$$\left[E_\mu - w_2 + \frac{1}{2}\frac{d^2}{dz^2} - V(z)\right]W(z) = V'(z)\phi_\mu(z) \tag{2.31}$$

The matrix element may thus be written as

$$M = \frac{(2\pi)^2}{(w_1 w_2)^{3/2}} \hat{\epsilon}_1.\hat{K}\ \hat{\epsilon}_2.\hat{K} N\ \delta(K_p - K_{p'}) \qquad (2.32)$$

where N is a matrix element obtained by doing one-dimensional integrals over the z coordinates

$$N = \langle \phi_{\mu'} | V'(z) | U_\mu \rangle + \langle \phi_{\mu'} | V'(z) | W_\mu \rangle + \langle \phi_{\mu'} | V''(z) | \phi_\mu \rangle \qquad (2.33)$$

Inserting Eq. (2.32) into Eq. (2.24) gives

$$\frac{dY}{dw_2 d\ \Omega_2} = \frac{1}{\pi c^4 w_1^3 w_2} \sum_{\mu,\mu'} \int d^2 K_p\ \Theta(-\phi - E_\mu - \frac{K_p^2}{2}) \Theta(E_{\mu'} + \phi + \frac{K_p^2}{2}) \times$$

$$|N|^2 (\hat{\epsilon}_1.\hat{K}\ \hat{\epsilon}_2.\hat{K})^2 \delta(w_1 - w_2 + E_\mu - E_{\mu'}) \qquad (2.34)$$

Here we have performed the integration over K'_p using the $\delta(K_p - K'_p)$ term and have summed over spins.

If we have unpolarized incident light and do not measure the polarization of the outgoing light we may further simplify this by summing over the final polarization vectors ($\hat{\epsilon}_2$) and averaging over the initial polarization vectors ($\hat{\epsilon}_1$) . Let θ_1 be the angle between the normal to the surface and the incident propagation vector of the photon , similarly let θ_2 be the angle between the outgoing photon's wave vector and normal. Then

$$\sum_{\hat{\epsilon}_2} \langle (\hat{\epsilon}_1.\hat{K}\ \hat{\epsilon}_2.\hat{K})^2 \rangle_{\hat{\epsilon}_1} = \frac{1}{2} (\sin\theta_1 \sin\theta_2)^2 \qquad (2.35)$$

In Eq.(2.34) we may integrate over K_p so we obtain

$$\frac{dY}{dw_2 d\ \Omega_2} = \frac{(\sin\theta_1 \sin\theta_2)^2}{2\pi c^4 w_1^3 w_2} \sum_{\mu,\mu'} |N|^2 [-\phi - E_\mu - max(-\phi - E_{\mu'}, 0)] \times$$

$$\Theta[-\phi - E_\mu - max(\epsilon_f - E_{\mu'}, 0)] \delta(w_1 - w_2 + E_\mu - E_{\mu'}) \qquad (2.36)$$

It is convenient to introduce the one-dimensional density of states

$$D(E) = \sum_{\mu} \delta(E - E_{\mu}) \tag{2.37}$$

so that Eq. (2.36) may finally be expressed as

$$\frac{dY}{dw_2 d\Omega_2} = \frac{(\sin\theta_1 \sin\theta_2)^2}{2\pi c^4 w_1^3 w_2} \int dE D(E) D(E + w_1 - w_2) |N|^2 \times$$

$$[-\phi - E - max(0, -\phi - E - w_1 + w_2)]\Theta[-\phi - E - \max(0, -\phi - E - w_1 + w_2)] \tag{2.38}$$

This may alternatively be written as

$$\frac{dY}{dw_2 d\Omega_2} = \frac{(\sin\theta_1 \sin\theta_2)^2}{2\pi c^4 w_1^3 w_2} \int dE D(E) D(E + w_1 - w_2) |N|^2 \times$$

$$\Theta(w_1 - w_2)\Theta(-\phi - E)\min(w_1 - w_2, -E - \phi). \tag{2.39}$$

This quantity is zero if $w_1 < w_2$, so at T=0K there will only be Stokes scattering. At finite temperatures we can expect an exponential tailing off of the Raman scattering on the anti-Stokes side of the incident frequency. Now we will consider the specific form of the potential.

THE STEP POTENTIAL

Before going on to a more general case let us look at the idealized model where the potential function V(z) is simply a step, i.e.,

$$V(z) = \begin{cases} -V_0 & \text{if } z < 0 \\ 0 & \text{if } z > 0 \end{cases} \tag{2.40}$$

The depth of the step is the sum of the work function and the Fermi energy

$$V_0 = \phi + \epsilon_f \tag{2.41}$$

For energies which lie below the vacuum level but above the bottom of the band, the normalized eigenfunctions of Eq.(2.26) are

$$\phi_\mu = \begin{cases} \sqrt{\frac{2}{L}}\sin(K_\mu z + \delta_\mu) & \text{if } z < 0 \\ \sqrt{\frac{2}{L}}\sin\delta_\mu \exp(-q_\mu z) & \text{if } z > 0 \end{cases} \tag{2.42}$$

Here

$$k_\mu = [2(E_\mu + V_0)]^{1/2}$$

$$q_\mu = [-2E_\mu]^{1/2}$$

and

$$\delta_\mu = -\cot^{-1}\left(\frac{q_\mu}{K_\mu}\right)$$

The normalization length is chosen to extend from -L to +L, where eventually the limit $L \to \infty$ will be taken.

We may use Eq.(2.42) along with the formula $V'(z) = V_0\delta(z)$ to plug into the right-hand sides of Eqs.(2.30) and (2.31). The resulting inhomogeneous equation is then solved subject to the following boundary conditions. If the solution is of a propagating nature then the wave should propagate away from the surface. If the solution is of an attenuated nature then it should attenuate away from the surface. Thus from Eq.(2.30) we find

$$U(z) = \begin{cases} D_1 exp(-i\sigma_1 z) & \text{if } z < 0 \\ D_1 exp(i\tau_1 z) & \text{if } z > 0, \end{cases} \tag{2.43}$$

where

$$\sigma_1 = \begin{cases} [2(w_1+E_\mu+V_0)]^{1/2} & \text{if } w_1+E_\mu+V_0>0 \\ i\,[-2(w_1+_\mu+V_0)]^{1/2} & \text{if } w_1+E_\mu+V_0<0 \end{cases} \tag{2.44}$$

$$\tau_1 = \begin{cases} [2(w_1+E_\mu)]^{1/2} & \text{if } w_1+E_\mu>0 \\ i\,[-2(w_1+E_\mu)]^{1/2} & \text{if } w_1+E_\mu<0, \end{cases} \tag{2.45}$$

and

$$D_1 = \frac{-2i}{\sigma_1+\tau_1} V_0\phi_\mu(0). \tag{2.46}$$

Likewise

$$W(z) = \begin{cases} D_2\exp(-i\,\sigma_2 z) & \text{if } z<0 \\ D_2\exp(i\,\tau_2 z) & \text{if } z>0, \end{cases} \tag{2.47}$$

where

$$\sigma_2 = \begin{cases} [2(-w_2+E_\mu+V_0)]^{1/2} & \text{if } E_\mu+V_0-w_2>0 \\ i\,[-2(-w_2+E_\mu+V_0)]^{1/2} & \text{if } E_\mu+V_0-w_2<0, \end{cases} \tag{2.48}$$

$$\tau_2 = \begin{cases} [2(-w_2+E_\mu)]^{1/2} & \text{if } E_\mu-w_2>0 \\ [2(w_2-E_\mu)]^{1/2} & \text{if } E_\mu-w_2<0, \end{cases} \tag{2.49}$$

and

$$D_2 = \frac{-2iV_0}{\sigma_2+\tau_2}\phi_\mu(0) \tag{2.50}$$

In terms of Eqs.(2.42), it is now very simple to evaluate the matrix element appearing in Eq.(2.33). Thus the individual contributions are

$$\langle\phi_{\mu'}|V'(z)|U_\mu\rangle = \frac{-4iV_0^2}{\sigma_1+\tau_1}\frac{\sin\delta_\mu\sin\delta_{\mu'}}{L} \tag{2.51}$$

$$\langle\phi_{\mu'}|V'(z)|W_\mu\rangle = \frac{-4iV_0^2}{\sigma_2+\tau_2}\frac{\sin\delta_\mu\sin\delta_{\mu'}}{L} \tag{2.52}$$

and

$$<\phi_{\mu'}|V''(z)|\phi_{\mu}>=\frac{2V_0}{L}(q_{\mu}+q_{\mu'})\sin\delta_{\mu}\sin\delta_{\mu'} \tag{2.53}$$

Note that

$$\sin\delta_{\mu}\sin\delta_{\mu'}=\frac{K_{\mu}K_{\mu'}}{2V_0} \tag{2.54}$$

so

$$N=\frac{K_{\mu}K_{\mu'}}{L}\left|q_{\mu}+q_{\mu'}-2iV_0\left(\frac{1}{\sigma_1+\tau_1}+\frac{1}{\sigma_2+\tau_2}\right)\right| \tag{2.55}$$

The density of states for the step potential is

$$D(E)=\frac{L\,\Theta(E+V_0)}{\pi[2(E+V_0)]^{1/2}}+\frac{L\,\Theta(E)}{\pi[2E]^{1/2}}. \tag{2.56}$$

Since we will restrict our attentions to energies lying below the vacuum level the second term may be omitted and Eq. (2.39) becomes

$$\frac{dY}{dw_2 d\,\Omega_2}=\frac{(\sin\theta_1\sin\theta_2)^2}{\pi^3 c^4 w_1^3 w_2}\int_{-V_0}^{-\phi}dE\,[(E+V_0)(E+w_1-w_2+V_0)]^{1/2}\times$$

$$\left|\left|q+q'-2iV_0\left(\frac{1}{\sigma_1+\tau_1}+\frac{1}{\sigma_2+\tau_2}\right)\right|\right|\Theta(w_1-w_2)\min(w_1-w_2,-E-\phi). \tag{2.57}$$

Here $q'=(-2E_{\mu'})^{1/2}$evaluated at $E_{\mu'}=E'=E+w_1-w_2$. The formula for the yield has therefore been reduced to the evaluation of a one-dimensional integral. This integral may be computed numerically.

A MORE REALISTIC POTENTIAL

In the step potential model the abrupt change of the potential from $-V_0$ to 0 at z=0 is somewhat unrealistic. In reality the electrons penetrate in to the vacuum region and the potential change takes place more

gradually. Let us study the following model potential

$$V(z) = -V_0 \left| 1-[1+exp(-\alpha z)]^{-1} \right| \tag{2.58}$$

It rises from $-V_0$ to 0 in a characteristic distance of order $1/a$. While the Schrodinger equation for this potential may be solved analytically and the Green function may likewise be obtained , we have found it simpler to solve the equations numerically.

To obtain the eigenfunction we proceed as follows. We start at a large positive value of z and assign $\phi(z) = 1$ arbitrarily. Since for large z, $\phi(z) = exp[-z(-2\epsilon)^{1/2}]$ we know that $\phi'(z) = -(-2\epsilon)^{1/2}$. We numerically integrate the Schrodinger equation using a Runge-Kutta procedure down to some large negative value of z. There the wave function will be $\phi(z) = N \sin(z[(\epsilon+V_0)]^{1/2}+\delta)$. The normalization constant N can then be found from

$$N = \left| \phi^2(z) + \frac{1}{2E+2V_0}\left(\frac{d\phi}{dz}\right)^2 \right. \tag{2.59}$$

The wave function may then be rescaled so that $A = (2/L)^{1/2}$.

The solution to Eq.(2.30) is obtained by a slightly more complicated procedure. For large positive z we know from our experience with the step potential that

$$\frac{U'(z)}{U(z)} \Big|_{-\infty} \rightarrow i\tau_1, \tag{2.60}$$

while for large negative z,

$$\frac{U'(z)}{U(z)} \Big|_{-\infty} \rightarrow i\sigma_1, \tag{2.61}$$

Let us call the large positive value of z "L" and the large negative value of z "-L". If we would implement a Runge-Kutta integration procedure backwords in z we could express $U(-L)$ and $U'(-L)$ as linear combination of $U(L)$ and $U'(L)$. By using Eq.(2.60), however,

$$U(-L) = A + BU(L) \tag{2.62}$$

$$U'(-L) = C + DU(L) \tag{2.63}$$

where A, B, C, D are coefficients to be determined. What we do is make two trial integrations of Eq.(2.30) backwards in z. In the first trial we start with $U(L) = 0$ and call the resulting solution $U_0(z)$. From Eqs.(2.60) and (2.61) we then find that

$$A = U_0(-L) \tag{2.64}$$

and

$$C = U'_0(-L) \tag{2.65}$$

In the second trial we start with $U(L) = 1$ and call the resulting solution $U_1(z)$. Then from Eq.(2.62) and (2.63) we find

$$U_1(-L) = A + B, \tag{2.66}$$

$$U'_1(-L) = C + D. \tag{2.67}$$

Equations (2.64)-(2.67) are sufficient to determine A, B, C, and D. From Eqs.(2.62)-(2.64) we have

$$U(L) = -\frac{(i\sigma_1 A + C)}{D + i\sigma_1 B} \tag{2.68}$$

Inserting the solutions for A, B, C, D in to this expression tells us what the proper starting value for $U(L)$ should be

$$U(L) = -\frac{[U'_0(-L)+i\sigma_1 U_0(-L)]}{U'_1(-L)-U'_0(-L)+i\sigma_1[U_1(-L)-U_0(-L)]} \tag{2.69}$$

From Eq.(2.69) and (2.60) we then know the correct starting values for the functions $U(L)$ and $U'(L)$ so a backward Runge-Kutta integration yields the entire function $U(z)$. An identical procedure may be used to determine $W(z)$.

The density of states is again given by Eq.(2.56). Since the density of states is singular at $E+V_0=0$ (and at $E=0$) it is useful to make the change of variables $x^2 = E+V_0$. Then

$$\frac{dY}{dw_2 d\Omega_2} = \frac{(\sin\theta_1 \sin\theta_2)^2}{2\pi c^4 w_1^3 w_2} \int_0^{\epsilon_f^{1/2}} dx\,(x^2+w_1-w_2)^{-1/2} |N|^2 \times\Theta(w_1-w_2)\min(w_1-w_2, \epsilon_f - x^2), \tag{2.70}$$

and the integrand is now manifestly nonsingular.

RESULTS AND DISCUSSION

In the previous section we have developed a theory for continuum Raman scattering produced when a photon impinges on a free electron gas bounded by a surface potential. Let us now apply this theory to some simple metals. In order to do so we will need to know numerical values for the model potential of Eq.(2.58). Smith[17] has derived a model potential based on the density functional formalism and this may be used as a starting point. We have slightly modified the Smith potentials by regarding the background ion density as a variable which can be used to fit the experimental values for V_0 based on the work function and the Fermi energy. A least squares fitting procedure was then used to fit Eq.(2.58) to the Smith potential. The two parameters varied were the constant 'a' of Eq.(2.58) and the location of the origin of the Smith potential relative to our model

potential. Typical values of a for Al, Ag, and Au were found to be 0.91, 0.81, and 0.81, respectively. The corresponding values for V_0 were 0.59, 0.36, 0.36.

In Fig.2. we show typical wave functions appearing in our theory. In Fig.(2a).the eigenfunction $\phi(z)$ for Al corresponding to an energy E=-0.2 a.u. is shown along with the perturbed function U(z). Since U(z) is complex we graph both the real and imaginary parts of U(z) separately. The photon energy was taken to be $w_1 = 0.1 a.u.$. In Fig.(2b). we again plot $\phi(z)$ along with the real and imaginary parts of W(z). As might be expected each of these functions is oscillatory inside the solid and decays more or less exponentially into the vacuum. For comparison's sake in Fig.3. we illustrate what happens to the perturbed function U(z) at higher frequencies corresponding to transitions to states above the vacuum level. Now $w_1 = 0.5$ a. u. and the perturbed function is oscillatory over all space. Our attention , however, will be restricted to photon energies $\hbar w_1$ smaller than the work function, so the wave functions will look typically like those of Fig.2.

First we considered the idealized case of Raman scattering from a theta function step potential ,then we studied the scattering from the more realistic potential given by Eq.(2.58). The step potential case has the advantage that it is almost completely tractable analytically whereas the realistic potential requires some numerical integration of differential equations. In Fig.5. we compare the ratio of the square of typical matrix elements $|N|^2$ for the realistic potential to those of the step potential. As the parameter 'a' gets larger the realistic potential gets to look more like an abrupt step so the ratio approaches unity, as expected. For lower values of a, however, $|N|^2$ is significantly lower than the corresponding value for

the abrupt step. One may note that this is expected since the magnitude of $V'(z)$ gets to be smaller as the potential gets to be more gradual in its behavior. Hence the size of the matrix element is diminished.

Let ΔY denote the differential yield divided by the $(\sin\theta_1 \sin\theta_2)^2$ factor, i.e.,

$$\Delta Y = (\sin\theta_1 \sin\theta_2)^{-2} \frac{dY}{dw_2 d\Omega_2} \tag{2.71}$$

In Fig.4. we graph ΔY as a function of outgoing photon frequency for Al, Ag, and Au. Since the free electron parameters are the same for Ag and Au the theory predicts the same spectrum. In this graph the incident photon was taken to have an angular frequency=0.1 a.u., corresponding to an optical wavelength of 4850A . We note the differential yield rises gradually from zero as one proceeds more to the Stokes side of the incident photons. The typical scale over the optical region would be approximately 10^{-7}.

The gradual rise in the differential yield as one progresses into the Stokes region of the spectrum is largely due to a density of states effect. This may be seen in Fig.6. where we have graphed ΔY for a hypothetical case in which the matrix element N was taken to be 0.5. The Fermi energy was taken to be that appropriate to Ag, ie., $\epsilon_f = 0.20$a.u. The similarity of Fig.4 and 6 , the calculation with and without the energy variation of N, indicates that the shape of the differential yield curve is determined mainly by the density of states.

Let us now make rough numerical estimates. We choose these hypothtical experimental parameters to correspond to experiments done on Ag[5]. Consider the case of Ag and calculate the counting rate for Stokes shifted photons at an 1800cm^{-1} Raman shift. Assume an incident power of

0.2 W hitting the surface. Let us take θ_1 and θ_2 to be both 45^0 Let the incident laser wavelength be 4850A, corresponding to the calculations in Fig.4. The detector will be assumed to have a frequency resolution of $\Delta w = 2cm^{-1} = 0.91\times10^{-5}$ a.u. and an optical acceptance cone of $\Delta\Omega = 1$ steradian. The absolute yield into the detector is then $Y = 0.95\times10^{-15}$ per incident photon. The number of incident photons per second is 4.6×10^{17} so the counting rate would be 440 counts per second. Assuming a detector effiency of approximately 25% this would yield an observed counting rate of 110 counts per second. This is in very good agreement with the experimentally observed counting rate. Experiment[4] also indicate a gradual rise in the continuum background over $3500cm^{-1}$ range, followed by a gradual decline in the rate. It is this feature which we will address below.

For many purposes Ag may be treated as a free electron metal. This is because the density of states at the Fermi level is given correctly by the free electron Sommerfeld theory[18]. However, a glance at the bulk density of states function of Ag[19] will show that in reality band structure effects are important and that the density of states hardly follows a monotonic behavior. Theory[19] predicts that in the immediate neighborhood of the Fermi level the density of states goes through a maximum and minimum. The behavior of the density of states is reproduced in Fig.6. It is perhaps not unreasonable to assume that the equivalent one-dimensional density of states such as given by Eq.(2.37) will also display such a peak in the vicinity of the Fermi level. Since we have seen that the form of the differential yield function is approximately reproduced by neglecting the variation of the matrix element with energy, it is worthwhile to repeat the calculation for a density of states function such as in Fig.7. As a model we approximate Fig.7 by the function

$$D(E) \approx \begin{cases} (E_1 - E)(E - E_2) & \text{if } E_2 < E < E_1 \\ 0 & \text{otherwise} \end{cases} \tag{2.72}$$

For Ag we choose $E_1 = -0.151 a.u.$, $E_2 = -0.1867$ and $\phi = 0.1581$. From Eq. (2.70) the yield is then proportional to the integral

$$I \propto \int_{E_1}^{-\phi} dE D(E) D(E + \Delta) \Theta(E + \Delta + V_0)[-(\phi + E)\Theta(-\phi - E)\Theta(E + \phi + \Delta) +$$

$$\Delta \Theta(\Delta)\Theta(\Delta - E - \phi)] \tag{2.73}$$

where $\Delta = w_1 - w_2$. The result of this integral is plotted in Fig.8 as a function of the Stokes shift $w_1 - w_2$. We note that a broad maximum occurs at 0.015 a.u., or about 3300cm^{-1}. This is in good agreement with the observed maximum in the Ag spectrum, although this maximum may also be due in part to water molecular vibrations.

The implications of these crude calculations are very important. It means that by using a totally optical experiment one is able to measure some features of the band structure of solids to spectroscopic accuracy. This would put rather stringent requirements on any theoretical band structure calculations to reproduce the experimental features. Consequently the existing Raman experiments should be extended to larger Stokes shifts and to higher incident photon energies.

A comparison may be made between this theory and that of photoemission. In photoemission an electron is excited by an incident photon to an energy sufficient to overcome the work function and to leave the solid. If the energy is less than the work function then the excited electron is not emitted and will eventually relax. One of the process for relaxation is by emitting a photon. Here we have calculated the yield for coherently exciting such a photon.

In photoemission it is known that both the surface potential and the bulk potential play a role in determining the photoyield. Here we have just calculated the surface contribution to the Raman scattering and have neglected the bulk contribution. It is an approximation and this approximation can be remedied by suitably modifying the potential $V(\vec{r})$. The theory will still be described by Eq.(2.24) and (2.20). However, it should be noted that the experiments were done on a roughened silver surface, and on such a surface the ratio of surface area to mass is very high. Thus one would expect bulk effects to be not as important. Furthermore, the bulk effect is not very important unless a very large sample of bulk actually has radiation photons w_1 and w_2 passing through it. Because of screening the internal potential is rather smooth, as is evidenced by pseudopotential descriptions of the properties of the bulk metals. However, the final work on the relative importance of surface and bulk contributions must await a more complete analysis.

In photoemission one essentially measures the joint density of states for electrons above the vacuum level and below the Fermi level. In the theory outlined above one measures the joint density of states of electrons below the vacuum level (but above the Fermi level) with those below the Fermi level. Like inverse photoemission[20] it therefore provides complimentary information to that of photoemission. However, it has the potential advantage over inverse photoemission in that electron beams and their inherent difficulties and poor resolution are not needed.One may also study the solid-gas or solid-liquid interface by a purely optical technique. This theory should also be applicable to the case of ordinary photoemission.

References

1. For a recent review see "Surface Enhanced Raman Scattering", edited by R. K. Chang and T. E. Furtak (Plenum, New York, 1982)

2. A. Otto, Surf. Sci. 75, L392 (1972)

3. E. Burstein, Y. J. Chen, C. Y. Chen, S. Lundquist, and E. Tosatti, Solid State Commun. 29, 567 (1979)

4. J. I. Gersten, R. L. Birke, and J. R. Lombardi, Phys. Rev. Lett. 43, 71 (1979)

5. J. P. Heritage and J. G. Bergman, in Proceedings of the Second USA-USSR Light Scattering Symposium, edited by J. L. Birman, H. Z. Cummins, and K. K. Rebane (Plenum, New-York, 1979), p. 167

6. A. Otto, J. Timper, J. Billman, and I. Pockrand, Surf. Sci. 92, L55 (1980)

7. A. Otto, J. Timper, J. Billman, and I. Pockrand, Phys. Rev. Lett. 45, 46 (1980)

8. J. Timper, J. Billman, A. Otto, and I. Pockrand, Surf. Sci. 101, 348 (1980)

9. I. Pockrand and A. Otto, Solid State Commun. 37, 109(1981)

10. J. I. Gersten, R. L. Birke, and J. R. Lombardi, Phys. Rev. Lett. 43, 147 (1979)

11. A. Otto, Surf. Sci. 92,145 (1980)

12. J. C. Tsang, J. R. Kirtley, and T. N. Theis, Solid State Commun. 35, 667 (1980)

13. B. Pettinger, Chem. Phys. Lett. 78, 404 (1981)

14. C. K. Chen, A. R. B. deCastro, and Y. R. Shen, Phys. Rev. Lett.46, 145 (1981)

15. J. P. Heritage, J. G. Bergman, A. Pinczuk, and J. M. Worlock, Chem. Phys. Lett. 67, 229 (1979)

16. E. Burstein and C. Y. Chen, in Proceedings of the 7th International Conference on Raman Spectroscopy, Ottowa, 1980, edited by W. E. Murphy (North-Holland, Amsterdam, 1980), p.346.

17. J. R. Smth, Phys. Rev. 181, 522 (1969)

18. C. Kittel, Introduction to Solid State Physics,4th ed. (Wiley, New-York, 1971).

19. E. C. Snow, Phys. Rev. 172 708 (1968)

20. V. Dose, Progr. Surf. Sci. 13, 225 (1983)

Figure Caption

Fig.1. Diagrams corresponding to Raman scattering process. Diagram a, b, c, and d are second order processes whereas diagram e is a first order process. Electrons and holes are described by solid lines and photons by dashed lines.

Fig.2. a). Wave functions as a function of distance. Here ϕ is an eigen function for aluminium. Re U and Im U are the real and imaginary parts of the perturbed wave functions for w=0.1 a.u. b). same as Fig.2(a) except that RE W and Im W are compared with ϕ.

Fig. 3. Perturbed function U(z) at higher frequencies corresponding to transitions to states above the vacuum level $w_1 = 0.5$.

Fig. 4. Differential yield of Eq. (4.13) divided by $(\sin\theta_1 \sin\theta_2)^2$ as a function of scattered photon frequency, w_2, for Al, Ag, and Au. Both abscissa and ordinates are in atomic units.

Fig.5. Ratio of matrix elements squared $|N|^2/|N|^2_{step}$ for the realistic potential and the abrupt step potential. Here $V_0 = 0.3$, $\epsilon = -0.2$, $w_1 = 0.1$, and $w_2 = 0.075$ a.u. The abscissa is the slope parameter, a, of Eq.(4.1) expressed in Bohr radii.

Fig.6. Same as Fig. 5 but for a constant matrix element N=0.5.

Fig.7. Theoretical density of states function as computed by Snow (Ref. 19) in the vicinity of the Fermi level.

Fig.8. Differential yield based on theorical density of states as a function of the Stokes shift in photon energy, $w_1 - w_2$

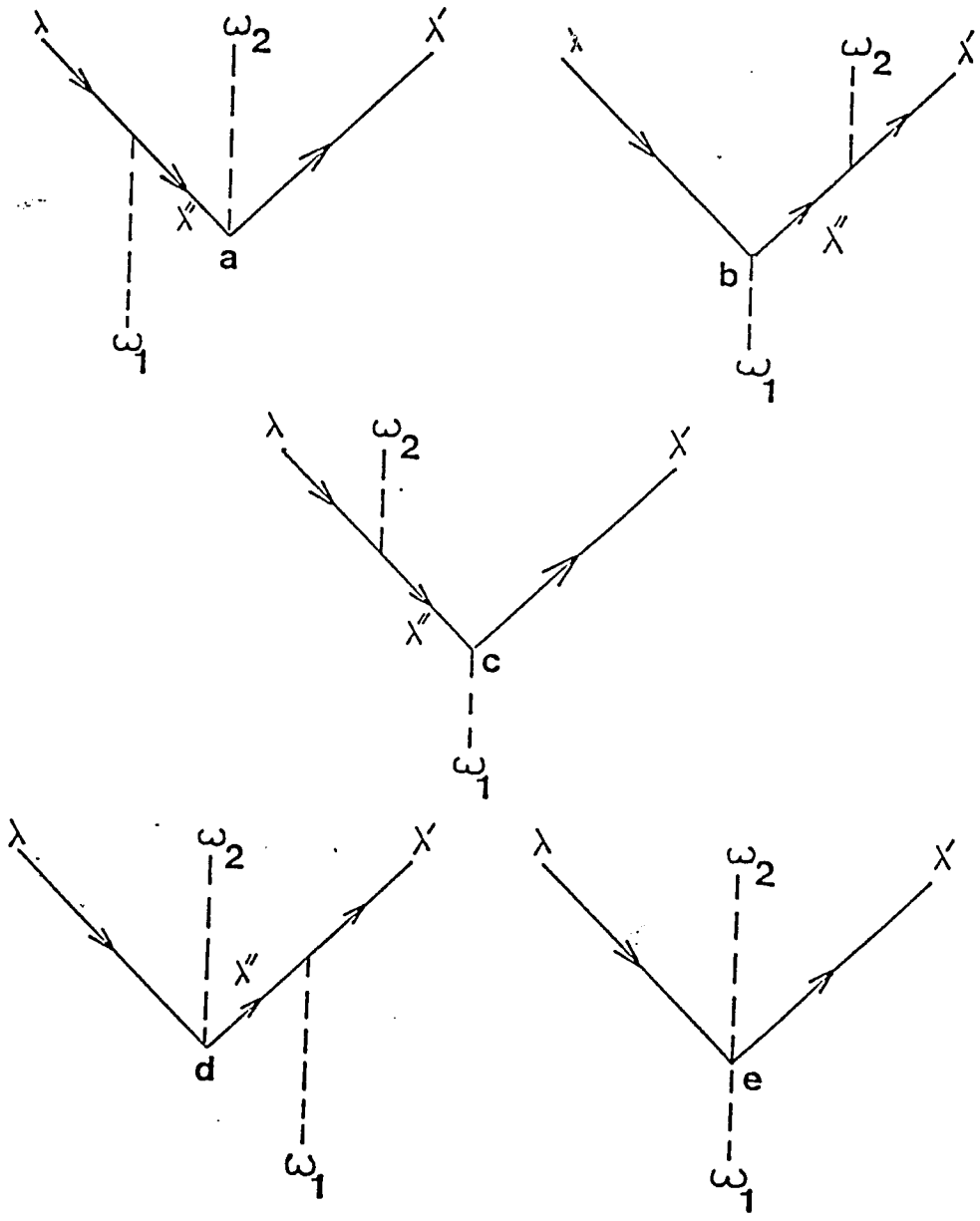

Fig. 1

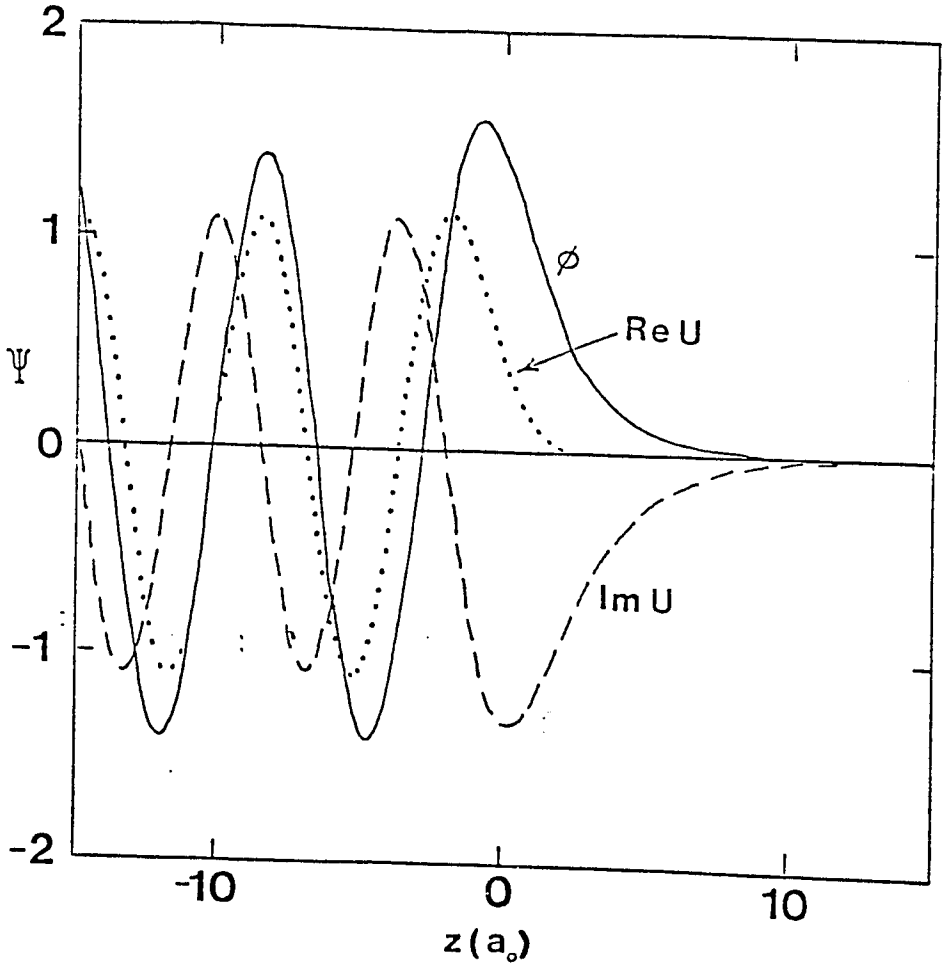

Fig. 2a

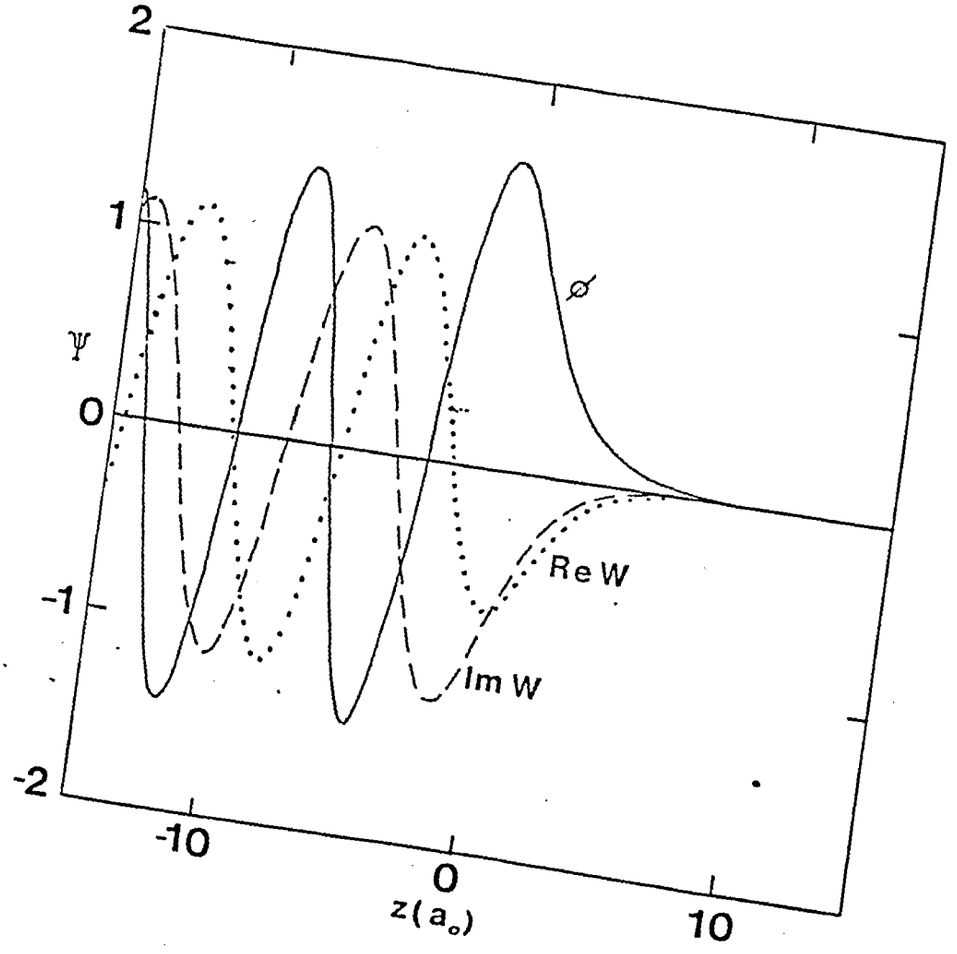

Fig. 2b

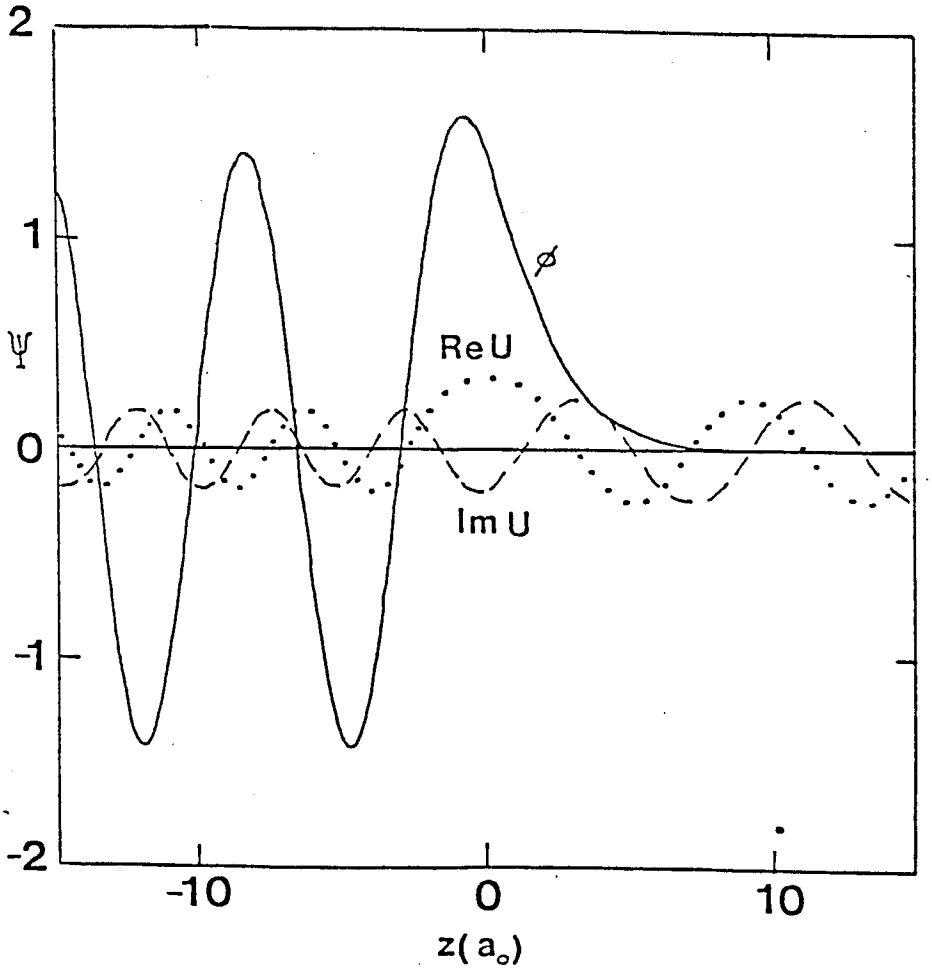

Fig. 3

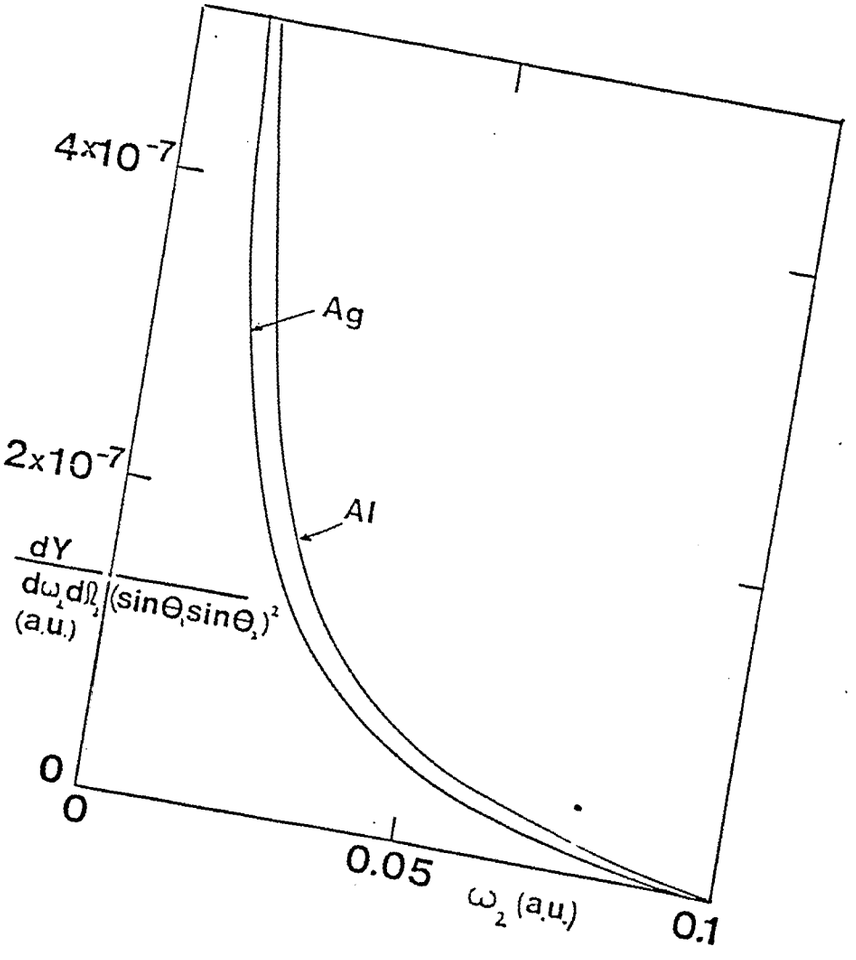

Fig. 4

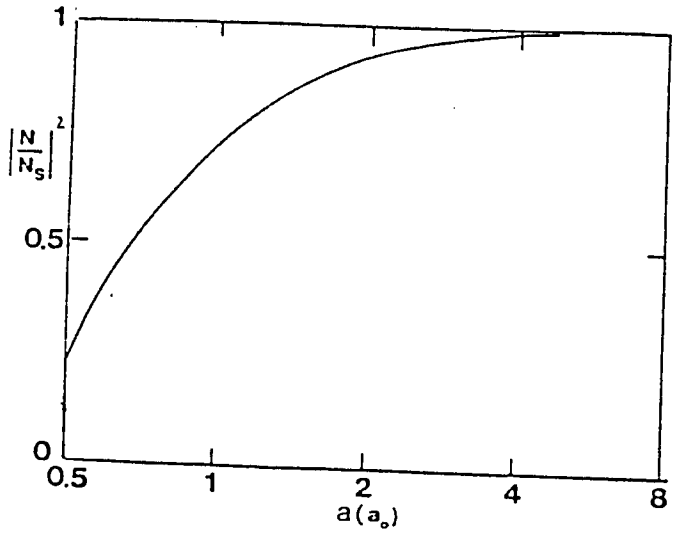

Fig. 5

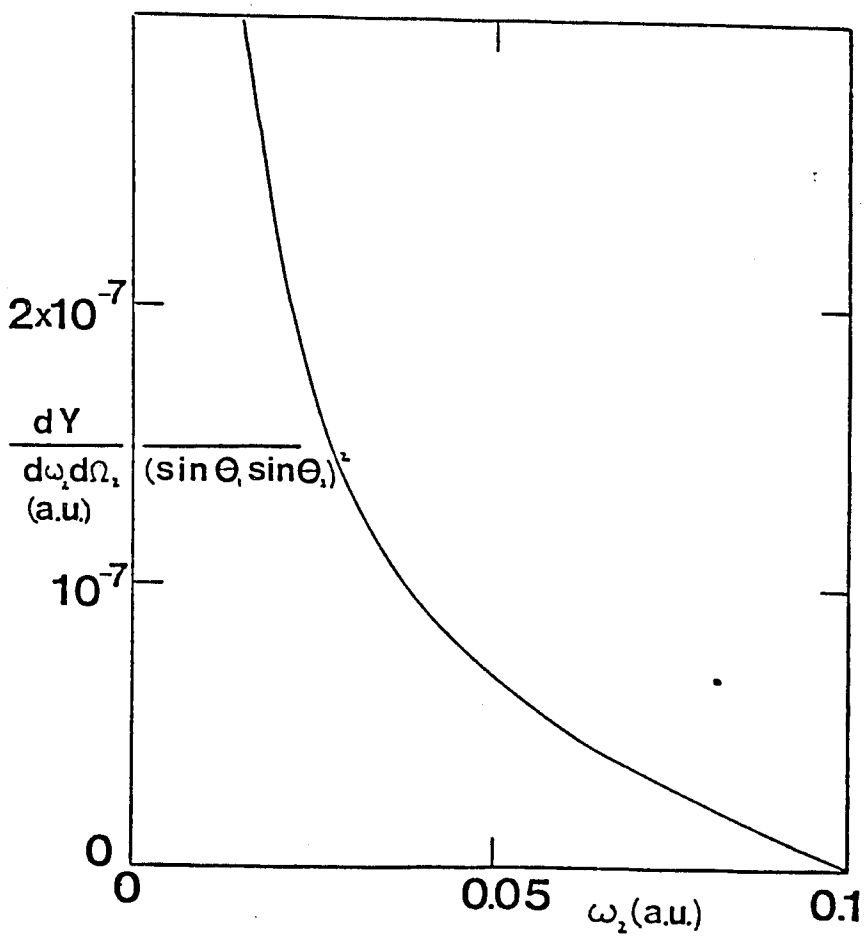

Fig. 6

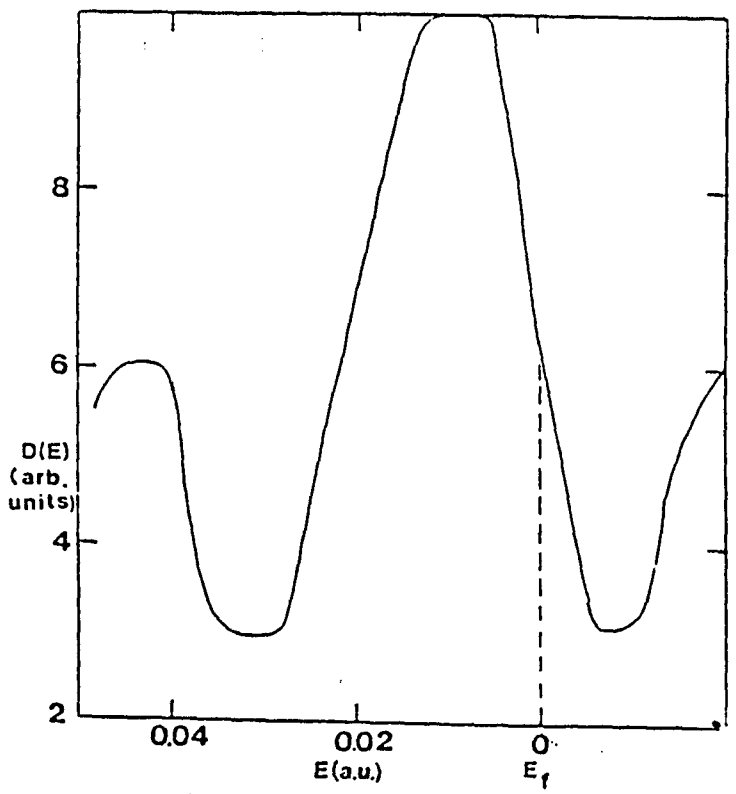

Fig. 7

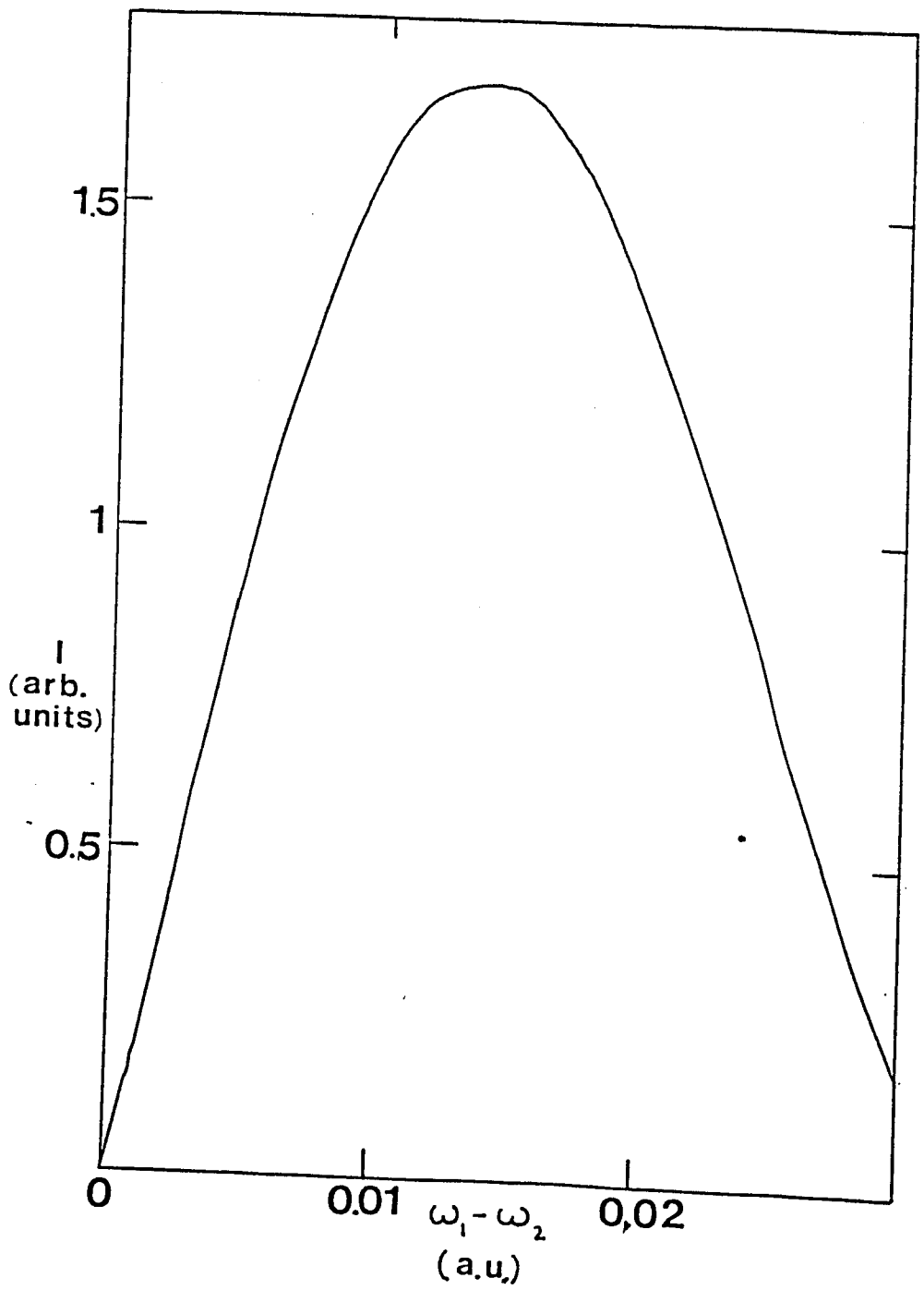

Fig. 8

2. Electronic Raman Scattering From Spherical Particles

1. Introduction

Light scattering from the surface of a solid or from a small solid state particle has been a subject of considerable interest in recent years. Some of this interest has centered on the study of surface enhanced Raman scattering (*SERS*)[1]. The Raman spectrum is that of molecule, adsorbed on the surface of the solid , and has been observed for adsorbates both on rough surfaces and on solid state particles. Associated with this spectrum is a background continuum spectrum[2–5], which appears to be characteristic of the solid itself[6–9].

In the first part of this thesis and in a recent paper[10] we studied a flat metallic surface subjected to electromagnetic radiation and found that continuum electromagnetic radiation is emitted. The origin of this radiation may be regarded as a kind of Raman process involving the solid state electrons. An electron from below the Fermi surface is excited by the incident photon and raised to a virtual level. As the electron falls back to some unoccupied state above the Fermi level, an outgoing photon is emitted. The surface potential provides the necessary momentum transfer to allow this transition to occur. An attractive feature of doing a purely electromagnetic experiment of course, is that results may be obtained to optical spectroscopic accuracy. Thus such an experiment has an advantage over photoemission or inverse photoemission.

Small solid state particles and atomic clusters have been studied intensively in recent years. Significant information concerning these clusters can be obtained from a variety of physical measurements. Light scattering has been employed[12] primarily in such studies. For example by studying the low frequency Raman Scattering associated with small particles on surfaces or in colloids, it is possible to get interesting information concerning their size and shape[13] . Recently these low frequency vibrations have also been seen from microcrystallites in glass[14]. Either of these systems may be used to study the electronic Raman scattering to be discussed here, although isolated levitated particles provide the cleanest system.

In addition it has been noted that there are anomalies associated with small particles. Schmidt-Ott et.al[15] have measured the photoelectric yield from small metal particles and found it to be nearly two orders of magnitude larger than would be expected on the basis of extrapolations from planar surface measurements. This problem has received some theoretical consideration recently[16]. In order to clarify the electronic properties of small particles it is desirable to have as many experimental probes available as possible .

A cluster or small particle may be regarded as a giant molecule. As such, it is expected to have a rich spectrum of both vibrational and electronic excitations. The primary focus of this section is on the latter. It is possible, using short pulses of exciting light, to study electronic excitations without the need for considering vibrational excitations. We shall discuss this more later. Electronic Raman scattering can be used to study the transition from a giant molecule to a bulk solid as the size of the particle is increased.

The existence of 'electronic Raman scattering' could be of considerable importance in interpreting astronomical data. It is known that various regions of the universe are permeated with dust particles. If it is indeed possible to lower the frequency of a Raman scattered photon, it is possible that this effect could contribute to the 'apparent red shift' of various galactic and intergalactic objects. Effects of a similar but unrelated nature have been discussed in the literature lately[17].

Furthermore, a distribution of particle sizes would tend to resonate with certain incident frequencies and make them more efficient Raman scatterers. This could also be of some relevance to the identification of atomic elements and their abundances in distant stars.

Additional motivation for this study is that electronic Raman scattering could be used to characterize the shape and size of small particles, including those etched onto microcircuit wafers. There is also the possibility of having such particles serve as nonlinear optical elements useful for down-converting light.

In our theory we calculate not only the spectrum (which is rather trivial) but the excitation strength of each line (which requires more detailed study). Our theory makes use of the electron in a spherical potential well to determine the energy level spectrum and the associated excitation strength.

In the next section we describe the model and develop the theory. This is followed by some detailed calculation and a discussion of the results. In order to keep this section self contained some of the arguments presented in the previous chapter are duplicated here.

2. Theory

The physical process we are considering is one in which an incident photon characterized by a frequency w_1 and polarization ϵ_1 virtually excites an electron from an occupied state below the Fermi level to a state above the Fermi level . The excited electron then relaxes to some empty state above Fermi level emitting a secondary photon characterized by frequency w_2 and polarization ϵ_2. Our goal is to calculate the yield for this Raman process. The electrons in the solid are described by the Sommerfeld model in which they are bounded by a spherically symmetric surface potential. The electromagnetic field corresponding to the photons at frequencies w_1 and w_2 are described by the vector potentials $\vec{A}_1$ and $\vec{A}_2$. We are working in the long wave length limit, so that retardation effects are neglected and $\vec{A}_1$ and $\vec{A}_2$ can be taken as spatially homogeneous. We also neglect the 'eletron-electron' interaction. Atomic units are used, so that m=e= $\hbar$ =1. The one electron Schrodinger equation is given by

$$\left\{ \tfrac{1}{2}[\vec{P} + \frac{1}{c}(\vec{A}_1 + \vec{A}_2)]^2 + V(\vec{r}) - i\frac{\partial}{\partial t} \right\} \psi(\vec{r}, t) = 0 \tag{2.1}$$

where

$$V(\vec{r}) = \begin{cases} -V_0 & \text{if } r < a \\ 0 & \text{if } r > a \end{cases} \tag{2.2}$$

Here a is the radius of the sphere and V_o is the well depth.

Making a gauge transformation of the type[10]

$$\psi(\vec{r}, t) = e^{i[(\alpha_1 + \alpha_2).\vec{r} + \beta]} \chi(\vec{r}, t) \tag{2.3}$$

where

$$\alpha_j = -\frac{1}{c}\int_0^t A_j(t')dt' \tag{2.4}$$

$$\beta = -\frac{1}{2c^2}\int_0^t [A_1(t')+A_2(t')]^2 dt' \tag{2.5}$$

and making use of the commutation relation $[\vec{p}_k, \vec{r}_l] = -i\,\delta_{kl}$, Eq. (2.1) can be rewritten as

$$\left[\frac{\vec{p}^2}{2}+V(\vec{r}-\alpha_1-\alpha_2) - i\frac{\partial}{\partial t}\right]\chi(\vec{r},t) = 0 \tag{2.6}$$

Thus in this gauge the electrons respond to a time-dependent potential which oscillates at the frequency of both the incident and the out-going photons.

In discussing Raman scattering we are only interested in terms bilinear in $\vec{A}_1$ and $\vec{A}_2$, so we will make a perturbation expansion of V. Thus

$$V(\vec{r}-\alpha_1-\alpha_2) \approx V(r)-(\alpha_1+\alpha_2).\nabla V + \tfrac{1}{2}(\alpha_1\alpha_2+\alpha_2\alpha_1):\nabla\nabla V \tag{2.7}$$

.The Hamiltonian may be written as the sum of three terms

$$H = H_0+H_1+H_2 \tag{2.8}$$

where H_0 is the unperturbed Hamiltonian describing the quiescent solid

$$H_0 = \frac{\vec{p}^2}{2}+V(\vec{r}) \tag{2.9}$$

H_1 is the part of the Hamiltonian linear in the electromagnetic field

$$H_1 = -(\alpha_1+\alpha_2).\nabla V \tag{2.10}$$

and H_2 is bilinear in the fields.

$$H_2 = \tfrac{1}{2}(\alpha_1\alpha_2+\alpha_2\alpha_1):\nabla\nabla V = \alpha_1\alpha_2:\nabla\nabla V \qquad (2.11)$$

In our calculation to lowest order in perturbation theory we consider the second order perturbation produced by H_1 and the first order perturbation by H_2. If we quantize the electromagnetic field we may write α_1 and α_2 in terms of the creation and annihilation operators for the photons. Since we are only interested in the process in which photon w_1 is absorbed and photon w_2 is emitted we have

$$\alpha_1 = -\hat{\epsilon}^1 a_1 (2\frac{\pi}{\Omega w_1^3})^{\frac{1}{2}} \qquad (2.12a)$$

$$\alpha_2 = -\hat{\epsilon}^2 a_2^+ (2\frac{\pi}{\Omega w_2^3})^{\frac{1}{2}} \qquad (2.12b)$$

where Ω is the quantization volume of all space. The second quantized Hamiltonian for the system may now be written in terms of the matrix elements involving the eigenstates of the unperturbed Hamiltonian

$$(\epsilon_\lambda - H_0)\,|\lambda> = 0 \qquad (2.13)$$

Thus

$$H = w_1(a_1^+ a_1+\tfrac{1}{2})+w_2(a_2^+ a_2+\tfrac{1}{2})-(2\frac{\pi}{\Omega w_1^3})^{\frac{1}{2}}\sum_{\lambda,\lambda',\sigma} <\lambda'|\hat{\epsilon}^1.\nabla V\,|\lambda> \times$$

$$a_1 b_{\lambda'\sigma}^+ b_{\lambda\sigma} - (\frac{2\pi}{\Omega w_2^3})^{\frac{1}{2}}\sum_{\lambda\lambda'\sigma} <\lambda'|\hat{\epsilon}^2.\nabla V\,|\lambda> a_2^+ b_{\lambda'\sigma}^+ b_{\lambda\sigma} -$$

$$\frac{2\pi}{\Omega}(w_1 w_2)^{-\frac{3}{2}}\sum_{\lambda\lambda'\sigma} <\lambda'|\hat{\epsilon}^1.\nabla\hat{\epsilon}^2.\nabla V\,|\lambda> a_2^+ a_1 b_{\lambda'\sigma}^+ b_{\lambda\sigma} \qquad (2.14)$$

where σ is the spin index, a_μ and $b_{\lambda\sigma}$ are the destruction operators for photons and electrons, a_μ^+ and and $b_{\lambda\sigma}^+$ are the corresponding creation operators.

The physical processes corresponding to Raman Scattering are shown in Fig. (1) by the 5 diagrams. In each process a photon of frequency w_1 is absorbed and a photon of frequency w_2 is emitted. A hole is produced in state $|\lambda>$ and an electron is excited to state $|\lambda'>$. In diagrams (a) and (c) the intermediate state involves a hole whereas in diagram (b) and (d) it involves an electron. In (b) and (c) the absorption occurs prior to emission whereas the reverse is true for diagrams (a) and (d). Diagram (e) is a process in which absorption and emission occurs simultaneously. The explicit expression for the matrix element corresponding to these five diagrams has been calculated in our previous paper [10]. Their sum is given by

$$M = 2\frac{\pi}{(w_1 w_2)^{3/2}} <\lambda'| [\hat{\epsilon}^2.\nabla V G(w_1+\epsilon_\lambda)\hat{\epsilon}^1.\nabla V + \hat{\epsilon}^1.\nabla V G(\epsilon_\lambda - w_2)\hat{\epsilon}^2.\nabla V + \hat{\epsilon}^1.\nabla\hat{\epsilon}^2.\nabla V]|\lambda> \quad (2.15)$$

where we have introduced the Greens function $G(\epsilon)$ defined by

$$G(\epsilon) = \sum_{\lambda'} |\lambda'><\lambda'| \frac{1}{\epsilon - H_0} \quad (2.16)$$

The boundary condition corresponding to this function is chosen to result in outgoing states.

We are interested in obtaining the yield for producing outgoing photons that reach the detector per incident photon. We calculate the scattering rate by using Fermi's Golden Rule and dividing by the incident flux of photons. Thus summing over the initial and the final states of the electron and final states of the photon , the cross sectional yield is given by

$$Y = \frac{2\pi}{c} \sum_{k_2,\lambda,\lambda',\sigma} f_{\lambda^-} f_{\lambda^+} |M|^2 \delta(w_1 - w_2 + \epsilon_{nl} - \epsilon_{n'l'}) \quad (2.17)$$

Here ϵ_{nl} and $\epsilon_{n'l'}$ are the initial and final state energy of the electron and $\vec{k}_2$ is the direction of final photon wave vector. The summation over final states is given by the integral

$$\sum_{k_2} = \int w_2^2 dw_2 \frac{d\Omega_2}{(2\pi c)^2} \tag{2.18}$$

The differential yield for producing a photon in a frequency range dw_2 around w_2 and a solid angle range $d\Omega_2$ is given by

$$\frac{dY}{dw_2 d\Omega_2} = \frac{w_2^2}{4\pi^2 c^4} \sum_{\lambda,\lambda',\sigma} f_\lambda^- f_{\lambda'}^+ |M|^2 \delta(w_1 - w_2 + \epsilon_{nl} - \epsilon_{n'l'}) \tag{2.19}$$

where σ is the spin index. f_λ^- is the Fermi factor for an occupied electron state $|\lambda>$ while $f_{\lambda'}^+$ is the Fermi factor for the unoccupied state $|\lambda'>$. Note that $f_\lambda^- + f_{\lambda'}^+ = 1$. In our work we are primarily concerned with situations in which thermal effects are not important. So we have used the relation

$$f_\lambda^- = \Theta(\epsilon_f - \epsilon_\lambda) \tag{2.20}$$

Θ being the unit step function, and $-\epsilon_f$ the work function. For convenience vacuum level is taken at $\epsilon = 0$. Conservation of energy for the overall process demands $w_1 + \epsilon_\lambda = w_2 + \epsilon_{\lambda'}$

Spherical Potential

With the potential given by equation (2.2) the eigenfunctions are given by

$$<\vec{r}|\lambda> = \phi_{nl}(r) Y_{lm}(\hat{r}) \tag{2.21}$$

$$<\lambda'|\vec{r}'> = \phi_{n'l'}(r') Y_{lm}^*(\hat{r}') \tag{2.22}$$

where $\lambda = (n, l, m)$. Inserting the complete set of states in the expression for the matrix element in equation. (2.15) we get

$$M = \frac{2\pi}{(w_1 w_2)^{3/2}} \int d\vec{r} \int d\vec{r}\,' \langle \lambda' | [\hat{\epsilon}^2.\nabla V \; | \vec{r}\,' \rangle \langle \vec{r}\,' | G(w_1+\epsilon_\lambda) | \vec{r} \rangle \langle \vec{r} \; | \hat{\epsilon}^1.\nabla V +$$

$$\hat{\epsilon}^1.\nabla V \; | \vec{r}\,' \rangle \langle \vec{r}\,' | G(\epsilon_\lambda - w_2) | \vec{r} \rangle \langle \vec{r} \; | \hat{\epsilon}^2.\nabla V +$$

$$| \vec{r}\,' \rangle \langle \vec{r}\,' | \vec{r} \rangle \langle \vec{r} \; | \hat{\epsilon}^1.\nabla \hat{\epsilon}^2.\nabla V \;] | \lambda \rangle \qquad (2.23)$$

The matrix element of the Greens function $\langle \vec{r}\,' | G(w_1+\epsilon_\lambda) | \vec{r} \rangle$ is a scalar function of the variables $\vec{r}$, $\vec{r}\,'$ and $\hat{r}.\hat{r}\,'$, so we can express it in terms of spherical harmonics as

$$\langle \vec{r}\,' | G(w_1+\epsilon_\lambda) | \vec{r} \rangle = \sum_{L,M} G_L(r, r'; \epsilon_\lambda + w_1) Y^*_{LM}(\hat{r}\,') Y_{LM}(\hat{r}) \qquad (2.24)$$

With equations (2.21) and (2.22) we obtain

$$\langle \lambda' | \hat{\epsilon}^2.\nabla V \; | \vec{r}\,' \rangle = \hat{\epsilon}^2.\hat{r}\,' \frac{\partial V(r')}{\partial r'} \phi_{n'l'}(r) Y^*_{l'm'}(\hat{r}\,') \qquad (2.25)$$

$$\langle \vec{r} \; | \hat{\epsilon}^1.\nabla V \; | \lambda \rangle = \hat{\epsilon}^1.\hat{r} \frac{\partial V(r)}{\partial r} \phi_{nl}(r) Y_{lm}(\hat{r}) \qquad (2.26)$$

where we have introduced the spherical vectors

$$\hat{\epsilon}^2.\hat{r}\,' = c \sum_{\mu'} \epsilon^2_{\mu'} Y^*_{1\mu'}(\hat{r}\,') \qquad (2.27)$$

$$\hat{\epsilon}^1.\hat{r} = c \sum_{\mu} \epsilon_\mu{}^{1^*} Y_{1\mu}(\hat{r}) \qquad (2.28)$$

with $c = \sqrt{\frac{4\pi}{3}}$. From Eq. (2.23) M can be written as sum of three terms, given by

$$M = \frac{2\pi}{(w_1 w_2)^{3/2}} [M_a + M_b + M_c] \qquad (2.29)$$

Inserting all those values defined above in Eqs. (2.24) - (2.28) and using the 3j symbols[11] the three matrix element may be expressed in the form

$$M_a = \frac{3}{4\pi}\sqrt{(2l+1)(2l'+1)}\sum_{L,M,\mu,\mu'} Q_n^{(L)}{}_{l',nl}(\epsilon_{nl}+w_1)(2L+1)c^2\epsilon_\mu^{2}\epsilon_\mu^{1*}$$

$$\begin{pmatrix}1 & l' & L\\ \mu' & m' & M\end{pmatrix}\begin{pmatrix}1 & l & L\\ \mu & m & M\end{pmatrix}\begin{pmatrix}1 & l' & L\\ 0 & 0 & 0\end{pmatrix}\begin{pmatrix}1 & l & L\\ 0 & 0 & 0\end{pmatrix} \qquad (2.30a)$$

$$M_b = \frac{3}{4\pi}\sqrt{(2l+1)(2l'+1)}\sum_{L,M,\mu,\mu'} Q_n^{(L)}{}_{l',nl}(\epsilon_{nl}-w_2)(2L+1)c^2\epsilon_\mu^{1}\epsilon_\mu^{2*}$$

$$\begin{pmatrix}1 & l' & L\\ \mu' & m' & M\end{pmatrix}\begin{pmatrix}1 & l & L\\ \mu & m & M\end{pmatrix}\begin{pmatrix}1 & l' & L\\ 0 & 0 & 0\end{pmatrix}\begin{pmatrix}1 & l & L\\ 0 & 0 & 0\end{pmatrix} \qquad (2.30b)$$

$$M_c = \frac{3}{4\pi}\sqrt{(2l+1)(2l'+1)}\sum_{L,M,\mu,\mu'} \tilde{Q}_n^{(L)}{}_{l',nl}(2L+1)c^2\epsilon_\mu^{2}\epsilon_\mu^{1*}$$

$$\begin{pmatrix}1 & l' & L\\ \mu' & m' & M\end{pmatrix}\begin{pmatrix}1 & l & L\\ \mu & m & M\end{pmatrix}\begin{pmatrix}1 & l' & L\\ 0 & 0 & 0\end{pmatrix}\begin{pmatrix}1 & l & L\\ 0 & 0 & 0\end{pmatrix} \qquad (2.30c)$$

Where Q and $\tilde{Q}$ are given by

$$Q_n^{L}{}_{l',nl}(\epsilon_{nl}+w_1) = \int dr r^2 \int dr' r'^2 \phi_{n'l'}(r')V'(r')G_L(r,r';\epsilon_{nl}+w_1)V'(r)\phi_{nl}(r) \qquad (2.31a)$$

$$Q_n^{L}{}_{l',nl}(\epsilon_{nl}-w_2) = \int dr r^2 \int dr' r'^2 \phi_{n'l'}(r')V'(r')G_L(r,r';\epsilon_{nl}-w_2)V'(r)\phi_{nl}(r) \qquad (2.31b)$$

$$\tilde{Q}_n^{L}{}_{l',nl} = \int dr r^2 \int dr' r'^2 \phi_{n'l'}(r')\frac{1}{r^2}\delta(r-r')V''(r)\phi_{nl}(r) \qquad (2.31c)$$

With the above expressions equation (2.29) becomes

$$M = \frac{2\pi}{(w_1 w_2)^{3/2}}\sqrt{(2l+1)(2l'+1)}\sum_{LM\mu\mu'}(2L+1)[A^L\epsilon_\mu^{2}\epsilon_\mu^{1*}+B^L\epsilon_\mu^{2*}\epsilon_\mu^{1}]\times$$

$$\begin{pmatrix} 1 & l' & L \\ 0 & 0 & 0 \end{pmatrix}\begin{pmatrix} 1 & l & L \\ 0 & 0 & 0 \end{pmatrix}\begin{pmatrix} 1 & l' & L \\ \mu' & m' & M \end{pmatrix}\begin{pmatrix} 1 & l & L \\ \mu & m & M \end{pmatrix} \tag{2.32}$$

where

$$A^L = Q^L_{n'l';nl}(\epsilon_{nl} + w_1) + \tilde{Q}^L_{n'l';nl} \tag{2.33a}$$

$$B_L = Q^L_{n'l';nl}(\epsilon_{nl} - w_2) \tag{2.33b}$$

After computing $|M|^2$ we wish to sum over m, m', $\hat{\epsilon}^2$ and average over $\hat{\epsilon}^1$. In this treatment we do not look specifically at polarization effects, although it is certainly possible to do this in our formalism. Let $\vec{k}_1$ be the incident photon wave vector and $\vec{k}_2$ be the outgoing photon wave vector. While summing over all these variables we use the relations

$$\sum_{\hat{\epsilon}^1} \epsilon^{1\,*}_{\mu_1} \epsilon^1_{\mu_2} = \alpha\delta_{\mu_1,\mu_2} + 4\pi\beta Y^*_{1\mu_1}(\hat{k}_1) Y_{1\mu_2}(\hat{k}_1) \tag{2.34}$$

It can be shown that $\alpha = 1$, and $\beta = -1/3$. By averaging Eq. (2.34) over all directions, we find

$$\langle \sum_{\hat{\epsilon}_2} \epsilon^{2\,*}_{\mu_2'} \epsilon_{\mu_1'}{}^2 \rangle_{\hat{k}_2} = \frac{2}{3}\delta_{\mu_1',\mu_2'} \tag{2.35}$$

$$\langle 1/2 \sum_{\hat{\epsilon}_1} \epsilon^{1\,*}_{\mu_1} \epsilon_{\mu_2}{}^1 \rangle_{\hat{k}_1} = \frac{1}{3}\delta_{\mu_1,\mu_2} \tag{2.36}$$

Combining these equations we get

$$\sum_{m,m'} \langle \sum_{\hat{\epsilon}_2} |M|^2 \rangle_{\hat{k}_1 \hat{k}_2 \hat{\epsilon}_1} = \frac{(2\pi)^2}{(w_1 w_2)^3} \frac{2}{9}(2l+1)(2l'+1) \sum_{LL'} (2L+1)(2L'+1)$$

$$[(A^L A^{L'} + B^L B^{L'})\delta_{\mu_1,\mu_2}\delta_{\mu_1',\mu_2'} + (-)^{\mu_1+\mu_2}(A^L B^{L'} + A^{L'} B^L)\delta_{\mu_1',-\mu_2'}\delta_{\mu_2',-\mu_1}]$$

$$\begin{pmatrix} 1 & l' & L \\ 0 & 0 & 0 \end{pmatrix}\begin{pmatrix} 1 & l & L \\ 0 & 0 & 0 \end{pmatrix}\begin{pmatrix} 1 & l' & L' \\ 0 & 0 & 0 \end{pmatrix}\begin{pmatrix} 1 & l & L' \\ 0 & 0 & 0 \end{pmatrix} \times$$

$$\sum_{M\,\mu_1\mu'_1M'\mu_2\mu'_2mm'} \begin{pmatrix} 1 & l' & L \\ \mu'_1 & m' & M \end{pmatrix} \begin{pmatrix} 1 & l & L \\ \mu_1 & m & M \end{pmatrix} \begin{pmatrix} 1 & l' & L' \\ \mu'_2 & m' & M' \end{pmatrix} \begin{pmatrix} 1 & l & L' \\ \mu_2 & m & M' \end{pmatrix}$$

$$= \frac{2}{9}\frac{(2\pi)^2}{(w_1 w_2)^3}(2l+1)(2l'+1)\sum_{LL'}(2L+1)(2L'+1)$$

$$[(A^L A^{L'}+B^L B^{L'})\frac{\delta_{LL'}}{(2L+1)}+$$

$$(A^L B^{L'}+A^{L'}B^L)S_2(l,l';L,L')] \qquad (2.37)$$

where

$$S_2(l,l';LL') = \sum_{mm'MM'\mu_1\mu_2}(-)^{\mu_1+\mu_2}\begin{pmatrix} 1 & l' & L \\ -\mu_2 & m' & M \end{pmatrix}\begin{pmatrix} 1 & l & L \\ \mu_1 & m & M \end{pmatrix}\times$$

$$\begin{pmatrix} 1 & l' & L' \\ -\mu_1 & m' & M' \end{pmatrix}\begin{pmatrix} 1 & l & L' \\ \mu_2 & m & M' \end{pmatrix}$$

Utilizing the dipole selection rules for the excitation and de-excitation processes, one finds only the following allowed transitions.

a.) $l'=(l+2), \quad L=(l+1), \quad L'=(l+1)$

b.) $l'=(l-2), \quad L=(l-1), \quad L'=(l-1)$

c.) $l'=l, \quad L=(l+1), \quad L'=(l+1)$

d.) $l'=l, \quad L=(l+1), \quad L'=(l-1)$

e.) $l'=l, \quad L=(l-1), \quad L'=(l+1)$

f.) $l'=l, \quad L=(l-1), \quad L'=(l-1)$

It can be shown that

$$S_2 = \begin{cases} \frac{2}{3(2l+3)} & \text{if } l'=l+2, \quad L=L'=l+1 \\ \frac{2}{3(2l-1)} & l'=l-2, \quad L=L'=l-1 \\ 0 & \textit{otherwise} \end{cases}$$

Inserting these values, the average of the differential yield from Eq.(2.19) can be written as

$$\sum_{\hat{\epsilon}_2} \left\langle \frac{dY}{dw_2} \right\rangle_{\hat{\epsilon}_1 \hat{k}_1} = \frac{8\pi}{9 w_1^3 w_2 c^4} \sum_{nl, n'l'} T f_{nl}^- f_{n'l'}^+ \cdot \delta(w_1 - w_2 + \epsilon_{nl} - \epsilon_{n'l'}) \quad (2.38)$$

where

$$T = \begin{cases} \frac{(l+1)^2}{(2l+3)}[A^{(l+1)^2} + B^{(l+1)^2}] + \frac{l^2}{(2l+1)}[A^{(l-1)^2} + B^{(l-1)^2}] & \text{if } l' = l \\ \frac{l(l-1)}{(2l-1)}[A^{(l-1)^2} + B^{(l-1)^2} + \frac{4}{3} A^{(l-1)} B^{(l-1)}] & \text{if } l' = l-2 \\ \frac{(l+1)(2+l)}{(2l+3)}[A^{(l+1)^2} + B^{(l+1)^2} + \frac{4}{3} A^{(l+1)} B^{(l+1)}] & \text{if } l' = l+2 \end{cases} \quad (2.39)$$

Thus the yield spectrum is nothing but a δ function spectrum multiplied by the weight factor T. Evaluation of T involves the evaluation of A^L and B^L given by the Eq. (2.33). With the potential given in Eq. (2.2) we have

$V'(r) = V_0 \delta(r - a)$ and Eq. (2.31a) becomes

$$Q^L_{nl,n'l'}(\epsilon_{nl} + w_1) = V_0^2 a^4 \phi_{n'l'}(a) G_L(a, a; \epsilon_{nl} + w_1) \phi_{nl}(a) \quad (2.40)$$

where $G(r, r')$ satisfies the wave equation

$$[w_1 + \epsilon_{nl} - \frac{p^2}{2} - V(r)] G(\vec{r}, \vec{r}') = \delta(\vec{r} - \vec{r}') \quad (2.41)$$

$G(\vec{r}, \vec{r}')$ can be expressed as sum of spherical harmonics

$$G(\vec{r}, \vec{r}') = \sum_{L,M} G_L(r, r'; \epsilon_{nl} + w_1) Y^*_{LM}(\hat{r}') Y_{LM}(\hat{r}) \quad (2.42)$$

Introducing a variable $\psi_L(r)$ defined by

$$\psi_L(r) = \int dr' G_L(r, r'; \epsilon_{nl} + w_1) \delta(r' - a) = G_L(r, a; \epsilon_{nl} + w_1) \quad (2.43)$$

we find

$$Q^{L}_{n'l',nl} = V_0{}^2 a^4 \phi_{n'l'}(a)\psi_L(a)\phi_{nl}(a) \tag{2.44}$$

The function $\psi_L(r)$ satisfies the wave equation

$$\left[w_1+\epsilon_{nl} - \frac{p^2}{2} - V(r) - \frac{L(L+1)}{2r^2}\right]\psi_L(r) = \frac{1}{a^2}\delta(r-a) \tag{2.45}$$

This equation can be solved analytically and the value of $\psi(r)$ at r=a is given by

$$\psi_L(a) = \begin{cases} \dfrac{2}{a^2}\dfrac{j_L(ka)h_L^1(qa)}{kj'_L(ka)h_L^1(qa) - qh'^1_L(qa)j_L(ka)} & \text{if } (w_1+\epsilon_{nl}+V)>0 \text{ and } (w_1+\epsilon_{nl})>0 \\ \dfrac{2}{a^2}\dfrac{j_L(ka)k_L(sa)}{kj'_L(ka)k_L(sa) - sk'_L(sa)j_L(ka)} & \text{if } (w_1+\epsilon_{nl}+V)>0 \text{ and } (w_1+\epsilon_{nl})<0 \\ \dfrac{2}{a^2}\dfrac{i_L(k_1a)k_L(sa)}{k_1 i'_L(k_1a)k_L(sa) - sk'_L(sa)i_L(k_1a)} & \text{if } (w_1+\epsilon_{nl}+V)<0 \text{ and } (w_1+\epsilon_{nl})<0 \end{cases} \tag{2.46}$$

where

$$k = \sqrt{2(w_1+\epsilon_{nl}+V)} \qquad \text{if } (w_1+\epsilon_{nl}+V)>0$$

$$k_1 = \sqrt{-2(w_1+\epsilon_{nl}+V)} \qquad \text{if } (w_1+\epsilon_{nl}+v)<0$$

$$q = \sqrt{2(w_1+\epsilon_{nl})} \qquad \text{if } (w_1+\epsilon_{nl})>0$$

$$s = \sqrt{-2(w_1+\epsilon_{nl})} \qquad \text{if } (w_1+\epsilon_{nl})<0$$

For small enough w_1 we can restrict the intermediate state ψ_L so as to never go to first condition of equation (2.46). Thus we never permit the intermediate state to rise above the vacuum level. Q and $\tilde{Q}$ expressed in terms of ψ_L are given by

$$Q^{L}_{n'l';nl}(\epsilon_{nl}+w_1) = V^2 a^4 \phi_{n'l'}(a)\psi_L(a)\phi_{nl}(a) \tag{2.47}$$

$$\tilde{Q}^{L}_{n'l';nl} = -V[\phi'_{n'l'}(a)\phi_{nl}(a)+\phi_{n'l'}(a)\phi'_{nl}(a)] \tag{2.48}$$

where the eigenfunctions $\phi_{n'l'}(a)$ satisfies the Schrodinger equation

$$\left[\frac{\vec{p}^2}{2}+V(r)-\epsilon_{nl}\right]\phi_{nl}(r)Y_{lm}(\hat{r}) = 0 \tag{2.49}$$

The solution of this equation is given by

$$\phi_{nl}(r) = \begin{cases} D j_l(pr)k_l(\lambda a) & \text{if } r < a \\ D k_l(\lambda r) j_l(pa) & \text{if } r > a \end{cases} \tag{2.50}$$

$$\text{where} \quad p = \sqrt{2(\epsilon_{nl}+V)}$$

$$\text{and} \quad \lambda = \sqrt{-2\epsilon_{nl}}$$

The normalization constant D is determined from the continuity of ϕ at r=a and is given by

$$D = \frac{1}{\sqrt{\int_0^a j_l^2(pr)k_l^2(\lambda a)r^2dr + \int_a^\infty k_l^2(\lambda r) j_l^2(pa)r^2dr}} \tag{2.51}$$

D can be determined analytically, and is given by

$$D = \left[\frac{\pi}{8a^2}e^{-2\lambda a}\frac{1}{\lambda^2 p^2}\left(a-\frac{\sin 2pa}{2p}\right)+\frac{1}{p^2\lambda^3}\sin^2 pa\right]^{-1/2} \tag{2.52}$$

$$\text{if } l = 0$$

and

$$D = \frac{a^3}{2}[k_{l-1}(\lambda a)k_{l+1}(\lambda a) j_l^2(pa) - j_{l-1}(pa) j_{l+1}(pa)k_l^2(\lambda a)]^{-1/2}$$

$$\text{if } l \neq 0$$

The eigenvalues are given by the condition

$$pa\, j'_l(pa)k_l(\lambda a) - \lambda a k'_l(\lambda a)\, j_l(pa) = 0 \qquad (2.52)$$

3. Results and Discussion

In the theory that we have just constructed a formalism for describing the Raman scattering from a small spherical metalic particle has been introduced. The formalism bears some similarity to atomic physics and some similarity to solid state physics. The spherical symmetry has been successfully employed, as in atomic physics, to reduce the theory to a compact form involving analytic formulas. The solid state physics appears in our use of the Sommerfeld model in describing the electronic states.

At first sight it appears that a rich spectrum of Raman Scattering frequencies would be seen and this would make it somewhat difficult to resolve individual lines. For example, consider Fig. 2. where a joint density of states for a spherical potential well is translated into a Raman spectra. The joint density of states is determined here naively by simply weighting each transition frequency by the degeneracy factor $(2l+1)(2l'+1)$ associated with that transition. The calculation was done for a potential well of diameter 29.7 angstroms, a well depth of V=8.16 eV, a work function of $|\epsilon_f|$=4.3 eV and an incident photon energy of 2.72 eV. These numbers typify common metalic situations and are suitable for silver. In order to provide a presentable spectrum the individual lines have been broadened by making them into Lorentzians with line width .01 eV . This simulates the effect of the finite resolution of a spectrometer. In the figure, the degeneracy is plotted as a function of the scaled Raman shift $(w_1 - w_2)/\epsilon_f$. We note that there is a tendency for the spectrum to increase for the larger shifts. This tendency was also noted in our previous work[10] on

Raman scattering from a planar surface. It comes about because there is a large phase space available to the outgoing photon when the (Stokes) Raman shift is increased. In our work it will be assumed that the temperature of the particle is sufficiently small, so that anti- Stokes shifts are not important.

A limitation of the above consideration is that the the weights associated with given lines are not simply the degeneracy. Important matrix element effects do enter and the primary goal of this work has been to describe and understand these effects. A Raman spectrum for the spherical particle just considered is given in Fig. 3. The abscissa is the same as in the previous case but the ordinate now includes the weighting of the given lines by the appropriate strengths derived from the matrix elements. A striking feature of the exact spectrum is that it is simpler than the joint density of states derived spectrum. The dominant lines have been labeled by letters A and B . These labels will be discussed soon. In our discussion of the Raman spectrum we have neglected the natural linewidth associated with the excited states. This puts a limitation on the theory. In our calculation the strength of the spectral line grows as one turns closer to resonance. However competing with this process is resonance fluorescence in which a real transition is made. In order to understand the reasons for this we will have to look at an energy level scheme for the particles.

In Fig. 4 we represent the energy levels as a series of points. The abscissa denotes the orbital angular momentum and the ordinate denotes the energy. Spin- orbit coupling effects are expected to be very weak and therefore unimportant. As expected, the spectrum has the characteristics of both a box potential and an atom. For a given l, the energy gap between successive states increases as the energy increases, just as in a spherical box.

On the other hand we see that the degeneracy between different orbital angular momenta is lifted due to penetration of the electron into the classically forbidden region.

We have labeled the transitions A and B on the energy level scheme and note that they correspond to our selection rules $\Delta l = \pm 2,0$. The dominant contribution to the spectrum come from those transitions in which the intermediate state (virtual) lies close to an actual energy level. It is precisely the analog of conventional resonant Raman scattering for the case of a spherical particle. When resonance occurs a large scattering occurs, while when one is off resonance, a small scattering occurs. This will be seen more clearly in Fig. 5,6, and 7, where a semilog scale is used to display the spectrum.

Since we are dealing with a resonant phenomenon we would expect the spectrum to be very sensitive to small changes in the physical parameters. This is illustrated in Fig.5 where the spectra for spheres of slightly different radii are shown. This ordinate denotes the strength of the Raman signal, the abscissa is again the scaled Raman shift. If we consider spheres of somewhat greater size difference the sensitivity becomes even more striking, as in Fig. 6.

In order to relate our calculations to experiment it is useful to convert our results into a form that will be of more utility to experimentalists. The quantity $\frac{dY}{dw}$ appearing in Eq.(2.38) represents the cross-section per unit scattered frequency expression in standard atomic units. An examination of Fig.(6) shows this number to be typically on the order of 10^{-4}, although because of resonance effects this number may be increased or decreased. We make the following estimate based on $\frac{dY}{dw} = 10^{-4}$.

Using a typical spectrometer resolution of $100cm^{-1}$ (5×10^{-4} atomic units) the cross section for Raman scattering light in to the spectromter would be $dw\frac{dY}{dw} = 5\times10^{-8}a_o^2$. Let I_1 represent the incident light intensity. So $\frac{I_1}{\hbar w_1}$ is the number of incident photons per unit area per unit time. Let n denote the number of spheres per unit volume and V denote the volume of illuminated spheres probed by the Raman spectrometer. The number of scattered photons per unit time is then

$$\dot{N} = \frac{dY}{dw}dw\frac{I_1}{\hbar w_1}nV \tag{3.1}$$

The density of spheres is typically expressed in terms of a filling factor, f, by $f = 4\pi na^3/3$, where "a" is the typical sphere radius. Taking a typical value[16] for f equal to 10^{-8}, $a=25a_o = 25\times.529\times10^{-8}$cm, $V = .1\,cm^3$, and $I = 100watt / cm^2$ for 2.7 eV incident photon gives a scattering rate of 3.3×10^5 photons per second. With a system with a solid angle acceptance of 1 steradian and a detector efficiency of 1 percent this gives about 260 counts per second. This number may be increased by increasing the laser intensity, the acceptance band width, the filling factor or any of the other parameters in the numerator of Eq.(3.1). We thus conclude that the experimental observation of the Raman scattering by spheres is feasible.

In Fig. 7 we illustrate the dependence of the spectrum on the incident light frequency. Again the sensitivity is apparent. The sensitivity is much less pronounced as the work function changes as in Fig. 8 . The reason for this is that both the energy level scheme and the matrix element are not dependent on the work-function. The work-function simply provides a parameter which makes part of the spectrum allowed or disallowed. Thus an allowed transition must always start from a state below the Fermi

level and terminate on a state above that level.

Until now we have considered only the effect of particle size on the spectrum, but not particle shape. We have not made a thorough study of this effect, but a simple exercise can give some insight into it. Let us compare the joint density of states of a sphere with that of a box potential. For simplicity we now allow the walls of the sphere and box to be impenetrable. The respective joint density of states spectrum is presented in Fig.9 and 10. We note that the spectrum for a box potential is richer, this is to be expected since the azimuthal degeneracy is lifted in the case of the box. However, we still expect the resonant Raman scattering mechanism to be operative in the case of the box. Thus the actual Raman spectrum will again appear to be much simpler .

In principle valuable information concerning the particle's shape can be extracted from either the electronic Raman scattering or the low frequency vibrational Raman scattering. At this time it is difficult to comment on the preferability of either method. The answer will depend upon the experimental ability to resolve individual spectral lines. The more lines that are seen, the more information can be obtained relating to particle shapes.

In Fig. 9 we present the spectrum for a sphere with infinitely high walls. The sphere radius and Fermi energy are taken to be the same as in Fig. 2. We note, however, that the spectra appear to be qualitatively quite different. This is due to the penetration of the electronic wave functions in to the vacuum. A more diffuse wave function can be expected to see less of the centrifugal barrier that a wave function confined to the interior of the box. This leads to a greater influence of the centrifugal barrier in the latter case and a broader distribution of energy levels, and hence

Raman frequencies. In the case of the sphere of finite well depth the spectrum is more compact as the degree of degeneracy among the orbital angular momentum state is greater.

If an experiment is done to measure the Raman spectrum for a particle, a possible complication arises due to the motion of the nuclei. This is analogous to Raman scattering in the case of a molecule where the nuclear vibrations modulate the electronic spectrum. In the molecular case this results in vibrational energy bands associated with the given electronic transitions. There the Frank-Condon factors must be introduced to give the measured spectrum. One would expect similar considerations to apply to the case of a small sphere. If the experiment were done with a CW laser the spectrum, indeed, would be quite dense.

It is possible, however, to excite the electronic spectrum by going to short optical pulses. If the scattering event is over before the molecule has had a chance to move, one would not expect the light to 'know' about the ions. The response would be due to the electrons alone. Broad band detection accomplishes the same thing. By averaging over the contribution from many vibrational transitions one is able to focus on the purely electronic contribution. In designing such an experiment the duration of a pulse must be shorter than a vibrational period, but not so short that its Fourier spectrum is broader than the Raman spectrum. We see from our analysis that the Raman spectrum does indeed tend to be sparse, so that the latter limitation is not severe, at all.

In summary we see that Raman scattering from a small solid state particle can provide valuable information concerning the size and shape of the particle. The detailed spectrum is indicative of the underlying electronic spectrum and is very sensitive to the parameters of the problem.

References

1. For a recent review see ' Surface Enhanced Raman Scattering ', edited by R. K. Chang and T. E. Furtak (Plenum, New York, 1982).

2. A. Otto, Surface Sci. 75, L392 (1982)

3. E. Burstein, Y. J. Chen, C. Y. Chen, S. Lundquist, and E. Tosatti, Solid State Commun. 29, 567(1979)

4. J. I. Gersten, R. L. Birke, and J. R. Lombardi, Phys. Rev. Lett. 43, 71 (1979)

5. J. P. Heritage and J. G. Bergman, in ' Proceedings of the second USA-USSR Light Scattering Symposium', edited by J. L. Birman, H. J. Cummins, and K. K. Rebane (Plenum, New York, 1979), p. 167

6. A. Otto, J. Timper, J. Billman, G.Kovacs, and I. Pockrand, Surf. Sci. 92, L55 (1980)

7. A. Otto, J. Timper, J. Billman, and I. Pockrand, Phys. Rev. Lett. 45,46 (1980)

8. J. Timper, J. Billman, A. Otto, and I. Pockrand, Surf. Sci. 101, 348 (1980)

9. I. Pockrand and A. Otto, Solid State Commun. 37, 109, (1981)

10. S. Das, and J. I. Gersten, J. Chem. Phys. 85 (2), 647 (1986)

11. "Angular Momentum in Quantum Mechanics" by A. R. Edmonds , Princeton University press, (1957)

12. S. X. Qian, J. B. S, R. K. Chang, Opt. Lett. (USA). 10, 10, 499-501 , J. B. S, S. X. Qian, R. K. Chang, Opt. Lett. (USA) 10, 1, 37-39, J F. Owen, R. K. Chang, Chem. Phys. Lett. 104, 5, 510-515, S. Ard and A.

B. Pluchi Appl. Opt. 21, 23, 4194-4196, S. Ard, E. K. Murphy, and G. Sageev, Appl. Opt. 24, 7, 1048-1053, L. M. Folan, S. Ard, S. D. Druger, Chem. Phys. Lett. 118, 3, 322-327

13. D. A. Weitz, T. J. Gramila, A. Z. Genack and J. I. Gersten, Phys. Rev. Lett. Vol 45, 5, 355-358,(1980), J. I. Gersten, D. A. Weitz, T. J. Gramila and A Z. Genack, Phys. Rev. B, 222, 10, 4562-4571, (1980), E. Duval, G. Mariotto, M. Montagna, O. Pilla, G. Viliani and M. Barland, Europhys. Lett. 3, 3, pp. 333-339(1987)

14. E. Duval, A. Boukenter, and B. Champagnon, Phys. Rev. Lett. Vol 56, no. 19, 2052-2055, (1986)

15. A. Schmidt-Ott, P. Schurtenberger, and H. C. Siegman, Phys. Rev. Lett. 45, 15, 1284, (1980)

16. Q. Y. Chen, and C. W. Bates, Jr. Phys. Rev. Lett. 57, 21, 2737 (1986)

17. Emil Wolf, Nature, 326, 363, (1987)

Figure Captions

FIG. 1. Diagrams corresponding to Raman scattering process. Diagrams a, b, c, and d are second order process whereas diagram e is a first order process. Electrons and holes are described by solid lines and photons by dashed lines.

FIG. 2. Degeneracy spectrum of a sphere with a finite potential. Here a=28.1 a. u., w_1=.1 a.u, ϵ_f =-.158 a.u.

FIG. 3. Transition Spectrum corresponding to the energy level diagram of fig. 4. (7,7) denotes transition from l=7, to l'=7, etc.

Fig. 4. Energy levels of the sphere. Abscissa represents the energy levels, ordinate is angular momentum. a=28.1 a.u., w_1=.1 a.u., e_f =-.158 a.u. Virtual levels in the transition are shown by the dotted lines.

FIG. 5. Transition showing three different radii very close to each other in the semi log plot. Abscissa shows transition probability, ordinate is the frequency difference normalised with respect to fermi energy.

FIG. 6. Transition showing 4 different radii, quite different from each other. Abscissa and ordinates are same as that of fg.5

FIG. 7. Spectrum with 5 different incident frequency. Abscissa and Ordinates are same as the fig. 5.

FIG. 8. Spectrum with different Fermi energies. The abscissa is the transition probability, the ordinate is the frequency difference.

FIG. 9. Spectrum of the sphere with infinite wall of radius 28.1 a. u.

FIG. 10. Spectrum of a cube of side 49.2 Angstroms with infinite wall . The abscissa is the degeneracy, and the ordinate is the frequency difference normalized with respect to Fermi energy.

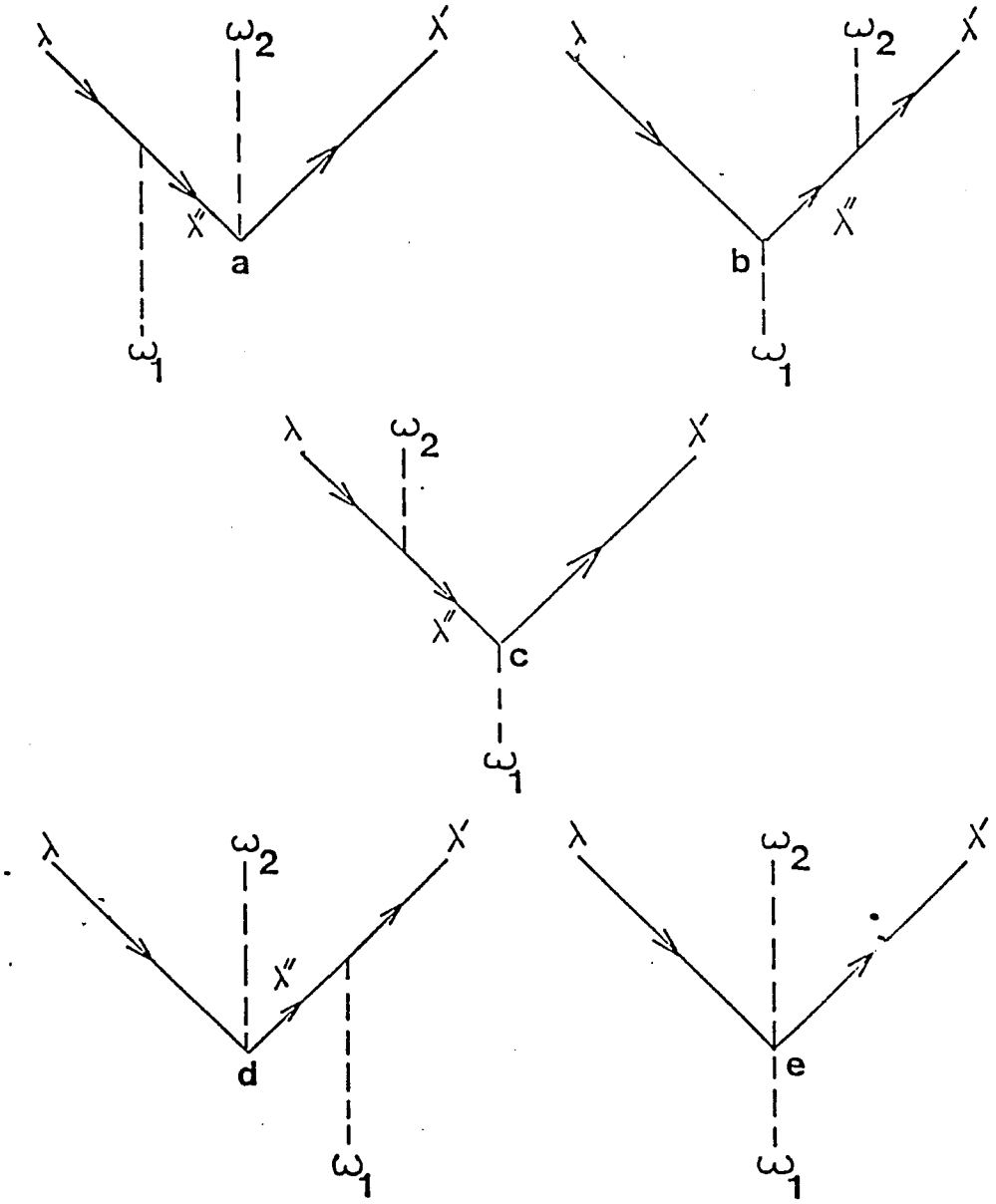

Fig. 1

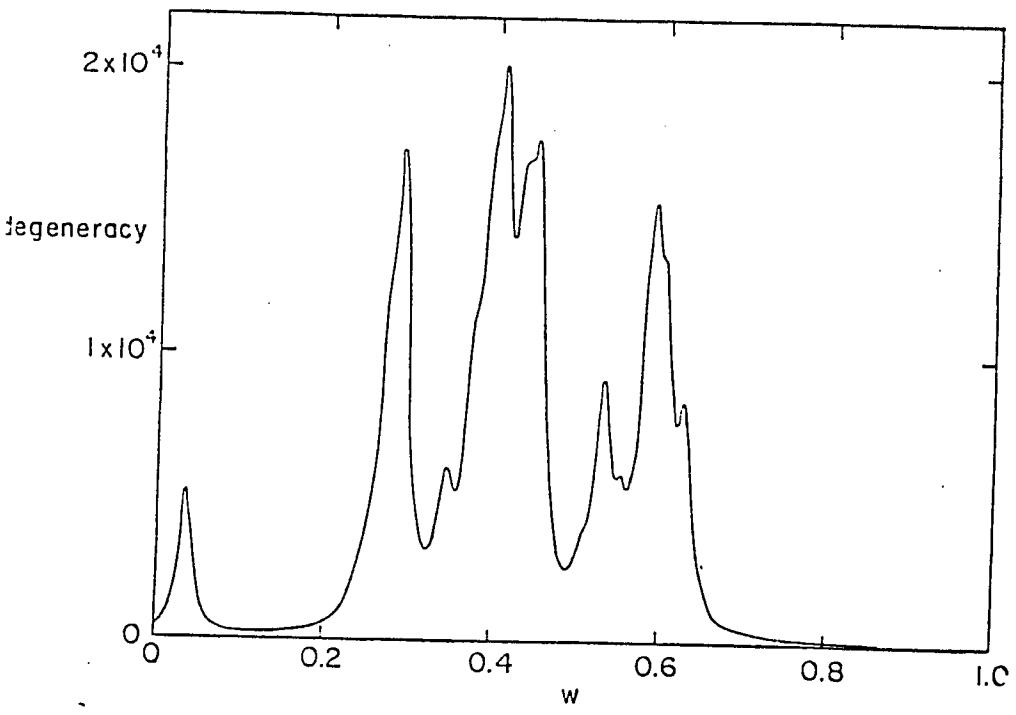

Fig. 2

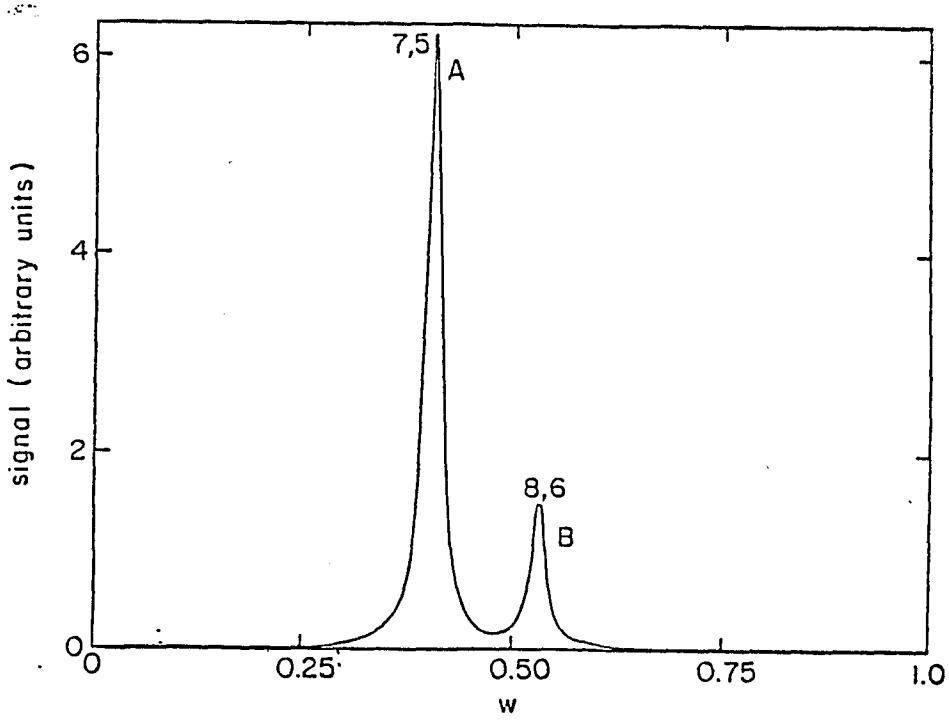

Fig. 3

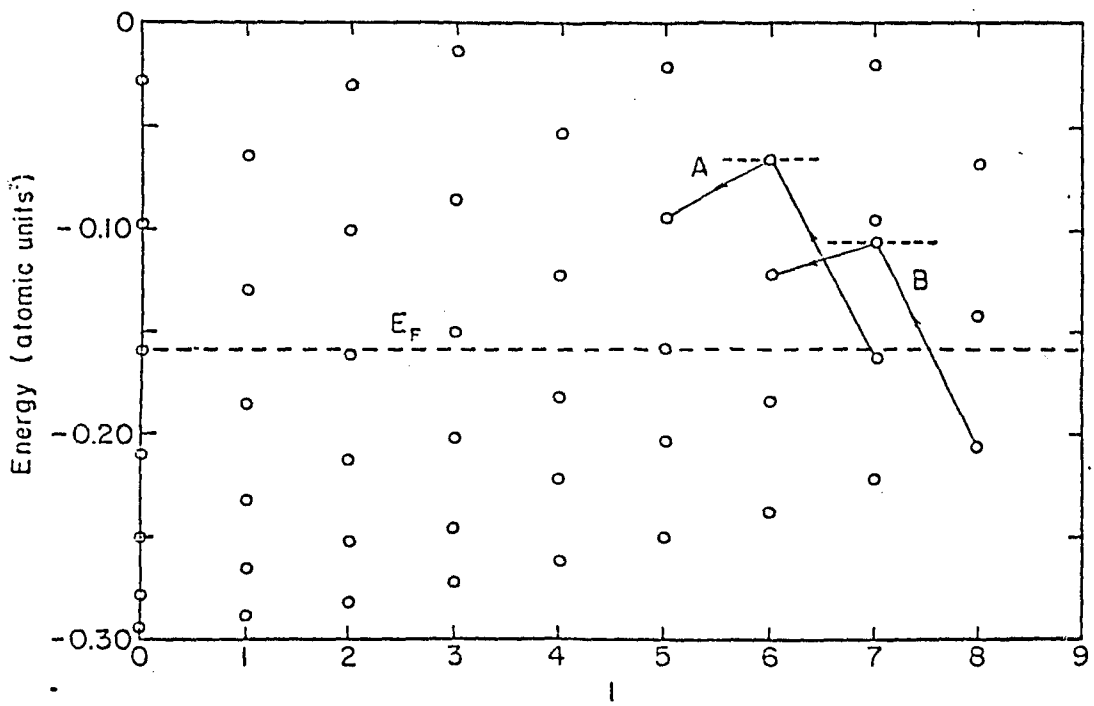

Fig. 4

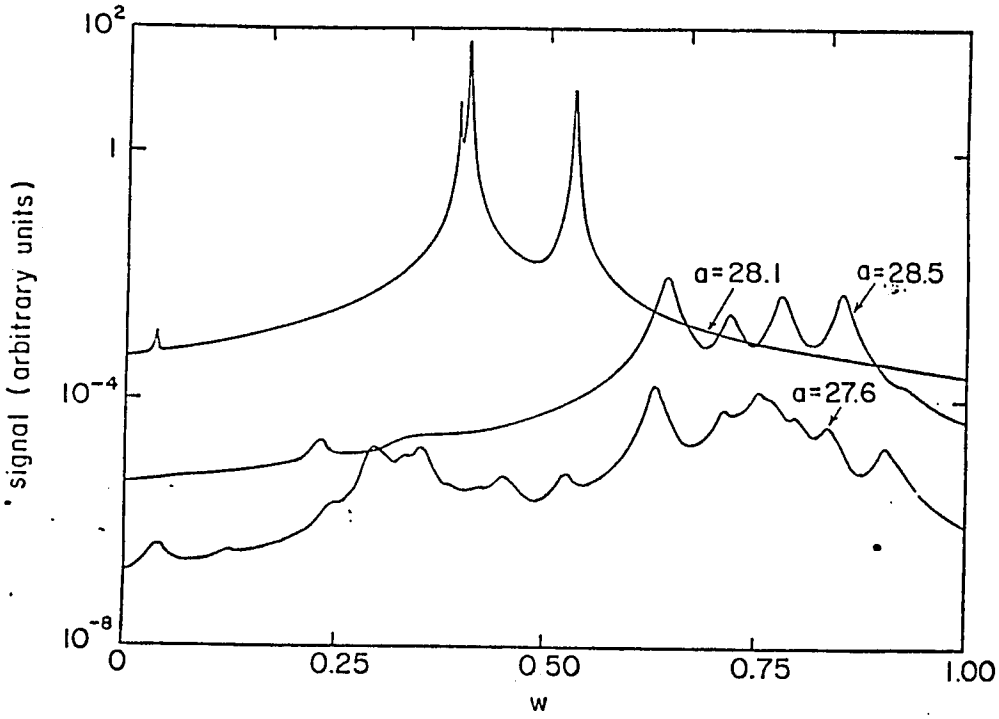
10^2
1
10^{-4}
10^{-8}
signal (arbitrary units)
a=28.1
a=28.5
a=27.6
0
0.25
0.50
0.75
1.00
w

Fig. 5

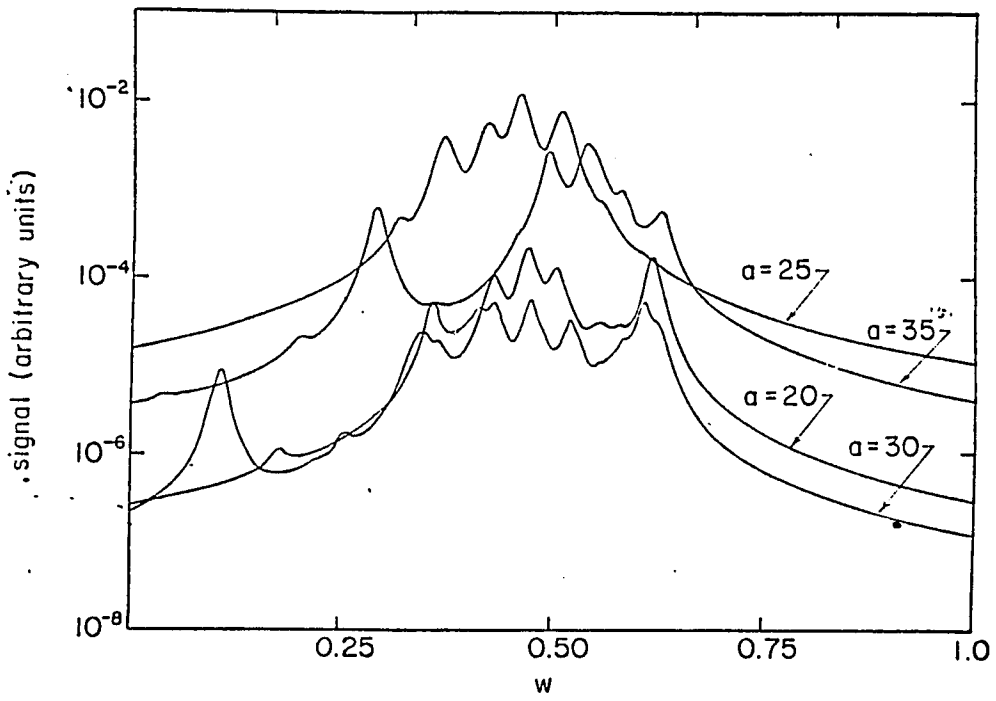
signal (arbitrary units)
10^{-2}
10^{-4}
10^{-6}
10^{-8}
0.25
0.50
0.75
1.0
w
a=25
a=35
a=20
a=30

Fig. 6

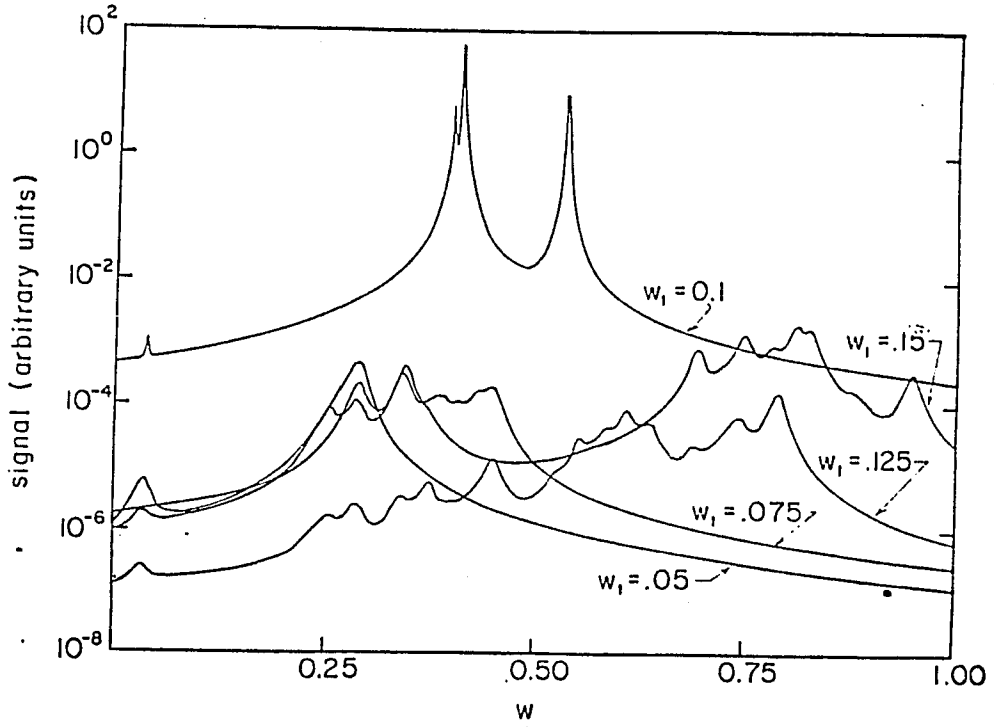
10^2
10^0
10^{-2}
10^{-4}
10^{-6}
10^{-8}
signal (arbitrary units)
$w_1 = 0.1$
$w_1 = .15$
$w_1 = .125$
$w_1 = .075$
$w_1 = .05$
0.25
0.50
0.75
1.00
w

Fig. 7

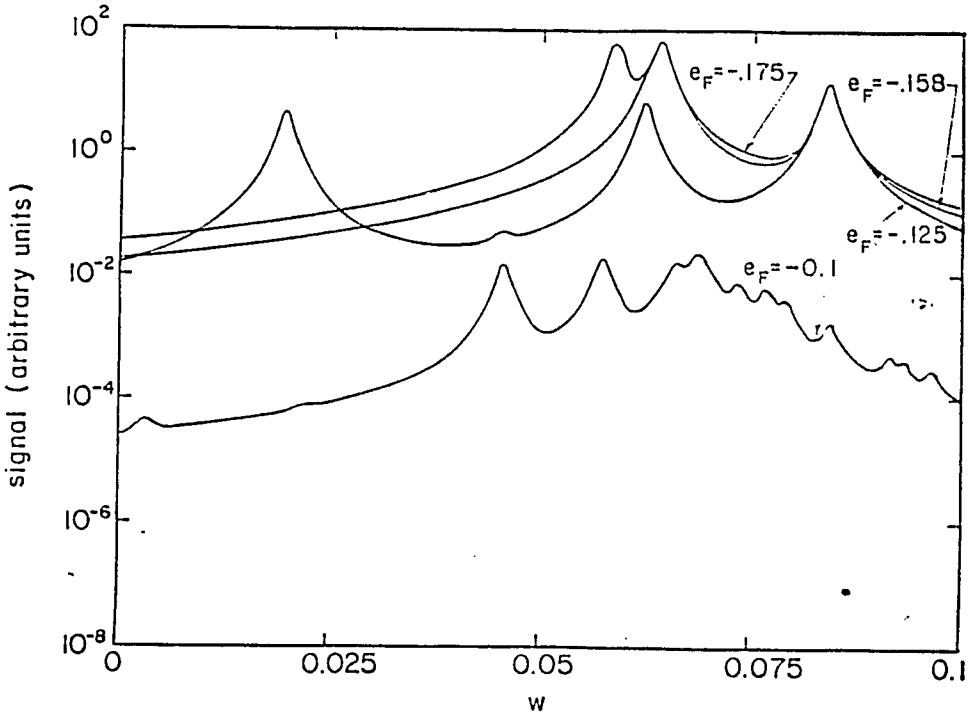
10^2
10^0
10^{-2}
10^{-4}
10^{-6}
10^{-8}
signal (arbitrary units)
e_F=-.175
e_F=-.158
e_F=-.125
e_F=-0.1
0
0.025
0.05
0.075
0.1
w

Fig. 8

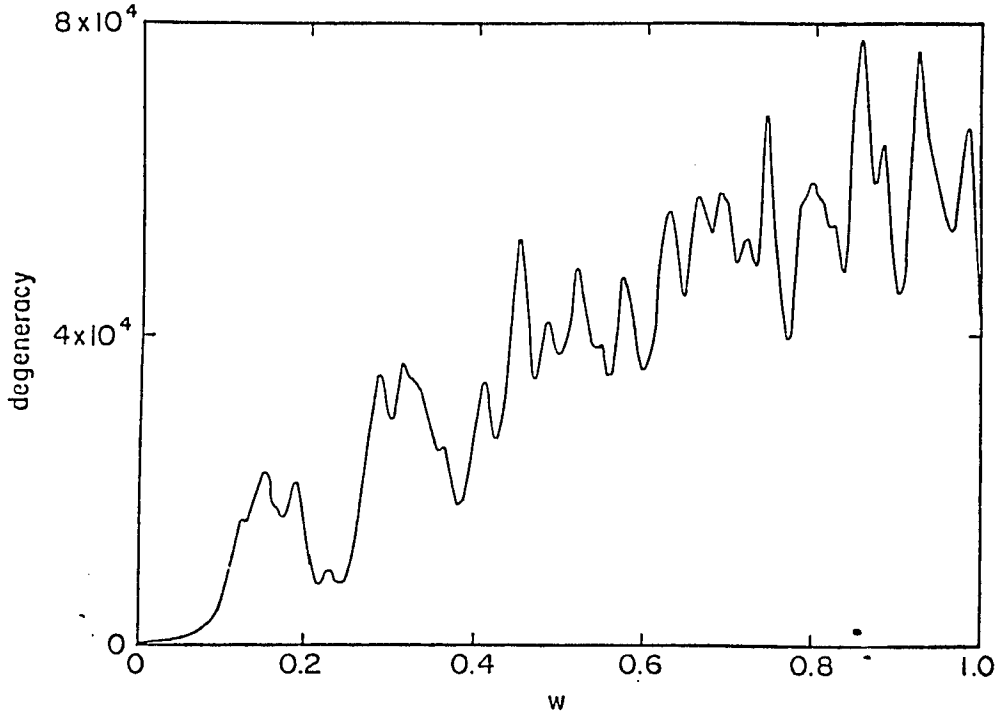

Fig. 9

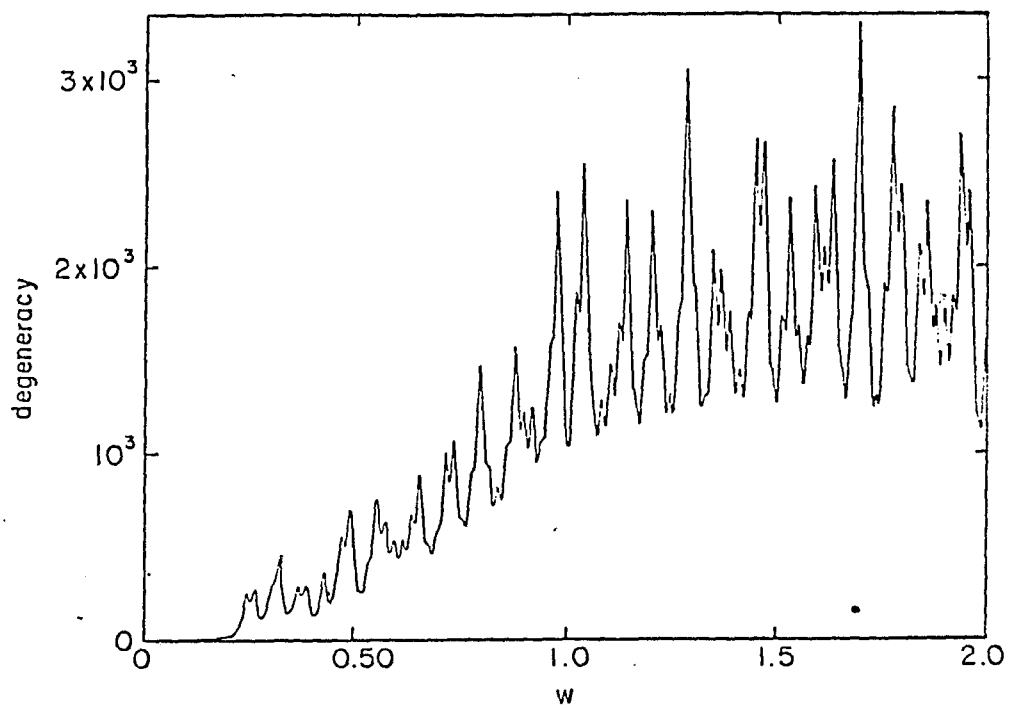

Fig. 10

PART II.

ELECTRON SCATTERING FROM SOLID SURFACES AND SMALL PARTICLES.

INTRODUCTION

The primary tool for the study of solid state surfaces is electron scattering. The earliest applications of this technique date back to Davisson and Germer who studied the Bragg reflection of electrons from solids. The important distinctions between light and electrons that made them suitable for the study of solid state surfaces was

a. The characteristic wave length for electrons at low energies was on the order of the lattice spacing and could be continuously varied.

b. The electrons that were scattered were those which did not penetrate the solid that readily and thus were strongly affected by surface properties.

c. The electrons were readily prepared, focused and detected.

However, progress in the full use of electron spectroscopy was slow due to the need for ultrahigh vacuum techniques and the need for developing methods for preparing and characterizing clean surfaces. Today a whole range of techniques exist including low energy electron diffraction (LEED), Auger electron spectroscopy (AES), low energy electron loss spectroscopy (LEELS), Surface extended X-ray absorption fine structure (SEXAFS), photoemission, ellipsometry and various ion scattering probes. The state of the art is perhaps best characterized by the recent invention of the vacuum electron tunneling microscope. Recent work has been reviewed by Raether.

Because of the importance of surfaces for science and technology we have chosen two aspects of the interaction of electrons with surfaces for analysis in this part of the thesis. In the first problem we look at the inelastic excitation of a flat surface by electrons. Our goal will be to see what the effect of solid state structure has on the excitation spectra of the solid. As we shall see, interesting information may be extracted from the data. Secondly, we turn our attention to rough surfaces or small particles. Again we look into the question of how the structure influences the scattering, but now focus our attention on the finite size of the particle or the surface roughness feature. We will see that, because of the spatial dispersion of the dielectric function of matter, there is indeed a shift of the excitation spectra with size.

In the first project of this part of the thesis we look at interference effects in electron energy loss spectroscopy. Previous calculations of EELS were based on a model of the solid in which the potential the electron experiences is simply a step potential. Thus the interior of the solid is treated as a free electron gas confined by a wall of finite height. The theory predicts an EELS spectrum for the surface plasmon loss peak which falls off monotonically with increasing electron energy. This, perhaps can be understood as an effect related to the duration of a collision. As the energy of the electron increases the electron spends less time in the vicinity of the surface. Hence the probability for exciting the plasmon also gets to be less.

Recently experiments were carried out at the University of Puerto Rico for electrons incident on silver. Contrary to theoretical expectations the EELS intensity of the plasmon loss peak relative to the elastic peak did not fall off monotonically but rather had some regions where it actually

increased considerably with increasing energy.

We attempt to explain this behavior on the basis of a possible quantum interference effect caused by the electrons scattered off of the various ionic planes of the solid. For certain energies the quantum mechanical amplitude for an electron to be near the surface will be different than for others. This amplitude will depend on the comparison of the lattice constant and the electron wave length. Since the surface plasmon is most easily excited when the electron is near the surface we also expect the probability for its excitation to be correlated to the electron is being found on the surface.

The second project of this part of the thesis involves studying EELS from small spherical particles. This could serve as a model for island films. In spite of its experimental interest the theoretical formulation of the energy loss probability for a charged particle passing near a general polarizable sphere is incomplete. For closer trajectories we expect larger contributions from higher multipoles since it must approach the planar limit. The calculation for the dipole mode is relatively easy and has been done. Ferrel et.al. have done calculations for all multipoles with a dielectric constant which is only a function of frequency. We would like to generalize the theory to include spatial dispersion .

In order to consider such effects we have introduced the frequency and wave- vector dependent dielectric function $\epsilon(\vec{k}, w)$. The problem gets complicated due to the presence of finite boundary effects. We develop an approximate method for incorporating such effects by replacing $\epsilon(\vec{k}, w)$ by an effective dielectric constant $\epsilon_l(w)$, where l is the multipolar index of the excitation.

3. Interference effect in Electron Energy Loss Spectroscopy

1.INTRODUCTION

At present, electron scattering from solid state surfaces provides two complementary ways of probing the solid. On the one hand low energy electron diffraction (LEED) is a valuable tool to characterize the surface structure[1]. On the other hand, low energy electron loss spectroscopy (LEELS)[2] is useful in determining the excitation spectrum of the solid. The combination of the two techniques provide surface scientists with a powerful tool for studying the dynamics and statics of surfaces. In this paper we will study the consequences of interference effects on the LEELS spectrum and thus probe the common boundary of the above two methods. From our analysis, we will see that additional information concerning the solid may be obtained from such a study.

The origin of the interference effects in LEELS may be understood simply as follows. The scattering electron couples to typical excitations of the solid such as surface plasmons, bulk plasmons and electron-hole pairs. The probability for making an inelastic transition depends on a matrix element involving states of the scattering electron and the potential which describes the collective excitation. Since surface excitations have potentials which are peaked in the surface region, these matrix elements will tend to accentuate the behavior of the electron wave functions near the surface. The electronic wave functions, however are determined by the superposition of the incident wave with the waves reflected from the various ionic planes in the solid. The reflection from these planes may interfere either constructively or destructively depending on the particular value of the wave length and the geometric structure of the solid. Thus one would

expect the LEELS spectrum to contain information about the underlying structure as well as the inelastic scattering spectrum. Furthermore, since the wave function of the electron near the surface is playing a more important role, it might be expected that the information contained in the LEELS spectrum might be more specific to the surface region than the bulk region. This would allow the energy of the incident electron to be raised without the drawback that occurs in LEED when the energy is raised, namely that the electron samples a good portion of the bulk as well as the surface.

Previous theoretical descriptions of the LEELS spectrum relied on two models. On the one hand, dielectric theory[3–6] provides a formalism in which it is simple to describe the inelastic excitations. On the other hand, the Sommerfeld model[7] for an electron interacting with a solid provides a natural description for the dynamics of the electron. Combined, the two methods allow one to describe LEELS spectra. This program has been carried out in the literature[8] and applied to the excitation of surface plasmons. The basic conclusion drawn by such a study is that the excitation spectrum as a function of the primary electron energy falls off with energy at high energies. In the context of the model, this is reasonable, since the time that the electron spends in the vicinity of the surface is a function of the energy and decreases as the energy increases, going roughly as the inverse square root of the energy. One may argue that when the electron is near the surface it is able to excite surface plasmons, when it is away from the surface, it cannot.

The above model, however clearly leaves out several elements which are of significance to us here. In particular, the Sommerfeld model does not include the spatially modulated ionic potential which is the

source of the interference pattern seen in LEED. In our model this will be included. We also will consider other possible excitation channels: the bulk plasmons and the electron-hole pairs. As we will see, these contribute significantly to the inelastic background.

2. THEORY

The interference effects seen in LEED come about because of the scattering from the ions. One may identify two key elements in this process. One is due to scattering from the two-dimensional periodic array of atoms parallel to the surface while the other is due to the superposition of waves scattered from successive layers of atoms in the solid. The two effects play a somewhat different role in LEED. The former effect is largely responsible for Bragg scattering. The latter effect gives rise mainly to a modulation of the reflected intensity as a function of primary electron energy. In more refined multiple scattering formulations of LEED, these two effects are, of course, interconnected. Bragg scattering is very well understood and is not of much interest here. We therefore will focus our attention on the interlayer scattering.

In order to accomplish this let us introduce a simplified model in which the ionic potential is a function of one spatial variable, z. The particular form we choose for this potential consists of a periodic piece to describe the bulk of the solid and a surface potential. Thus

$$V(z) = \begin{cases} -Vo - Uo\cos(2\pi\frac{z}{b}) & \text{if } \cos(2\pi\frac{z}{b}) < 0, \\ -Vo & \text{if } \cos(2\pi\frac{z}{b}) > 0, \end{cases} \tag{2.1a}$$

when $|z| < \left(N + \frac{1}{4}\right) b$,

and

$$V(z) = -V_0 e^{-c[|z| - (N+\frac{1}{4})b]}, \tag{2.1b}$$

when $|z| > \left(N + \frac{1}{4}\right) b$,

Here V_0 is the complex optical potential, U_o is the strength of the lattice potential, b equals the lattice constant, N is the number of ionic planes taken to represent the solid and c determines how fast the potential goes to zero beyond the surface. In our calculation we model the solid by a finite number of planes and solve the problem numerically. The solid is taken to extend from -L to +L, where L=Nb.

In order to describe the LEELS process we will be applying 'Fermi's Golden Rule'. An electron in an incoming state $\phi_{in}(z)$ excites a surface excitation and scatters into an outgoing state; $\phi_{out}(z)$. As in LEED the 'in' and 'out' states may be expressed in terms of transmission and reflection coefficients outside the solid. Inside the solid, however, they will have to be obtained numerically. We begin by determining the 'in-state'.

a. The in-state

Since the potential varies only along z direction we can write the incoming wave as

$$\psi_{in} = \phi_{in} e^{i\vec{k}_p \vec{r}_p} \tag{2.2}$$

with $\vec{k}_p = (k_x, k_y)$ and $\vec{r}_p = (x, y)$, where $\vec{k}_p$ and $\vec{r}_p$ are the planar projections of $\vec{k}$ and $\vec{r}$. Here

$$\phi_{in}(z) = \begin{cases} e^{ikz} + Re^{-ikz} & \text{if } z < L \\ Te^{ikz} & \text{if } z > L \end{cases} \tag{2.3}$$

where

$$k = \sqrt{2\epsilon} \tag{2.4}$$

$$\epsilon = E - \frac{k_p^2}{2} \tag{2.5}$$

and E is the energy of the incoming electron. R and T are the reflection and transmission coefficient respectively. The function $\phi_{in}(z)$ satisfies the one - electron Schrodinger equation

$$[-\tfrac{1}{2}\partial_z^2 + V(z) - \epsilon]\,\phi_{in}(z) = 0. \tag{2.6}$$

The function $\phi_{in}(z)$ can also be written as a linear combination of parity eigenstates

$$\phi_{in}(z) = c_+\phi_+(z) + c_-\phi_-(z), \tag{2.7}$$

where

$$\phi_\pm = \pm\phi_\pm(-z), \tag{2.8}$$

Here the k dependence has been supressed. The parity eigenstates may be written as

$$\phi_\pm(z) = \begin{cases} \cos kz + \alpha\, sgn(z) \sin kz \\ \sin kz + \beta\, sgn(z) \cos kz \end{cases} \qquad \text{for } |z| > L \tag{2.9}$$

where $sgn(z) = z/|z|$ is an odd function of z. Equating Eqs. (2.3) and (2.7) for $z > L$ and $z < L$, yields

$$c_+ = \frac{1}{1+i\,\alpha} \tag{2.10a}$$

$$c_- = \frac{i}{1-i\,\beta} \tag{2.10b}$$

$$T = \frac{1-\alpha\beta}{(1+i\,\alpha)(1-i\,\beta)} \tag{2.10c}$$

$$R = -\frac{i\,(\alpha+\beta)}{(1+i\,\alpha)(1-i\,\beta)} \tag{2.10d}$$

The eigenstates $\phi_\pm$ for $|z| < L$ are calculated by numerical integration. Our procedure is as follows: start at z=0 and assign $\tilde{\phi}_+(0) = 1$ and $\tilde{\phi}'_+(0) = 0$, where prime denotes differentiation with respect to z and $\tilde{\phi}$ differs from ϕ by a normalization factor to be determined. Then we numerically integrate the Schrodinger equation by a Runge-Kutta procedure out to z=L. There $\tilde{\phi}_+(L)$ will be given by

$$\tilde{\phi}_+(L) = (\cos kL + \alpha \sin kL)\Gamma_+, \tag{2.11}$$

$$\tilde{\phi}'_+(L) = (k \sin kL + k\,\alpha \cos kL)\Gamma_+, \tag{2.12}$$

The normalization constant Γ_+ is determined from Eq. (2.9) and (2.12)

$$\Gamma_+ = |\tilde{\phi}_+(L)|\left[\frac{(1+|r_+|^2)}{(1+|\alpha|^2)}\right]^{1/2} \tag{2.13}$$

where we have defined

$$r_+ = \frac{\tilde{\phi}'_+(L)}{k\,\tilde{\phi}_+(L)}$$

$$= -\frac{\tan kL + \alpha}{1+\alpha \tan kL} \tag{2.14}$$

and

$$\alpha = \frac{r_+ + \tan kL}{1 - r_+ \tan kL} \tag{2.15}$$

Renormalizing the temporary function $\tilde{\phi}(z)$ gives

$$\phi_+(z) = \frac{\tilde{\phi}_+(z)}{\Gamma_+} \tag{2.16}$$

The eigenfunction $\phi_-(z)$ will be detrmined in the same way as $\phi_+(z)$ except that at z=0, we start with $\tilde{\phi}_- = 0$ and $\phi'(0) = 1$, and integrate to z=L:

$$\tilde{\phi}_-(L) = (\sin kL + \beta \cos kL)\Gamma_- \tag{2.17}$$

$$\tilde{\phi}'_-(L) = (k \cos kL - \beta k \sin kL)\Gamma_- \tag{2.18}$$

The quantities Γ_-, β, γ_- are given by

$$\Gamma_- = |\tilde{\phi}_-(L)| \sqrt{\frac{1 + |r_-|^2}{1 + |\beta|^2}} \tag{2.19}$$

$$\beta = \frac{1 - r_- \tan kL}{r_- + \tan kL} \tag{2.20}$$

$$r_- = \frac{\tilde{\phi}'_-(L)}{k\,\tilde{\phi}_-(L)} \tag{2.21}$$

and

$$\phi(z) = \frac{\tilde{\phi}_-(z)}{\Gamma_-} \tag{2.22}$$

Having characterized the 'in-state' let us now turn our attention to the 'out-state'.

b. The Out-state

The outgoing wave can be written as

$$\psi_{out}(\vec{r}) = e^{i\vec{k}'_p \cdot \vec{r}_p} \phi_{out}(z) \tag{2.23}$$

By the same argument as used in the case of the in-wave we can write

$$\phi_{out}(z) = \begin{cases} e^{ik'z} + \rho e^{-ik'z} & \text{if } z < L \\ \tau e^{ik'z} & \text{if } z > L \end{cases} \tag{2.24}$$

with

$$k' = \sqrt{2}\epsilon' \tag{2.25}$$

$$\epsilon' = E' - \frac{k'^2}{2} \tag{2.26}$$

where E' is the energy of the scattered electron.

The function $\phi_{out}(z)$ satisfies the Schrodinger equation

$$[-\tfrac{1}{2}\partial_z^2 + V(z) - \epsilon']\,\phi_{out}(z) = 0 \tag{2.27}$$

As before ϕ_{out} may be written as

$$\phi_{out}(z) = c'_+ \phi_+(z) + c'_- \phi_-(z) \tag{2.28}$$

with

$$\phi_\pm = \begin{cases} \cos k'z + \alpha' sgn(z) \sin k'z \\ \sin k'z + \beta' sgn(z) \cos k'z \end{cases} \tag{2.29}$$

when $|z| > L$.

Comparing the equations of the out-wave with the in-wave we see that they are identical provided

$$k \rightarrow k'$$

$$i \rightarrow -i$$

$$R \rightarrow \rho$$

$$T \rightarrow \tau$$

The expressions for $c_+, c_-, \rho, \tau, \alpha', r'_+, \Gamma_+, \phi_+, \beta', r'_-, \phi_-$ are obtained from the corresponding expressions for the in-wave simply by making the above replacement. Thus

$$c'_+ = \frac{1}{(1-i\,\alpha')} \tag{2.30a}$$

$$c'_- = -\frac{i}{(1+i\,\beta')} \tag{2.30b}$$

$$\tau = \frac{1-\alpha'\beta'}{(1-i\,\alpha')(1+i\,\beta')} \tag{2.30c}$$

$$\rho = i\frac{\alpha'+\beta'}{(1-i\,\alpha')(1+i\,\beta')} \tag{2.30d}$$

$$\alpha' = \frac{r'_+ + \tan k'L}{1-r'_+\tan k'L} \tag{2.31}$$

$$r'_+ = \frac{\tilde{\phi}(L)}{k'\tilde{\phi}_+(L)} \tag{2.32}$$

$$\Gamma_+ = |\tilde{\phi}_+(L)|\,[\frac{1+|r'_+|^2}{1+|\alpha'|^2}]^{1/2} \tag{2.33}$$

$$\phi_+(z) = \frac{\tilde{\phi}_+(z)}{\Gamma_+} \tag{2.34}$$

$$\beta' = \frac{1-r'_-\tan k'L}{r'_-+\tan k'L} \tag{2.35}$$

$$r'_- = \frac{\tilde{\phi}'_-(L)}{k'\tilde{\phi}_-(L)} \tag{2.36}$$

$$\phi_- = \frac{\tilde{\phi}_-(z)}{\Gamma_-} \tag{2.37}$$

C. Matrix element for surface plasmon excitation

Having determined the in and out -waves we now calculate the matrix elements involved in the excitation of a surface plasmon wave. With b as the lattice constant and N the number of layers, the surface plasmon wave can be represented by a potential field of the form

$$\phi = \gamma e^{-q\,|z+Nb\,|} \tag{2.38}$$

where $\vec{q} = \vec{k}_p - \vec{k}'_p$ is the wave-vector of the plasmon and γ is the appropriate coupling constant. The desired matrix element is

$$I = \int e^{-q\,|z+nb\,|}\phi^*_{out}(z)\phi_{in}(z) \tag{2.39}$$

$$= I_L + I_M + I_R$$

where we have divided the integration range into three regions:

$$I_L = \int_{-\infty}^{-L} dz e^{q(z+nb)}\phi^*_{out}(z)\phi_{in}(z)$$

$$= \int_{-\infty}^{-L} dz e^{qz}\left[e^{-k'z} + \rho e^{ik'z}\right]^*\left[e^{ikz} + Re^{-ikz}\right]e^{qnb}$$

$$= e^{-q(L-nb)}\left|\frac{e^{-i(k+k')L}}{q+i(k+k')} + \rho^*\frac{e^{i(k'-k)L}}{q-i(k-k')} + R\frac{e^{i(k-k')L}}{q-i(k-k')} + R\rho^*\frac{e^{i(k+k')L}}{q-i(k+k')}\right| \tag{2.40}$$

$$I_R = \int_{L}^{\infty} dz e^{-q(z+nb)}\left[\tau e^{-ik'z}\right]^*\left[Te^{ikz}\right]$$

$$= T\tau^* e^{-qnb}\frac{e^{[-q+i(k+k')]L}}{q-i(k+k')} \tag{2.41}$$

$$I_M = \int_{-L}^{L} dz e^{-q\,|z+nb\,|}\phi^*_{out}(z)\phi_{in}(z)$$

$$= \int_0^L dz e^{-q|-z+nb|} \phi_{out}^*(-z)\phi_{in}(-z) + \int_0^L dz e^{-q|z+nb|} \phi_{out}^*(z)\phi_{in}(z) \quad (2.42)$$

Inserting the expressions for ϕ_{out} and ϕ_{in} from (2.26) and (2.7) we get

$$I_M = \int_0^L dz \Big[c'_+ \phi_+^*(z) c_+ \phi_+(z) + c'_- \phi_-^*(z) c_- \phi_-(z) \big)\big(e^{-q|z+nb|} + e^{-q|nb-z|}\big)\Big] +$$

$$\Big[c'_- \phi_-^* c_+ \phi_+(z) + c'_+ \phi_+^*(z) c_- \phi_-(z) \big]\big[e^{-q|z+nb|} - e^{-q|nb-z|}\big] \Big] \quad (2.43)$$

From (2.38) and (2.39) note that as $L \to \infty$ both I_L and $I_R \to 0$, so that the main contribution comes from I_M. Of course, I_M must be evaluated numerically. In order that the wave-function be continuous at -L both in magnitude and phase, I_M is multiplied by a phase factor, given by

$$\eta = \frac{e^{-ikL} + Re^{ikL}}{c_+ \phi_+(L) - c_- \phi_-(L)} \quad (2.44)$$

The differential scattering rate is determined from the formula

$$\frac{d\Gamma}{d\Omega dE'} = \frac{1}{4\pi^2 h} \sqrt{2E' - k_p'^2}\, |\gamma(q_p)|^2 |I|^2 \delta(E' + w_{q_p} - E) \quad (2.45)$$

where γ is the plasmon coupling constant and is given by $[2\pi h / q_p \frac{\partial \epsilon}{\partial w}]^{1/2}$.

Using this value for γ we obtain the differential scattering rate

$$\frac{d\Gamma}{d\Omega dE'} = \left\{ \frac{1}{2\pi q_p \frac{\partial \epsilon}{\partial w}\Big|_{w_q}} \sqrt{2E' - k_p'^2}\, |I|^2 \right\} \delta(E' + w_{q_p} - E)$$

$$= P(E)\delta(E' + w_{q_p} - E) \quad (2.46)$$

d. Scattering geometry

Our work is motivated by some experiments currently in progress[6]. In order to compare our results with these experiments we must take the geometry of the experiments into account and relate our theoretically calculated differential scattering rate to the signal to be determined experimentally. In Fig.(1) we show the experimental arrangement that is being used. The line A A' denotes the surface of the solid. The normal to the solid is along the direction $\hat{n}$. An incident beam of wave vector $\vec{k}$ impinges on the solid and scatters into an outgoing state with wave vector $\vec{k}'$. The detector is taken to be a cylindrical analyzer with a circular entrance slit around the base of a cone whose apex angle is θ. The geometric relation between the various vectors are described by angles θ,θ', and ψ. Thus

$$\vec{k}_p = \sqrt{2E}\,\sin\theta\,\hat{i} \tag{2.47}$$

$$\vec{k}'_p = \sqrt{2E'}\sin\theta'(\hat{i}\cos\phi' + \hat{j}\sin\phi') \tag{2.48}$$

$$k = \sqrt{2E}\,\cos\theta \tag{2.49}$$

$$k' = \sqrt{2E'}\cos\theta' \tag{2.50}$$

where $\epsilon = \frac{k^2}{2}$ and $\epsilon' = \frac{k'^2}{2}$

$$\vec{q} = \vec{k}'_p - \vec{k}_p$$

$$= (\sqrt{2E}\,\sin\theta'\cos\phi' - \sqrt{2E}\,\sin\theta)\hat{i} + \sqrt{2E'}\sin\theta'\sin\phi'\hat{j} \tag{2.51}$$

The angles ψ,θ,and θ', shown in fig(1b) are related by the equation

$$\sin\theta' = \frac{2(\sin\theta\cos\phi'\cos\psi) \pm \sqrt{4(\sin^2\theta\cos^2\phi'\cos^2\psi) - 4(\sin^2\theta\cos^2\phi' + \cos^2\theta)(\cos^2\psi - \cos^2\theta)}}{2(\sin^2\theta\cos^2\phi' + \cos^2\theta)} \tag{2.52}$$

Naturally we define the physical branch as that sign which gives us a real solution.

3. BACKGROUND SCATTERING

In addition to the plasmon peak one expects other excitations to be present. Let us try to identify and estimate the various background contributions due to these excitations. The two main sources of background come from electron-hole pairs and bulk plasmon emission. In order to estimate the electron-hole pair contribution we will study the direct excitation process induced by the interaction with the incident electron. The bulk plasmon excitation process, on the other hand, is more naturally describable in a dielectric formalism.

a. Electron hole-pair contributions

As an electron impinges on the solid it will interact with the tails of the solid's electrons which penetrate the vacuum region. It may be argued that this represents the major source for the electron-hole background contribution because this interaction is unscreened. Once the electron penetrates the solid the extent of its Coulomb interaction with electrons is limited by the screening effect of other electrons. In the course of the excitation process the solid's electron make a transition from some initial state $|i>$ to a final state $|f>$. The transition amplitude is given in time-dependent perturbation theory by

$$A = -i\int_{-\infty}^{\infty} dt e^{-i(\epsilon_i-\epsilon_f)t} <f| \frac{\Theta(z)}{|\vec{r}-\vec{R}(t)|} |i> \qquad (3.1)$$

where $\vec{R}(t)$ defines the classical trajectory of the projectile and ϵ_i and ϵ_f denote the energies of the respective states. The unit step function $\Theta(z)$ allows a Coulomb coupling only if the electron is in the the vacuum

region.

Let $P(\epsilon)d\epsilon$ represent the probability of having an energy loss between ϵ and $\epsilon+d\epsilon$. $P(\epsilon)$ is given by

$$P(\epsilon) = \sum_{i,f} f_f^+ f_i^- |A|^2 \delta(\epsilon_i - \epsilon_f - \epsilon)$$

$$= 2\int_{\epsilon_f}^{\infty} d\epsilon_f \, D(\epsilon_f) \int_{-\infty}^{\epsilon_f} d\epsilon_i \, D(\epsilon_i) |\bar{A}|^2 \delta(\epsilon_i - \epsilon_f - \epsilon)$$

$$= 2\int_{\epsilon+\epsilon_f}^{\epsilon_f} d\epsilon_i \, D(\epsilon_i) D(\epsilon_i - \epsilon) |\bar{A}|^2$$

$$= 2|\bar{A}|^2 \int_{\epsilon+\epsilon_f}^{\epsilon_f} d\epsilon_i \, D(\epsilon_i) D(\epsilon_i - \epsilon) \qquad (3.2)$$

Here ϵ is the energy lost by the incident electron in producing the electron-hole pair. The quantities f^- and f^+ are the Fermi-factors for the occupied and unoccupied electronic states . If we neglect thermal effects they are represented by Θ functions. $D(\epsilon)$ denotes the density of states and $\bar{A}$ represents an average transition matrix element. Note that the probability function involves the joint density of states. The density of states of silver is modeled as shown in the Fig(2) . In this model one simplifies matters by including only s and d band contributions. The mathematical form we use is

$$D(E) = \begin{cases} \dfrac{F\sqrt{2(E+V_o)}}{2\pi^2} & \text{if } -V_o < E < E_1 \\ \dfrac{G + F\sqrt{2(E+V_o)}}{2\pi^2} & \text{if } E_1 < E < E_2 \\ \dfrac{F\sqrt{(2(E+V_o)}}{2\pi^2} & \text{if } E_2 < E < 0 \\ \dfrac{F[\sqrt{2(E+V_o)} + \sqrt{2E}\,]}{2\pi^2} & \text{if } E > 0 \end{cases} \qquad (3.3)$$

where E_1 and E_2 are determined by band edges. The constants F and G are evaluated by using the normalization conditions given by

$$\int_{-V_o}^{\epsilon_f} D_s(E)dE = n_s \tag{3.4}$$

$$\int_{\epsilon_1}^{\epsilon_2} D_d(E)dE = n_d \tag{3.5}$$

where n_s and n_d are the number densities of s and d electrons, respectively. With this, our model density of states becomes

$$D(E) = 8.6\times10^{-3}\left|\frac{10}{\epsilon_2-\epsilon_1}\Theta(E-\epsilon_1)+\frac{3}{2.\sqrt{2}(\epsilon+V_o)^{\frac{3}{2}}}\sqrt{2(E+V_o)}\Theta(E+V_o)+\right.$$

$$\left.\frac{3}{2.\sqrt{2}(\epsilon+V_o)^{\frac{3}{2}}}\sqrt{2E}\,\Theta(E)\right| \tag{3.6}$$

The first term in the above expression is the contribution from the localized d electrons, This term is relatively unimportant since we are considering only the coupling of the projectile with the electrons which tail into the vacuum.

In order to calculate the transition amplitude one must specify the initial and final states of the solid electrons, which are obtained by solving the Schrodinger equation

$$[-\tfrac{1}{2}\nabla^2+V(z)-E]\psi = 0 \tag{3.7}$$

with

$$V(z) = \begin{cases} -V_o & \text{if } z<0 \\ 0 & \text{if } z>0 \end{cases} \tag{3.8}$$

As before z=0, represents the surface. Since the potential varies only in the z direction , the solution of the above equation may be written as

$$\psi = \phi(z)e^{i\vec{k}_p \cdot \vec{r}_p} \tag{3.9}$$

Two cases are of interest : bound-bound transitions and bound-continuum transitions. In the bound-bound transition the excited electron remains below the vacuum level whereas in the bound-continuum transition it is excited above the vacuum level.

For a bound state $E - \frac{k_p^2}{2} < 0$ and

$$\phi(z) = \begin{cases} Ne^{-Qz} & \text{if } z > 0 \\ N\dfrac{\sin(qz+\delta)}{\sin\delta} & \text{if } z < 0 \end{cases} \tag{3.10}$$

where $Q = \sqrt{k_p^2 - 2E}$ and $q = \sqrt{2(E+V_o) - k_p^2}$.

The constants N and δ are determined from the boundary conditions and are given by

$$\delta = cot^{-1}(-\frac{Q}{q}) \tag{3.12}$$

$$N = \sqrt{\frac{2}{L}}\sin\delta \tag{3.13}$$

For a continuum state $E - \frac{k_p^2}{2} > 0$ and

$$\phi(z) = \begin{cases} \bar{N}[e^{ik_z z} + Re^{-ik_z z}] & \text{if } z < 0 \\ \bar{N}Te^{iqz} & \text{if } z > 0 \end{cases} \tag{3.14}$$

where R and T are the reflection and transmission coefficients respectively, and are obtained by matching ϕ and ϕ' at z=0,

$$R = \frac{k_z - q}{k_z + q} \tag{3.15}$$

$$T = 1 - R$$

$$k_z = \sqrt{2E - q_p^2} \tag{3.16}$$

$$\overline{N} = [2L(1 + R + R^2)]^{-1/2} \tag{3.17}$$

In terms of these states we may now study the transitions.

The matrix element for bound-bound transition is given by

$$A_1 = \frac{4\pi i N N'}{(Q + Q')^2 - q^2} \left[\frac{2(Q + Q')v_z}{(Q + Q')^2 v_z^2 + \tilde{w}^2} - \frac{2qv_z}{q^2 v_z^2 + \tilde{w}^2} \right] \tag{3.18}$$

where

$$\tilde{w} = w + (\vec{k}'_p - \vec{k}_p).\vec{v}_p \tag{3.19}$$

Here v_z is the z component of the velocity of the electron, and $\vec{v}_p$ is the velocity of the projectile electron parallel to the surface.

The matrix element for the bound - continuum transition is given by

$$A_2 = \frac{4\pi i N N'}{(Q + ik_z)^2 - q^2} \left[\frac{2(Q + ik_z)v_z}{(Q + ik_z)^2 v_z^2 + \tilde{w}^2} - \frac{2qv_z}{q^2 v_z^2 + \tilde{w}^2} \right] +$$

$$\frac{4\pi i N \overline{N} R}{(Q - ik_z)^2 - q^2} \left[\frac{2(Q - ik_z)v_z}{(Q - ik_z)^2 v_z^2 + \tilde{w}^2} - \frac{2qv_z}{q^2 v_z^2 + \tilde{w}^2} \right] \tag{3.20}$$

The total matrix element is the sum of the above two terms

$$A = A_1 + A_2 \tag{3.21}$$

As before, in order to correlate our theory with experiments[6] we will evaluate this for a particular detector arrangement. The detector function is included to account for the fact that only some scattered electrons enter the detector. It is determined by the geometry of the experiment. One

must include the detector function corresponding to the scattering geometry shown in the fig.(1) in order to compare our results with the experiment. It is given by the formula

$$\Delta = \left| \Theta(X_o + \frac{\delta\psi}{2}\sqrt{1-X_o^2} - X_-)\Theta(X_- - X_o + \frac{\delta\psi}{2}\sqrt{1-X_o^2}) + \right.$$

$$\left. \Theta(X_o + \frac{\delta\psi}{2}\sqrt{1-X_o^2} - X_+)\Theta(X_+ - X_o + \frac{\delta\psi}{2}\sqrt{1-X_o^2}) \right| \qquad (3.22)$$

Here ψ_o refers to Fig.1 and $\delta\psi$ represents the angular width of the detecting slit. We have let

$$X_o = \cos\psi_o \qquad (3.23)$$

and

$$X_\pm = \frac{1}{v'}\left\{ \sin\theta(Q\cos\lambda - v\sin\theta) \pm \cos\theta\sqrt{-Q^2 - v^2\sin^2\theta + 2Qv\cos\lambda\sin\theta + v'^2} \right\} \qquad (3.24)$$

λ is the angle between two planer componets of the change in momentum in the natural coordinate systrm , v' is the speed of the scattered electron and v is the velocity of the incident electron.

The net transition probability, taking the detector function into account is

$$P_{\text{det}}(w) = \sum_{i,f} f_i^- f_f^+ |A|^2 \delta(\epsilon_f - \epsilon_i - w)\Delta$$

Using the definitions

$$D(\epsilon) = \sum_i \delta(\epsilon - \epsilon_i)$$

and

$$D(\epsilon') = \sum_f \delta(\epsilon' - \epsilon_f)$$

we obtain

$$P_{det}(w) = \int d\epsilon \int d\epsilon' \sum_{if} f_i^- f_f^+ \delta(\epsilon - \epsilon_i)\delta(\epsilon' - \epsilon_f)\delta(\epsilon_f - \epsilon_i - w) < |A|^2 \Delta > \tag{3.25}$$

where

$$< |A|^2 \Delta > = \frac{\sum_{if} f_i^- f_f^+ |A|^2 \Delta \delta(\epsilon_f - \epsilon_i - w)}{\int d\epsilon d\epsilon' \sum_{i,f} f_i^- f_f^+ \delta(\epsilon - \epsilon_i)\delta(\epsilon' - \epsilon_f)\delta(\epsilon' - \epsilon - w)} \tag{3.26}$$

The detection probability is therefore

$$P_{det}(w) = \int d\epsilon d\epsilon' D(\epsilon) D(\epsilon') \Theta(\epsilon_f - \epsilon)\Theta(\epsilon' - \epsilon_f)\delta(\epsilon' - \epsilon - w) < |A|^2 \Delta >$$

$$= J(w) < |A|^2 \Delta > \tag{3.27}$$

where $J(w)$ is the joint density of states corresponding to single particle density of states given by Eq.(3.3),

$$J(w) = \int d\epsilon d\epsilon' D(\epsilon) D(\epsilon') \Theta(\epsilon_f - \epsilon)\Theta(\epsilon' - \epsilon_f)\delta(\epsilon' - \epsilon - w) \tag{3.28}$$

In calculating $< |A|^2 \Delta >$ we make the simplifying assumption of using a free electron. The actual numerical calculation is done by a Monte-Carlo method.

b. Bulk-plasmon contributions

The electric field experienced by a charged particle scattering from a plane surface may be derived from the Poisson equation and is given by

$$\tilde{\vec{E}} = \int d^2k_p \int dw e^{i\vec{k}_p \cdot \vec{r}_p - iwt - k_p z} \frac{1}{k_p} \frac{1-\bar{\epsilon}(k_p, w)}{1+\bar{\epsilon}(k_p, w)}$$

$$(i\vec{k}_p + k_p \hat{z}) \int dt' e^{iwt' - i\vec{k}_p \cdot \vec{R}_p(t') - k_p z(t')} \tag{3.29}$$

where $\bar{\epsilon}$ is the effective dielectric constant defined by

$$\frac{1}{\bar{\epsilon}(\vec{k}_p, w)} = \frac{k_p}{\pi} \int \frac{dk_z}{(k_p^2 + k_z^2)\epsilon(\vec{k}, w)} \tag{3.30}$$

and $\vec{k} = (\vec{k}_p, k_z)$, $\vec{R} = (\vec{R}_p, z)$ where $\vec{k}_p$ and $\vec{R}_p$ are the planar components of $\vec{k}$ and $\vec{R}$ respectively.

The energy loss of the projectile is given by the equation

$$\Delta W = \mathrm{Re} Q \mid \int_{-\infty}^{+\infty} v.\tilde{\vec{E}} dt \mid_{r=R} \tag{3.31}$$

where Q is the charge of the projectile . The probability to lose energy $\hbar w$ is given by

$$P(\vec{q}, w) \equiv \frac{w}{\pi^2 q} \mathrm{Im} \frac{1}{1+\bar{\epsilon}} \mid \int_{-\infty}^{\infty} dt e^{iwt - i\vec{q}\cdot\vec{R}_p(t) - qz(t)} \mid^2 \tag{3.32}$$

As before, we must integrate the above probability over the detector function , to relate to experiments. Integrating over the plasmon wave vector $\vec{k}_p$ gives

$$P(w) = \int d\vec{q}_p \frac{w}{\pi^2 q} \mathrm{Im}\left(\frac{1}{1+\epsilon}\right)\Delta \mid \int_{-\infty}^{\infty} dt e^{iwt - i\vec{q}\cdot\vec{R}_p(t) - qz(t)} \mid^2$$

$$= \frac{w}{\pi^2} \int \frac{d^2q}{q} \mathrm{Im}\left(\frac{1}{1+\epsilon}\right)\Delta \frac{4q^2 v_{per}^2}{[(qv_{per})^2 + (w - \vec{q}.\vec{v})^2]^2} \tag{3.33}$$

where v_{per} is the perpendicular component of v. When the detector geometry is taken in to account we finally get

$$P(w) = S(w)\,\mathrm{Im}\left[\frac{1}{1+\epsilon}\right] \tag{3.34}$$

$$S(w) = \frac{wv^2\cos^2\theta}{2\pi^2}\int_0^1 dp\int_0^\pi d\,\lambda\sigma\Delta \tag{3.35}$$

where Δ is the detector function given by equation (3.22) and σ is given by

$$\sigma \equiv \frac{p^2}{[(pv\cos\theta)^2+(w-w_p-pv\cos\lambda\sin\theta)^2]^2} \tag{3.36}$$

Having determined the contributions from the surface plasmons, bulk plasmons and electron-hole pairs, let us now use them to calculate spectra.

4. RESULTS AND DISCUSSION

In the previous section we have developed a theory to describe interference effects that arise when electrons scattered inelastically from a metal and excite surface plasmons. The interference is caused by scattering from the various ion planes in the solid. Simply stated, the probability for an incident electron to be at the surface is not constant but depends on how the electron's wave length compares with the interionic separation. Since the excitation of surface plasmons is a local effect, taking place at the surface of the solid, we can understand the origin of the modulation.

In formulating our theory we also had to consider several background contributions to the inelastic spectrum which could possibly mask the interference effect. We have calculated the contribution due to electron-hole pair excitation as well as the contribution due to bulk plasmon excitation.

In our calculations we have made a number of simplifying assumptions. Perhaps the main one was to reduce the potential to a quasi-one-

dimensional form by neglecting the variation of the potential along the surface. It was pointed out that this assumption supresses the Bragg scattering but leaves the kind of interference we wish to study relatively unchanged. Thus the assumption permits us to focus on the essence of the physics without having to do the full three-dimensional calculation.

In doing our calculations we restricted our attention to the case of silver. The lattice constant was taken to be 2.36A , corresponding to the (1,1,1) direction interplanar spacing. In our calculations we took a finite slab of material with N planes. Typically N was taken to be around 20, because this yielded well-converged results.

As in the case of LEED we have introduced a complex potential[9]. The imaginary part of the potential is included to account for the depletion of current, due to inelastic process. Fig.(3) and Fig.(4) show the real and imaginary parts of the optical potential of Eq.(2.1). The real part represents the periodic part of the potential, whereas the imaginary part is responsible for the absorption. The curve for the potential is drawn taking N=5. The thickness of the solid is taken to be 37A

In Fig. (5) we plot the relative differential scattering rate as a function of the energy of the incident electron. The ordinate is in arbitrary units. The calculation was done for an incident angle $\theta = 30^{o}$, a cone angle of $\psi = 44^{o}$ and was integrated over all azimuthal angles, ϕ (see Fig.(1) for the scattering geometry). At high energies note that the curve falls with increasing energy, as would be expected on the basis of a classical analysis. However at lower energies some additional structure is observed. This structure arises from the interference effect discussed earlier. In addition to the fact that probability is decreasing with incident energy it is showing some additional structures in the low energy part. Here we have taken

the incident angle to be 30^0 and the cone angle to be 44^0, the ϕ integration was done over 360^0.

For comparison's sake, in Fig. (6) we display the results of the same calculation with the periodic part of the potential set equal to zero. This corresponds to the usual Sommerfeld free-electron model. Note that the interference structure present in Fig.(5) is now supressed, as would be expected. At high energy, the two graphs do behave similarly, i.e. the interference effects are less important. At low energies, however, gross discrepancies do occur.

In the above cases we have calculated the results when all azimuthally scattered electrons are detected. Let us now see what happens if we selectively detect electrons at a given azimuthal angle. Let us call this the angle-resolved signal. Fig.(7) shows the plasmon loss probability in the specular direction. Both the angle of incidence and reflection are taken to be 22^0 and the cone angle to be 44^0, and now ϕ is 180^0. Comparing Fig.(7) with Fig.(5) we see that there is a considerable difference. The sharp structure at E=24, 112 and 279 eV may be understood by examining the reflection coefficient for elastically scattered electrons. In Fig.8 we plot this reflection coefficient (given by Eq. 2.3). The reflection peaks are observed to occur in close proximity to the peaks in Fig.7. Thus we conclude that the specular interference pattern correlates with the elastic interference pattern. However, the detailed magnitudes of the two effects are different.

Finally Fig.(9) shows the azimuthal variation of plasmon probability. The abscissa denotes the angle ϕ. The incident electron energy is taken to be 100 eV, the angle of incidence was taken to be 21.15° and the scattered angle is given by Eq. (2.52). Note that some angle resolved structure is observed.

In summary we find that interference effects can be of considerable importance in understanding the systematics of inelastic processes, such as surface plasmon excitation, just as they are of importance in understanding the LEED intensities. This paper was designed primarily as an aid to experimental studies in this field.

The authors wish to acknowledge the suggestion for doing the present work to Prof. Y. Goldstein, A. Many and Z. Weiss and thank them for helpful discussions.

References

1. H. Raether. In Springer Tracts in Modern Physics. 38 (Springer, Berlin, Heidelberg, New York 1965) p.85

2. H. Froitzheim. In Topics in Current Physics. 4. ed. H. Ibach. (Springer - Verlag Berlin Heidelberg New York), 1977

3. E. Fermi: Phys. Rev. 57, 485 (1940)

4. J. Hubbard: Proc. Phys. Soc. (London) A 68, 976 (1955)

5. H. Frohlich: Max-Planck-Festschrift (BEB Deutscher Verlage der Wissenschaften, Berlin 1958) ed. H. Frohlich p. 277

6. H. Frohlich, H. Pelzer: Proc. Phys. Soc. (London) A 68, 525 (1955)

7. E. Evans, D.L. Mills: Phys. Rev. B 5, 4126 (1972)

8. Y. Goldstein (private communication)

9. J. B. Pendry: "Low Energy Electron Diffraction". (Academic Press. New York, 1974)

Figure Captions

Fig.(1). The scattering geometry. The quantities θ, θ', ψ, are the angle of incidence, angle of reflection, and cone angle respectively.

Fig.(2). The model density of states of Ag. Here ϵ_f is the Fermi level and the vacuum level is taken at 0.

Fig.(3). The real part of the ionic potential for the case where N=5, b=2.36 A , L=37 A .

Fig.(4). The Imaginary part of the ionic potential corresponding to the parameters of Fig.(3).

Fig.(5). The variation of the surface plasmon loss probability with the incident electron energy. Here θ = 30, ψ = 44, ϕ = (0, 360). b=2.36 A ,and N=20.

Fig.(6) Same as Fig.(3) with the strength of the ionic potential set equal to zero. Comparison of these two curves shows that the additional structures are due to the ionic potential.

Fig.(7) Plasmon loss probability in the specular direction. Here $\theta = \theta' = 22, \phi = 180$, b=2.36 A .

Fig.(8). The LEED spectrum corresponding to the parameters of Fig.(8)

Fig.(9). The variation of surface plasmon probability with azimuthal angle ϕ for 100 eV incident energy. Here θ = 21.15, and ψ = 42.3.

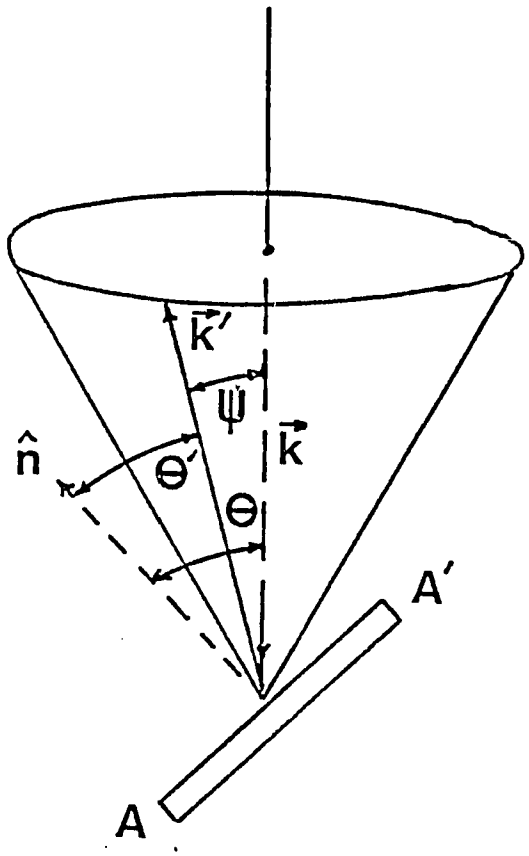

Fig. 1

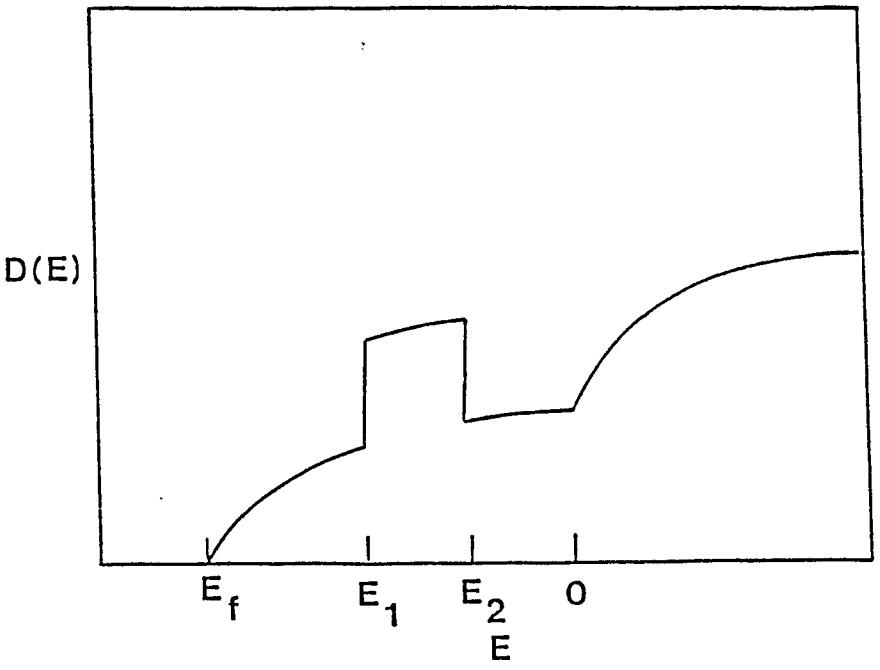

Fig. 2

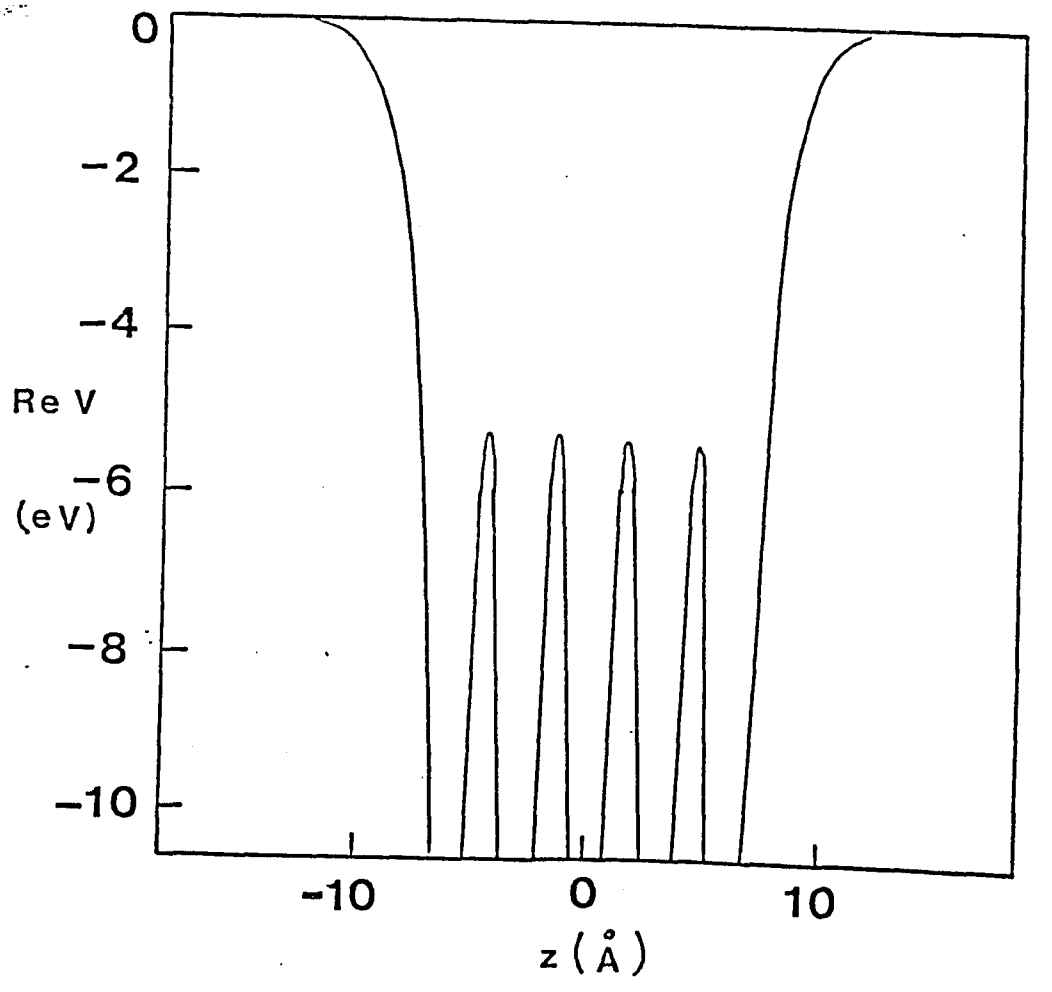

Fig. 3

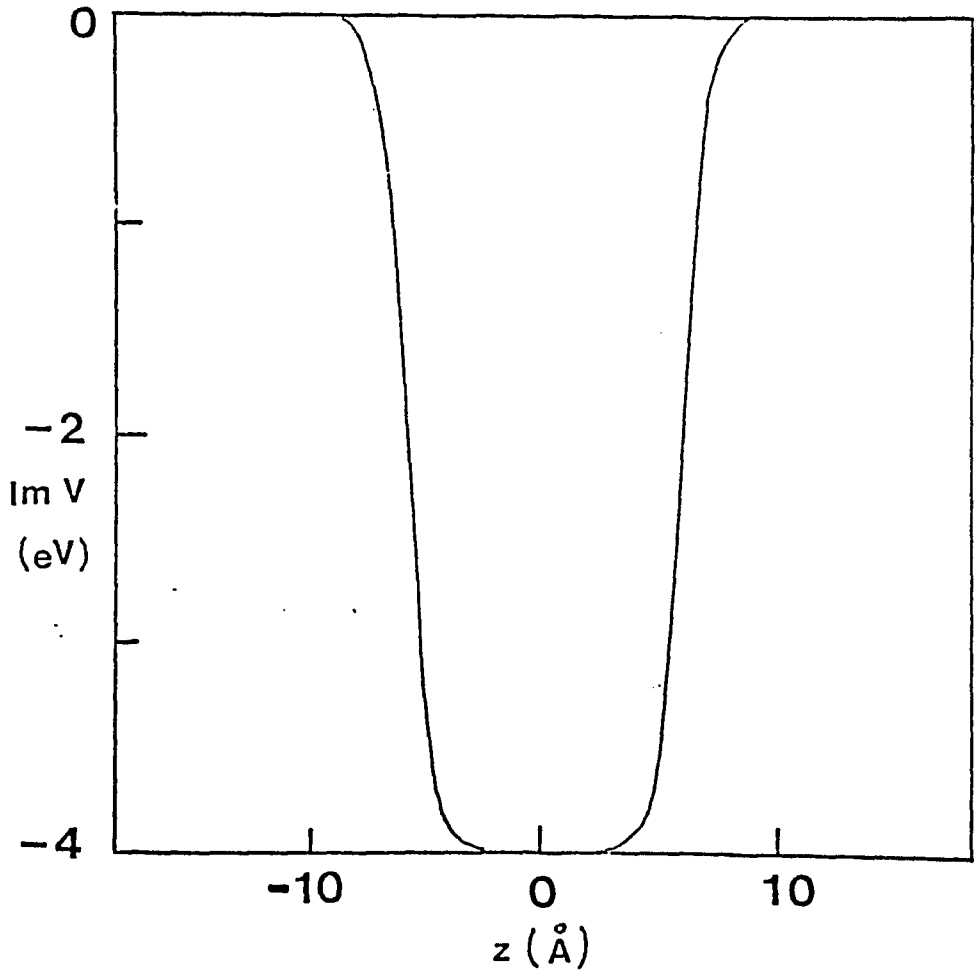

Fig. 4

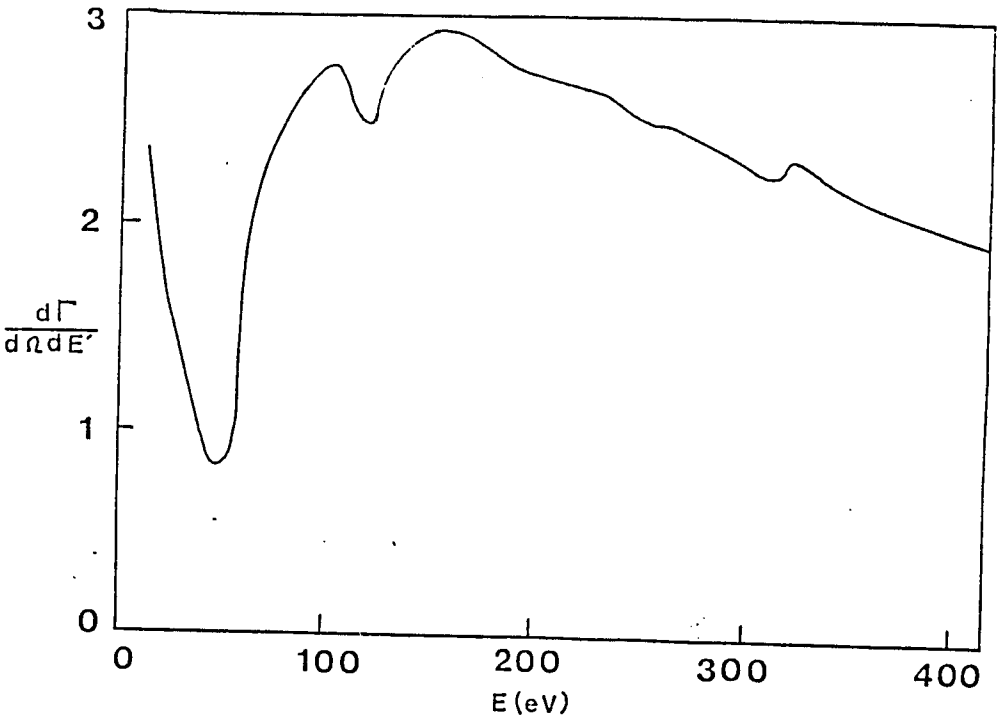

Fig. 5

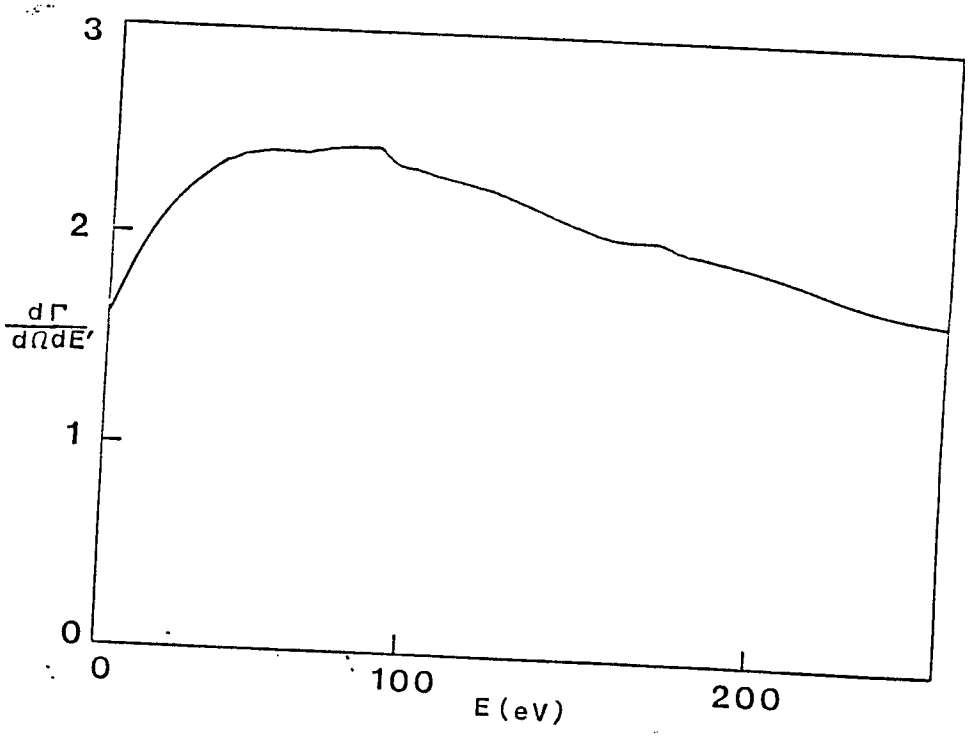

Fig. 6

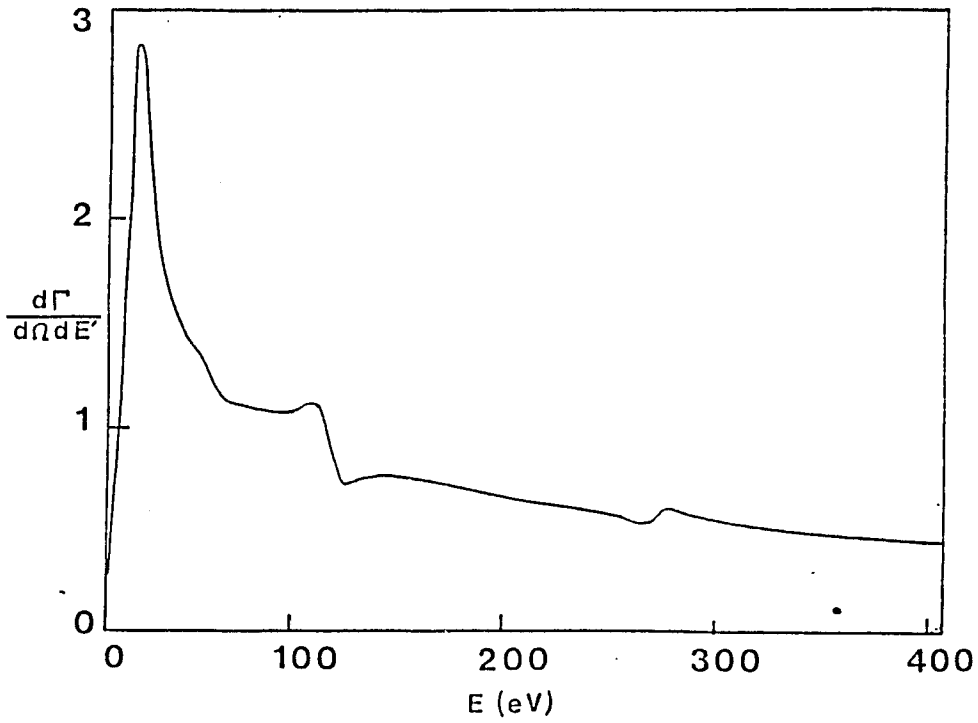

Fig. 7

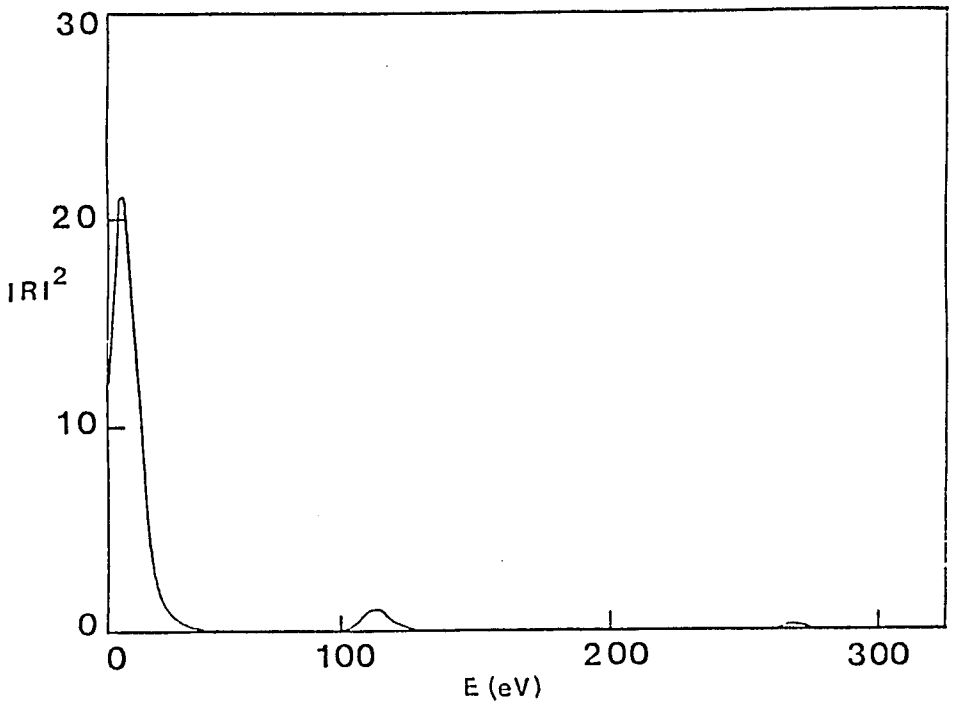

Fig. 3

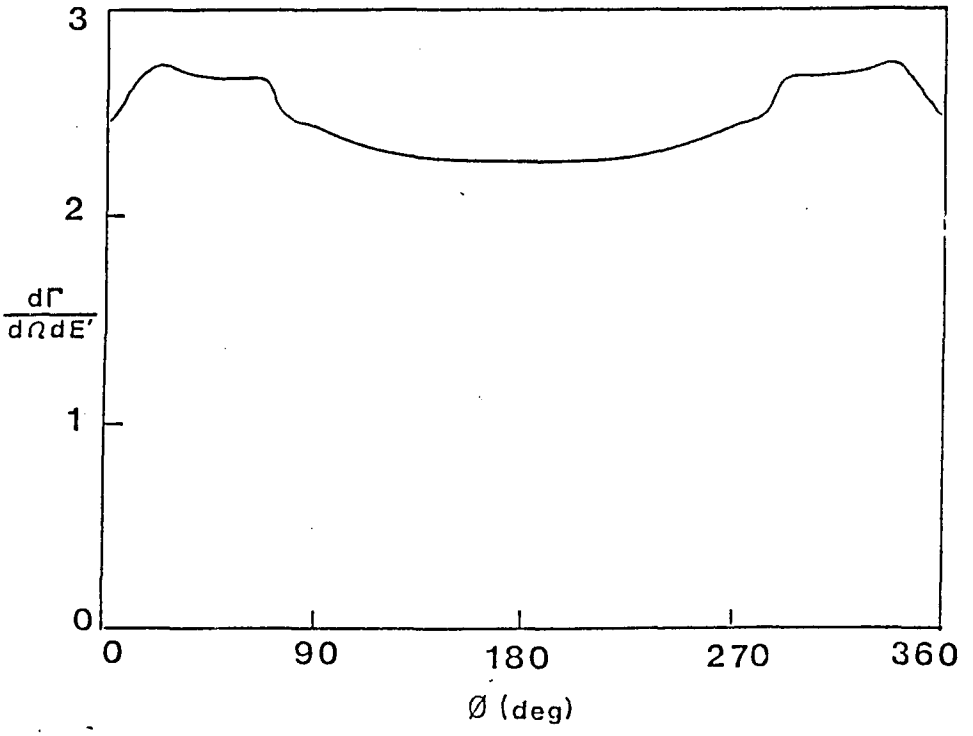

Fig. 9

4. Inelastic Scattering of an electron from a small sphere: Effect of non-local dielectric function on the excitation spectrum.

1. Introduction

In recent years the properties of small solid state systems such as isolated particles or surface roughness features has attracted considerable attention. The small particles could either be isolated levitated particles or could be on an inert substrate, in which case it forms what is known as island film. In this part of the thesis we study the properties of such systems interacting with electron beams. In particular we will study the inelastic loss spectrum of the electrons and try to relate it to elementary electronic and structural features of the small paricle.

The theoretical formulation of the energy loss spectrum for an electron scattering from a sphere has previously been given. Originally a theory has been given by Das and Gersten[1] for the excitation of dipolar collective excitations. This theory has been extended by Ferrel et. al.[2] who have computed the effect of multipolar excitations. Batson[4] studied the excitation of rough surfaces by means of electron scattering and focussed attention on the effect of a sphere near a plane. All of these formulations, however, involved an assumption that the spatial dispersion of the dielectric function could be neglected. For bulk matter, this is usually acceptable. For small particles, however, some care must be exercised before this assumption is used. In this chapter we will address this question.

In order to consider such effects we must introduce the frequency and wave-vector dependent dielectric function $\epsilon(\vec{k},w)$. The problem is complicated by the presence of finite boundary effects. In the present work we develop an approximate method for incorporating such effects by replacing $\epsilon(\vec{k},w)$ by a new effective dielectric constant $\epsilon_l(w)$, where l is the multipolar index of the excitation. As we will see, the l - dependence contains information concerning the spatial dispersion. We will include in our theory all higher order multipolar excitations, These are of interest since an electron whose wave length is small compared with the size of the particles will efficiently couple to such excitations.

2. Theory

The technique we will employ involves a semiclassical calculation in which the trajectory of the charged projectile is taken to be a classically prescribed one. The trajectory is given by $\vec{r} = \vec{R}(t)$ and the sphere which it interacts with is denoted by radius 'a'. The radius of the sphere is assumed to be much smaller than the wavelength of the light corresponding to the characteristic excitation frequency ($a << \lambda$), so that retardation effects can be neglected. The scattering geometry is illustrated in the Fig.(1a). The position of the electron at any instant of time is denoted by $\vec{R}(t)$, and 'a' denotes the sphere radius. The corresponding electrostatic potential satisfies the Laplace equation

$$\nabla^2\phi(\vec{r},t) = 0 \tag{2.1}$$

everywhere except at the position of the charge and the boundary. The solution is given by

$$\phi(r,t) = \frac{q}{|\vec{r}-\vec{R}(t)|} + \sum_{l,m} A_{lm}(t) r^{-(l+1)} Y_{lm}(\hat{r}) \quad \text{if} \quad r > a \tag{2.2a}$$

$$\phi(r,t) = \sum_{l,m} B_{lm}(t) r^{l} Y_{lm}(\hat{r}) \quad \text{if} \quad r < a \tag{2.2b}$$

The coefficients $A_{lm}(t)$ and $B_{lm}(t)$ could be determined by solving the Poisson equation and applying the boundary conditions. However, due to the finite size of the sphere, the non-local dielectric constant formalism can not be introduced. This is because the dielectric function is exppressed in terms of momentum eigenstates and is given as a function $\epsilon(\vec{k},w)$. For a finite sphere, momentum eigenstates are inappropriate. So an alternative method has to be developed.

We start by introducing a related problem which can be readily solved and show its relevance to the problem at hand. In this problem the sphere is replaced by an infinite medium through all space characterized by dielectric constant $\epsilon(\vec{k},w)$ and a fiduciary shell of charge at radius r=a, as shown in the Fig.(1b). Since the medium is now infinite there is no difficulty in introducing a momentum representation. We then demand that the field inside the shell be the same as in the first case i.e. ϕ is given by Eqn.(2.2b) for r< a. This technique has been used by Ferrel and Marusak[3] in the case of a semi- infinite crystal. They argued that when the electrons undergo specular reflection at the boundary, the electron dynamics is not influenced by the assumption. Here we extend their analysis to a spherical geometry and again assume specular reflection. The shell of charge is characterized by the charge density

$$\rho(\vec{r},t) = \delta(r-a) \sum_{l,m} \sigma_{lm}(t) Y_{lm}(\hat{r}) \tag{2.3}$$

The Poisson equation for ϕ corresponding to ρ is given by

$$\nabla^2 \phi = -4\pi \frac{\rho}{\epsilon} \tag{2.4}$$

The corresponding Fourier components are related by

$$k^2\epsilon(k,w)\phi(k,w) = 4\pi\rho(k,w) \tag{2.5}$$

With Eq. (2.3), $\rho(k,w)$ is expressed as

$$\rho(k,w) = \frac{1}{(2\pi)^4}\int d\vec{r}\int dt e^{-i(k.r-wt)}\delta(r-a)\sum_{lm}\sigma_{lm}(t)Y_{lm}(\hat{r}) \tag{2.6}$$

Using the spherical harmonic expansion of the plane wave we may write

$$\rho(k,w) = \frac{4\pi}{(2\pi)^4}a^2\int dt e^{iwt}\sum_{lm}(-i)^l\sigma_{lm}(t)j_l(ka)Y_{lm}(\hat{k})$$

$$= \frac{4\pi}{(2\pi)^3}a^2\sum_{lm}\sigma_{lm}(w)(-i)^l j_l(ka)Y_{lm}(\hat{k}) \tag{2.7}$$

where $j_l(ka)$ is the spherical Bessel function of the first kind and Y_{lm} are the spherical harmonics. Here $\sigma_{lm}(w)$ and $\sigma_{lm}(t)$ are the Fourier transforms of each other, i.e.

$$\sigma_{lm}(w) = \int_{-\infty}^{\infty}\frac{dt}{2\pi}e^{iwt}\sigma_{lm}(t) \tag{2.8}$$

With this form of ρ, Eq.(2.5) becomes

$$\phi(\vec{k},w) = \frac{2a^2}{\pi}\frac{1}{k^2\epsilon(\vec{k},w)}\sum_{l,m}\sigma_{lm}(w)(-i)^l j_l(ka)Y_{lm}(\hat{k}) \tag{2.9}$$

The electric field $\vec{E}$ and the displacement vector $\vec{D}$ are given by

$$\vec{E} = -\nabla\phi \tag{2.10}$$

$$\vec{D} = \int d\vec{k}\int dw\frac{2a^2}{\pi}(-ik)\frac{e^{i(\vec{k}.\vec{r}-wt)}}{k^2\epsilon(\vec{k},w)}\sum_{lm}\sigma_{lm}(w)(-i)^l j_l(ka)Y_{lm}(\hat{k}) \tag{2.11}$$

The radial component of $\vec{D}$ can be expressed as

$$D_r(\vec{r},t) = -2i\frac{a^2}{\pi}\int d\vec{k}dw\frac{\hat{k}.r}{k}e^{-iwt}\sum_{l,m,l',m'} 4\pi i^l\, j_l(kr)\times$$

$$Y^*_{lm}(\hat{k})Y_{lm}(\hat{r})\sigma_{l'm}(w)(-i)^{l'} j_l(ka)Y_{l'm}(\hat{k}) \qquad (2.12)$$

One may express the dot-product in the above expression as

$$\hat{k}.\hat{r} = P_1(\hat{k}.\hat{r}) = \frac{4\pi}{3}\sum_{\mu} Y_{1\mu}(\hat{k})Y^*_{1\mu}(\hat{r}) \qquad (2.13)$$

using the property of the 3j symbols, the radial component of the displacement vector may be expressed as

$$D_r(\vec{r},t)\,|_a = -4\pi\sum_{l,m}\sigma_{lm}(t)\frac{l}{2l+1}Y_{lm}(\hat{r}) \qquad (2.14)$$

The expression for the potential ϕ and radial components of D can also be obtained from Eq.(2.9) and is given by

$$\phi(\vec{r},t)\,|_a = 8a\sum_{l,m}\frac{\pi}{2l+1}\int dw\frac{\sigma_{lm}(w)}{\epsilon_l(w)}e^{-iwt}Y_{lm}(\hat{r}) \qquad (2.15)$$

where ϵ_l is the effective dielectric constant and is given by

$$\frac{1}{\epsilon_l(w)} = \frac{2a(2l+1)}{\pi}\int_0^{\infty}\frac{dk}{\epsilon(k,w)}j_l^2(ka) \qquad (2.16)$$

Here we have assumed the isotropy of the medium i.e.

$$\epsilon(\vec{k},w) = \epsilon(k,w)$$

A construct similar to that given in Eq. (2.16) has been given by Penn and Rendell[7] in their study of surface-enhanced photoabsorption and photoyield in small spheres.

We next demand that the quantities ϕ and D_r of both models match at the surface of the sphere (r=a). The potential and the radial components

of the displacement vectors from Eqs.(2.2),(2.14-15) are given by

$$\phi(\vec{r},t)|_a = q\sum_{l,m}\frac{4\pi}{2l+1}\frac{a^l}{R^{l+1}(t)}Y^*_{l,m}(\hat{k})Y_{lm}(\hat{r})+\sum_{l,m}A_{l,m}(t)r^{-(l+1)}Y_{l,m}(\hat{r}) \tag{2.17}$$

$$D_r(r,t)|_a = -q\sum_{l,m}\frac{4\pi}{2l+1}\frac{la^{l-1}}{R^{l+1}(t)}Y^*_{l,m}(\hat{k})Y_{l,m}(\hat{r})+\sum_{l,m}A_{l,m}(t)(l+1)a^{-(l+2)}Y_{l,m}(\hat{r}) \tag{2.18}$$

Thus

$$\frac{4\pi q}{2l+1}\frac{a^l}{R^{l+1}(t)}Y^*_{l,m}(\hat{k})+\frac{A_{l,m}(t)}{a^{l+1}} = \frac{4\pi a}{2l+1}\int dw e^{-iwt}\frac{\sigma_{l,m}(w)}{\epsilon_l(w)} \tag{2.19}$$

$$-\frac{4\pi q}{2l+1}\frac{la^{l-1}}{R^{l+1}(t)}Y^*_{l,m}(\hat{k})+A_{l,m}\frac{l+1}{a^{l+2}} = -\frac{4\pi l}{2l+1}\sigma_{l,m}(t) \tag{2.20}$$

After some simplification we get the expression for $\sigma_{l,m}(w)$

$$\sigma_{l,m}(w) = \frac{2l+1}{l+\frac{l+1}{\epsilon_l(w)}}\frac{q}{2\pi}\int_{-\infty}^{\infty}dt e^{iwt}\frac{a^{l-1}}{R^{l+1}(t)}Y^*_{l,m}(\hat{k}) \tag{2.21}$$

Putting the above value of $\sigma_{l,m}$ in Eqn. (2.19),we get

$$A_{l,m}(t) = a^{2l+1}4\pi q\left\{-\frac{1}{2l+1}\frac{Y^*_{l,m}(\hat{R}(t))}{R^{l+1}(t)}+\right.$$

$$\left.\frac{1}{2\pi}\int_{-\infty}^{\infty}dw e^{-iwt}\frac{1}{l\,\epsilon_l(w)+l+1}\int_{-\infty}^{\infty}dt' e^{iwt'}\frac{Y^*_{l,m}(\hat{R}(t'))}{R^{l+1}(t')}\right\} \tag{2.21b}$$

Thus the potential is given by

$$\phi(\vec{r},t) = 4\pi q\sum_{l,m}\frac{1}{2l+1}\frac{r^l_<}{r^{l+1}_>}Y^*_{l,m}(\hat{R}(t))Y_{l,m}(\hat{r})$$

$$4\pi q\sum_{l,m}a^{2l+1}\frac{Y_{l,m}(\hat{r})}{r^{l+1}}\left|-\frac{1}{2l+1}\frac{Y^*_{l,m}(\hat{R})}{R^{l+1}}+\right.$$

$$\frac{1}{2\pi}\int_{-\infty}^{\infty} dw \frac{e^{-iwt}}{l\,\epsilon_l(w)+l+1}\int_{-\infty}^{\infty} dt\, 'e^{iwt'}\frac{Y^*_{l,m}(\hat{R}(t'))}{R^{l+1}(t')}\Bigg| \qquad (2.22)$$

where $r_> = max(r, R(t))$, $r_< = min(r, R(t))$ The energy loss of the moving charge, "e", is given by

$$e = -\int_{-\infty}^{\infty} dt P(t) \qquad (2.23)$$

where $P(t) = -q\vec{v}(t).\vec{E}(t)$ is the power, E is the local electric field given by

$$\vec{E}(t) = -\nabla\tilde{\phi}(\vec{r})\,|_{\vec{r}=\vec{R}(t)} \qquad (2.24)$$

where $\vec{v}(t)$ is the velocity of the projectile. Thus "e" is given by

$$e = \int_{-\infty}^{\infty} dtq\dot{\vec{R}}(t).\vec{E}(t) \qquad (2.25)$$

When substituting the value of $\vec{E}(t)$ we take only the nonsingular part of $\phi(\vec{r},t)$ to avoid divergence problems with the self energy. This is given by

$$\tilde{\phi} = \sum_{l,m} A_{l,m}(t) r^{-(l+1)} Y_{l,m}(\hat{r}) \qquad (2.26)$$

Employing the expression for $A_{l,m}$ from Eq. (2.21), Eq. (2.25) we obtain

$$e = \int_{-\infty}^{\infty} dt\, 4\pi q^2 \Bigg| \dot{\vec{R}}.\nabla \sum_{l,m} a^{2l+1}\frac{Y_{l,m}(\hat{r})}{r^{l+1}}\Bigg\{-\frac{1}{2l+1}\frac{Y^*_{l,m}(\hat{R})}{R^{l+1}}+$$

$$\frac{1}{2\pi}\int_{-\infty}^{\infty} dw \frac{e^{-iwt}}{l\,\epsilon_l(w)+l+}\int_{-\infty}^{\infty} dt\, 'e^{iwt'}\frac{Y^*_{l,m}(\hat{R}(t'))}{R^{l+1}(t)}\Bigg\}\Bigg| \qquad (2.27)$$

Then the above expression may be written as

$$e = \int_{-\infty}^{\infty} e(w)dw \qquad (2.28)$$

where $e(w)dw$ is the energy loss in the frequency range between w and w+dw, factorizing the w integration from the two terms of the above equation yields

$$e(w) = 2q^2 \int_{-\infty}^{\infty} dt \sum_{l,m} a^{2l+1} e^{-iwt} \int_{-\infty}^{\infty} dt' e^{iwt'} \times$$

$$\frac{Y^*_{l,m}(\hat{R}')}{R'^{l+1}} \dot{\vec{R}}.\nabla_R \frac{Y_{l,m}(\hat{R})}{R^{l+1}} \left| \frac{-1}{2l+1} + \frac{1}{l\epsilon_l(w)+l+1} \right| \qquad (2.29)$$

$$= 2q^2 \sum_{l,m} a^{2l+1} \frac{l}{2l+1} \frac{1-\epsilon_l(w)}{l\epsilon_l(w)+l+1} \int_{-\infty}^{\infty} dt \int_{-\infty}^{\infty} dt' \times$$

$$e^{iw(t'-t)} \frac{Y^*_{l,m}(\hat{R}')}{R'^{l+1}} \dot{\vec{R}}.\nabla_R \frac{Y_{l,m}(\hat{R})}{R^{l+1}} \qquad (2.30)$$

From the above formula it is clear that $e(w)=0$, if $\epsilon_l(w) = 1$, as expected. If there is no sphere there is no loss. Furthermore

$$\frac{\partial f(\vec{R})}{\partial t} = \dot{\vec{R}}.\nabla_R f$$

$$\int_{-\infty}^{\infty} dt e^{-iwt} \dot{\vec{R}}.\nabla R \frac{Y_{l,m}(\hat{R})}{R^{l+1}} = iw \int_{-\infty}^{\infty} dt e^{-iwt} \frac{Y_{l,m}(\hat{R})}{R^{l+1}}$$

So Eq. (2.30) reduces to the form

$$e(w) = 2iwq^2 \sum_{l,m} a^{2l+1} \frac{l}{2l+1} \frac{1-\epsilon_l(w)}{l\epsilon_l(w)+l+1} \left| \int_{-\infty}^{\infty} dt e^{-iwt} \frac{Y_{l,m}(\hat{R})}{R^{l+1}} \right|^2 \qquad (2.31)$$

The real part of e(w) may be interpreted as the energy loss spectrum. The above equation can be written as

$$e(w) = -2wq^2 \sum_{l,m} a^{2l+1} \mathrm{Im} \frac{1}{l\epsilon_l(w)+l+1} \times \left| \int_{-\infty}^{\infty} dt e^{-iwt} \frac{Y_{l,m}(\hat{R})}{R^{l+1}} \right|^2 \qquad (2.32)$$

The total energy loss is expressible as the sum of the contributions due to exciting the individual multipoles, i.e.

$$e(w) = \sum_{l,m} e_{l,m}(w)$$

where $e_{l,m}(w)\,dw$ equals the energy lost to mode l,m between frequency w and w+dw. Here

$$e_{l,m}(w) = -2wq^2 a^{2l+1} \mathrm{Im} \frac{1}{l\epsilon_l(w)+l+1} \left| \int_{-\infty}^{\infty} dt e^{-iwt} \frac{Y_{l,m}(\hat{R})}{R^{l+1}} \right|^2 \qquad (2.33)$$

The probability for exciting a particular l,m mode between frequency w and w+dw is given by dividing this quantity by the photon energy $\hbar w$:

$$P_{l,m}(w)dw = \frac{e_{l,m}(w)dw}{\hbar w} \qquad (2.34)$$

The cross section for exciting a particular l,m mode between w and w+dw is thus

$$\frac{d\sigma_{l,m}}{dw} dw = \int_0^{2\pi} d\phi \int b db P_{l,m}(w)dw \qquad (2.35)$$

where b is the impact parameter and ϕ is the azimuthal angle.

Finally, using Eq. (2.33) the cross section is given by

$$\frac{d\sigma_{l,m}(w)}{dw} = -\int d\phi \int b db \frac{2q^2}{\hbar} a^{2l+1} \times \left| \int_{-\infty}^{\infty} dt e^{-iwt} \frac{Y_{l,m}(\hat{R})}{R^{l+1}} \right|^2 \mathrm{Im} \left| \frac{1}{l\epsilon_l(w)+l+1} \right| \qquad (2.36)$$

Thus the problem is reduced to the calculation of $\epsilon_l(w)$:

$$\frac{1}{\epsilon_l(w)} = \frac{2a(2l+1)}{\pi}\int_0^\infty dk \frac{j_l^2(ka)}{\epsilon(k,w)} \tag{2.37a}$$

This should be compared with the formula of Ritchie and Marusak[3] which gives

$$\frac{1}{\bar{\epsilon}(\vec{k},w)} = \frac{k_p}{\pi}\int dq_z \frac{1}{[k_p^2+q_z^2]\epsilon(\vec{q},w)} \tag{2.37b}$$

In order to assess the role played by spatial dispersion we need a model for the dielectric function $\epsilon(\vec{k},w)$. In general this can be a rather complicated task and is not really a solved problem, to this day. The difficulty lies in how to treat the one electron excitations of the system when spatial dispersion are present. While theoretical expressions may be constructed for $\epsilon(\vec{k},w)$ in terms of the electronic band structure, no simple method for their evaluation has been found.

In our work we are primarily concerned with collective excitations. For studying these it is possible to introduce a simple model which does include spatial dispersion effects. It is the hydrodynamical model. Let us derive the dielectric function as follows.

Hydrodynamic model

If an external test charge ρ_{ex} is introduced into the solid it produces a net charge ρ_{net}, which depends on the dielectric constant of the solid. These charge densities are given by the relations

$$\rho_{ex} = \rho_0 e^{i(\vec{k}\vec{r}-wt)} \tag{2.38}$$

$$\rho_{net} = \rho_1 e^{i(\vec{k}\vec{r}-wt)} \tag{2.39}$$

$$\rho_{net} = \frac{\rho_{ex}}{\epsilon(\vec{k},w)} \tag{2.40}$$

where ρ_0, ρ_1 are the corresponding amplitudes and $\epsilon(\vec{k}, w)$ is the dielectric constant of the solid. We follow the traditional Drude approach here. The dynamics is specified by Gauss's law, the continuity equation and a Newtonian equation of motion

$$\nabla.\vec{E} = 4\pi\rho_{net} \tag{2.41}$$

$$\nabla.\vec{J}_{net} + \frac{\partial\rho_{net}}{\partial t} = 0 \tag{2.42}$$

$$m\left[\frac{d\vec{v}}{dt} + \frac{\vec{v}}{\tau}\right] = -e\vec{E} - \chi_0\nabla n \tag{2.43}$$

where $\vec{J}_{net}$ is the net current in the solid due to the net external charge, $\vec{v}$ is the electron velocity, $e\vec{E}$ is the electrical force and $\chi_0\nabla n$ is the degeneracy force. Here χ_0 is derived from the Fermi energy and is given by

$$\chi_0 = \frac{\hbar^2}{2m}\frac{2}{3}\frac{(3\pi^2)^{2/3}}{n^{1/3}} \tag{2.44}$$

and

$$\rho_{net} = \rho_{ex} - e(n - n_0) \tag{2.45}$$

$$\vec{J}_{net} = -ne\vec{v} + \vec{J}_{ex} \tag{2.46}$$

$$n = n_0 + \nu(\vec{x}, t) \tag{2.47}$$

The quantity n is the induced electron charge density, n_0 is the back-ground ion charge density and ν represents the fluctuation in the background charge density. Linearizing the above set of equations yields, after some algebra, the expression for the dielectric function as

$$\epsilon(\vec{k}, w) = 1 - \frac{w_p^2}{w(w + \frac{i}{\tau}) - \chi_0\frac{k^2 n_0}{m}} \tag{2.48}$$

Using this value of the dielectric function the integral in Eq. (2.16) can be done analytically and is given by

$$\frac{1}{\epsilon_l(w)} = \frac{1}{\epsilon_d} + (2l+1)\frac{\epsilon_d - 1}{\epsilon_d} 2\frac{c}{\pi} i_l(c) k_l(c) \qquad (2.49)$$

where w_p is the free electron plasma frequency, ϵ_d is the Drude dielectric constant and c is a parameter,

$$w_p^2 = \frac{4\pi n e^2}{m}$$

$$\epsilon_d = 1 - \frac{w_p^2}{w(w + \frac{i}{\tau})}$$

$$c = w_p a \sqrt{\frac{m \epsilon_d}{\chi_0 n_0 (\epsilon_d - 1)}}$$

In Eq. (2.49) $i_l(c)$ and $k_l(c)$ are modified spherical Bessel functions of the first and second kind, respectively. Equation (2.49) provides us with the desired expression needed.

3. Results and discussion:

We have carried out a calculation of the frequencies for the resonant excitation of small spherical particles for both the Drude model and the hydrodynamiccal model. In the Drude case, where the dielectric function depends only on the frequency, $\epsilon = \epsilon(w)$, we do not expect the resonance frequencies to depend on the particle size at long wave-lengths. It is not until the wave-length gets to be comparable to the size of the particle that retardation effects enter and the Mie resonances display their variation with size. In Fig. 2 we show the variation of the Drude frequencies, determined from the equation $\epsilon(w) = -(l+1)/l$ as a function of l. As expected, the low modes are red-shifted away from the surface plasmon value

($\epsilon(w) = -1$). As l is increased the frequencies converge to the surface plasmon frequency.

In Fig.2 we also illustrate the result of the hydrodynamic calculation. The physical parameters chosen were those corresponding to a realistic model such as silver ($k_f = .645, \tau = 1500, \lambda = .13 a.u.$). The calculation was done for several particle sizes. The trends are clear. In each case, as l is increased the resonance frequency also increases. However, small "a" values have higher frequencies than large values. As "a" is increased the hydrodynamic results seem to converge to the Drude results. This is again illustrated in Fig. 3 where the frequencies are plotted as a function of sphere size for various order, l.

A qualitative understanding of these trends may be had by studying Eq. (2.48). The extent of the spatial dispersion of the dielectric function is governed by the extent of the $\vec{k}$-vectors involved . In a sphere of radius a the range of $\vec{k}$-vectors is determined by the uncertainty relation. Small a implies a large ∇k and vice versa. Thus for small spheres the effective dielectric function samples a higher range of frequencies than for large a. This accounts for the tendency of the frequencies to rise with decreasing a.

The effective dielectric function $\epsilon_l(w)$ should find application in problems relating to small particles. In this paper we have shown how it can be applied to the problem of inelastic electron scattering, but it could also find applicability in problems involving the interaction of light with particles or the interaction of atoms or molecules with particles.

References

1. P.Das and J. I. Gersten, Phys. Rev. B 27, 5912(1983)

2. T. L. Ferrel and P. M. Echenique, Phys. Rev. Lett, 55 14, 1526(1986)

3. Ritchie R. H. and Marusak A. L., Surf. Sci. 4, 234(1966)

4. P. E. Batson, Phys. Rev. Lett. 49, 936 (1982)

5. D. R. Penn and P. Apell, J. Phys C 16, 5729(1983)

6. N. Kreibig and P. Zachariao, Z. Phys. B 21 357(1975)

7. D. R. Penn and R. W. Rendell, Phys. Rev. Lett. 47, 1067, (1981)

Figure Captions

Fig.1. a). Scattering geometry. $\vec{R}(t)$ is the position of the projectile at any instant of time t, a is the sphere radius. b). Equivalent problem replaced by an infinite medium characterised by $\epsilon(\vec{k},w)$ and a shell of charge.

Fig.2. variation of frequency with l for different radius in hydrodynamic model

Fig.3. Variation of w with radius for different l.

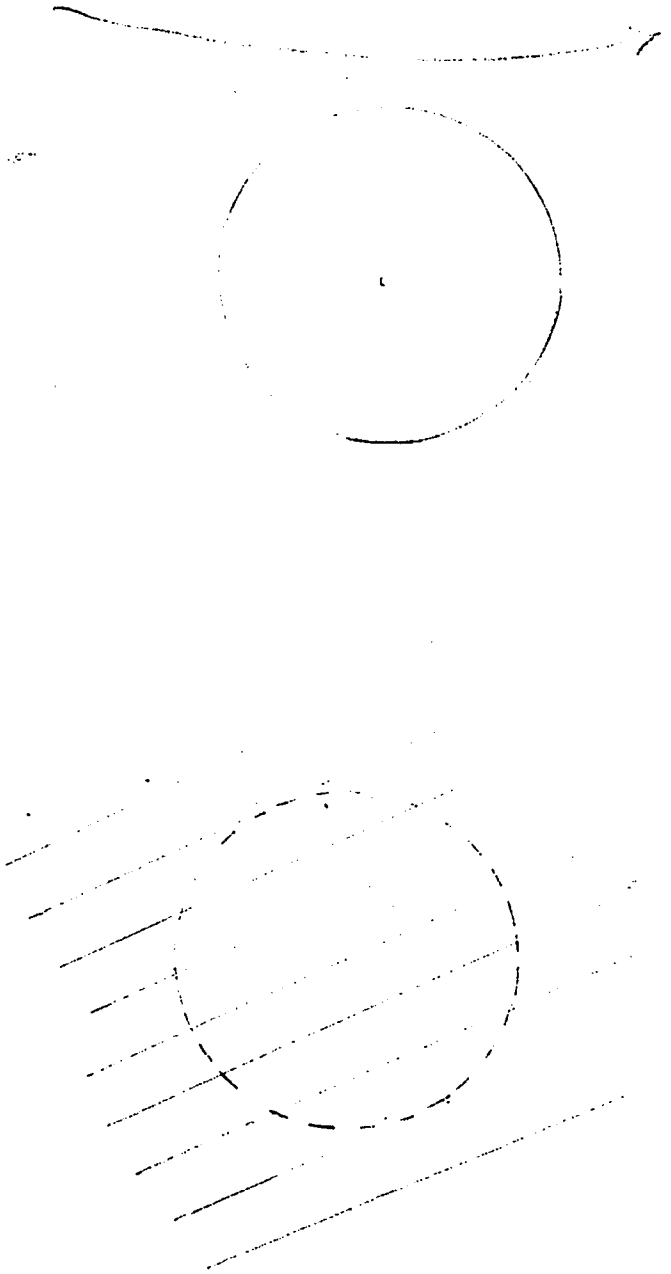

Fig. 1

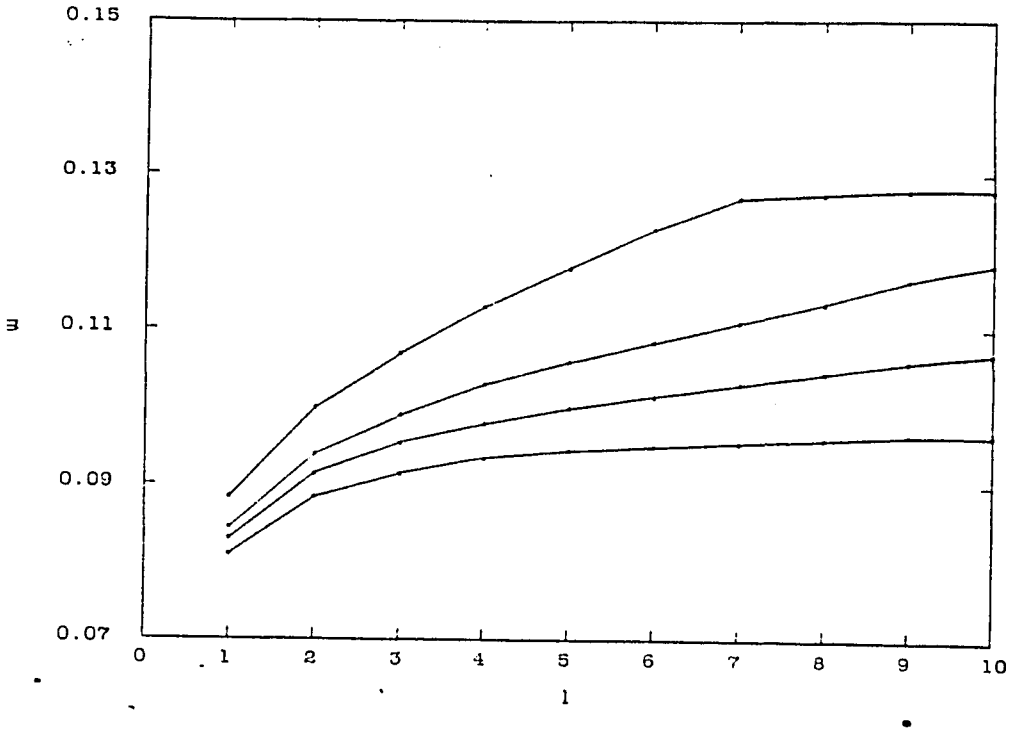

Fig. 2

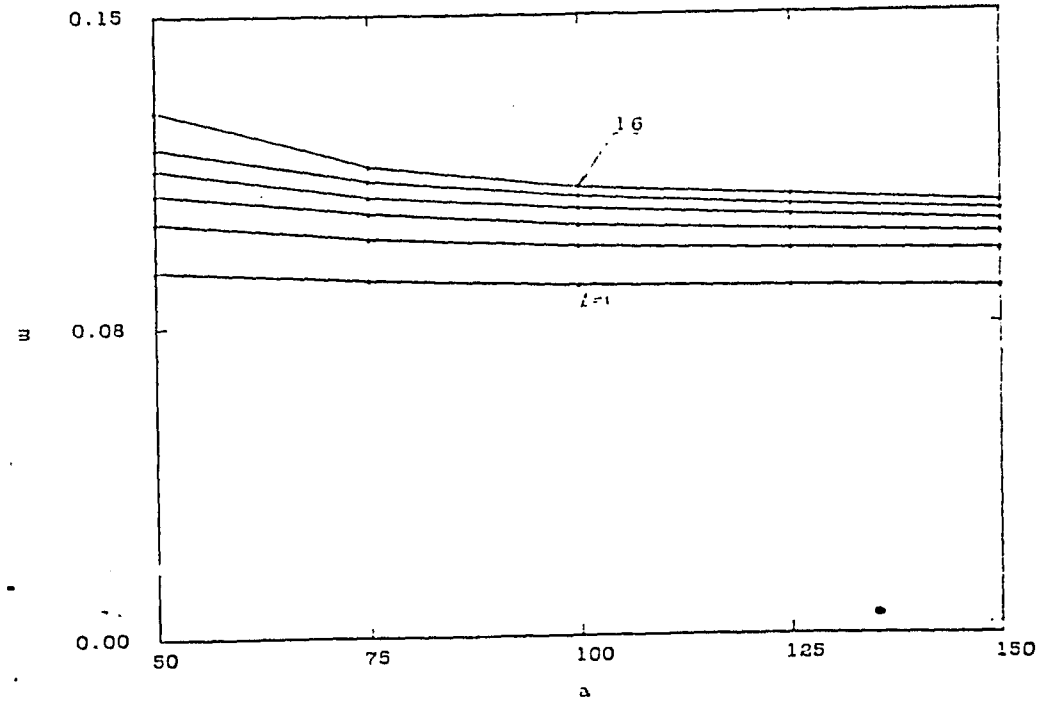

Fig. 3

CONCLUSION:

In conclusion we see that by careful analysis of the interaction of light or electrons with solids additional information concerning the structure and excitation properties of the solid may be obtained. In particular our first project indicates that the continuum electronic Raman scattering spectrum contains information about the density of states above the Fermi level. The second project shows how the Raman spectrum for a small particle can give information about the structure of the particle. Our third project, involving electron scattering from surfaces shows how the crystalline structure of the solid can influence even inelastic electron scattering properties. Finally our fourth project demonstrates how the excitation spectrum of a small particle can be influenced by the size of the particle. This thesis demonstrates that the well-studied fields of electron and light scattering with solids still provides a fertile area for research in condensed matter physics.